F_1F_0 ATP Hydrolysis is a Determinant of Metabolic Rate, a Correlate of Lifespan, and a Weakness of Cancer

Michael David Forrest Ph.D., (mikeforrest££hotmail.com (££=@))

ABSTRACT

Dramatic rectal temperature decrease, in mice administered with a drug that specifically inhibits F_1F_0 ATP hydrolysis, suggests that F_1F_0 ATP hydrolysis is a major determinant of metabolic rate *in vivo*. Across twelve investigated species, less F_1F_0 ATP hydrolysis correlates with greater maximal lifespan. Specific drug inhibition of F_1F_0 ATP hydrolysis exerts potent anti-cancer activity *in vitro*.

INTRODUCTION

Aerobic respiration converts the chemical energy of food into the chemical energy of ATP [1]. And because, by the 2nd Law of Thermodynamics, no energy conversion can be 100% efficient, heat is inherently generated as a by-product. An intermediate in this process is the generation of an electrochemical gradient of protons, a proton motive force (pmf), comprising ΔpH and voltage (Ψ_{IM}) components, across the inner mitochondrial membrane. ATP synthase is located in this membrane. It can use the pmf to generate ATP from ADP and inorganic phosphate (Pi). But ATP synthase is reversible and - depending on its substrate and product concentrations, and the pmf value - it can work "forwards" (passing protons, making ATP) or "backwards" (pumping protons, consuming ATP): its "forward" and "reverse" modes respectively. Which may also be termed F_1F_0 ATP synthesis and F_1F_0 ATP hydrolysis respectively.

IF1 protein is an endogenous protein that selectively blocks the reverse mode of ATP synthase (F_1F_0 ATP hydrolysis) [2]. It is widely considered irrelevant during aerobic respiration because (*i*) ATP synthase is solely performing F_1F_0 ATP synthesis, and (*ii*) IF1 protein activity is pH sensitive, being low at normal mitochondrial matrix pH (~pH 8). But it is considered significant upon matrix acidification. Caused by collapse of the pmf across the mitochondrial inner membrane. Which causes ATP synthase to reverse its operation, performing F_1F_0 ATP hydrolysis instead, consuming cellular ATP. This can occur, for example, during ischemia. When a tissue, or part(s) thereof, is completely/partially cut off

from blood flow, foregoing respiratory substrates and O_2 delivery. So, the present consensus is that IF1 protein is a safety device. Important in mitigating pathology, but irrelevant normally. By contrast, I herein report that some F_1F_0 ATP hydrolysis *does* occur normally. Whilst IF1 protein activity, although subdued by the normal alkaline pH of the mitochondrial matrix, is *usefully* non-zero.

RESULTS

This Results section comprises new experimental data. Presented first. Thereafter, in the light thereof, novel analysis of publicly available data. Then, disclosed at the end, more new experimental data.

Methods are presented later, as the penultimate section of this paper, before References.

New experimental results

Systemic inhibition of F_1F_0 ATP hydrolysis: If F_1F_0 ATP hydrolysis is a drive to greater metabolic rate, then systemic inhibition of F_1F_0 ATP hydrolysis should reduce metabolic rate in a subject. Which should, *if* the ambient temperature is lower than their normal body temperature, reduce their body temperature towards the ambient temperature. This is experimentally observed in Figure 1.

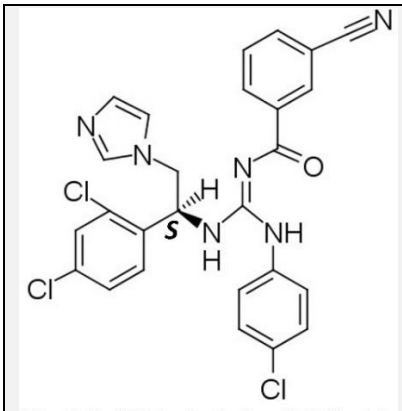

EC_{50} F_1F_0 ATP hydrolysis = **0.018 µM**

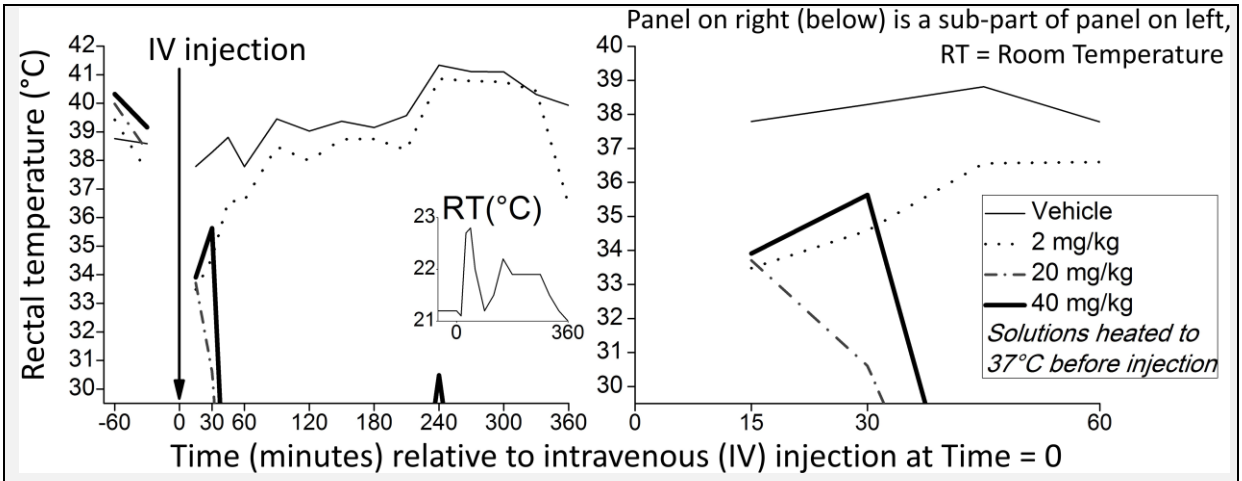

Figure 1 - Selectively inhibiting F_1F_0 ATP hydrolysis in mice reduces their rectal temperature towards room temperature. Room temperature (RT) was around 22°C. Drug structure shown (with enantiomeric excess (ee) of *S* stereoisomer ≥97%) was systemically (intravenously) administered to mice, whose rectal temperatures were monitored. This drug specifically, and potently, inhibits F_1F_0 ATP hydrolysis (EC_{50} = 0.018 μM, in a Sub-Mitochondrial Particle {SMP} assay) [3]. Four mice were used. One was administered vehicle (control), and the other three differing doses of the drug: 2 mg/kg, 20 mg/kg, and 40 mg/kg (all solutions heated to 37°C before administration). Rectal thermistor used couldn't measure rectal temperatures lower than 30°C. Both 20 and 40 mg/kg (but not 2 mg/kg) drug doses made rectal temperature fall below 30°C and out of range. Although the ensuing uncertainty is bounded because rectal temperature cannot fall below room temperature (RT): RT ≤ rectal temperature < 30°C. Rectal temperature was recorded every 15 minutes in the 1st hour after dosing, and every 30 minutes in the later hours shown. It was also recorded at 60 and 30 minutes before dosing. For each mouse, the 1st rectal temperature recording is typically of an atypically high body temperature. Which is associated with the stress of being handled, which a mouse typically becomes habituated to during the course of the experiment. This handling effect has been reported in other rectal thermistor studies of rodents, e.g. [4].

Figure 1 indicates that F_1F_0 ATP hydrolysis is a major determinant of metabolic rate. Its data (interpreted) suggests that during normal aerobic respiration, ATP synthase synthesizes ATP, but also hydrolyses a fraction of the ATP synthesized, which means more ATP needs to be synthesized. Which is a futile cycle, dissipating pmf, because of the inherent inefficiency of any energy conversion (2nd Law of Thermodynamics). And because it, by conferring a proportion of ATP synthase molecules not passing protons, but instead pumping protons

back, increases the rate of proton leak. Wherein pumped protons return to the mitochondrial matrix outside of ATP synthase. Their potential (electrochemical) energy dissipated as heat rather than partially captured in ATP. All of this drives a higher rate of aerobic respiration, conferring greater heat production. Where the amount of F_1F_0 ATP hydrolysis, increasing the rate of aerobic respiration (metabolic rate), is dictated by the amount of IF1 protein activity (per the amount of ATP synthase).

A prediction atop of Figure 1, for future testing, is that if the ambient temperature was instead at the mouse's normal body temperature (around 37°C [5]), or safely higher, then no body temperature drop would occur. Even at high drug doses. Because a mouse's body temperature cannot be at a lower temperature than its surround (2nd Law of Thermodynamics). To illustrate, by analogous example, anaesthetic can dramatically reduce a mouse's body temperature, but *not* when the mouse is kept at an ambient temperature of 37°C [6].

<u>Novel analysis of publicly available data</u> *(in light of the new experimental data above)*
Mammals (and birds) are endothermic and metabolically generate heat to maintain their body temperature. In Euclidean geometry, larger objects have a smaller surface-area (A) to volume (V) ratio. Because, where L is length, $A \propto L^2$ and $V \propto L^3$ ("square-cube law"). So, smaller mammal species have a larger surface-area to volume ratio than larger mammal species. And so they lose a greater proportion of their metabolically generated heat. Which means they must generate more heat per unit mass. Requiring them to have a higher metabolic rate per unit mass (serviced by a greater heart rate). Might this (at least partially) explain why smaller mammal species tend to age faster, and have shorter maximal lifespans, than larger mammal species? What sets this difference in specific metabolic rate?

Mouse data in Figure 1 has shown that F_1F_0 ATP hydrolysis is a causal input into metabolic rate. And further mouse data, later herein, shows that F_1F_0 ATP hydrolysis is a causal input into Reactive Oxygen Species (ROS) generation. Other subsequent data shows a *significant* correlation, across species, between greater specific F_1F_0 ATP hydrolysis *in vitro* and faster specific basal metabolic rate *in vivo*. Moreover, across species, a *significant* correlation is shown between less specific F_1F_0 ATP hydrolysis *in vitro* and less mitochondrial [ROS] *in vitro*, and to less ROS damage to DNA, mitochondrial DNA (mtDNA), and to cellular/membrane lipids. Furthermore, there is a *significant* correlation shown, across species, between less specific F_1F_0 ATP hydrolysis *in vitro* and greater maximal lifespan.

Wherein performed mediation analysis (and supporting interventional data) suggests that specific F_1F_0 ATP hydrolysis dictates maximal lifespan, via dictating specific basal metabolic rate. Thereby *possibly* explaining (at least partially) why different mammal species have different maximal lifespans. Therein *perhaps* teaching a mechanism, and compounds, to slow aging.

Less specific F_1F_0 ATP hydrolysis correlates with longer maximal lifespan

Figure 2 shows that, across twelve different mammal and bird species, less specific F_1F_0 ATP hydrolysis (*in vitro*, in Sub-Mitochondrial Particles {SMPs}; refer Methods) correlates with larger body mass, lower specific basal metabolic rate, slower heart rate, and greater maximal lifespan. The underlying data of this figure is in a table in the Methods section. With data sources disclosed there.

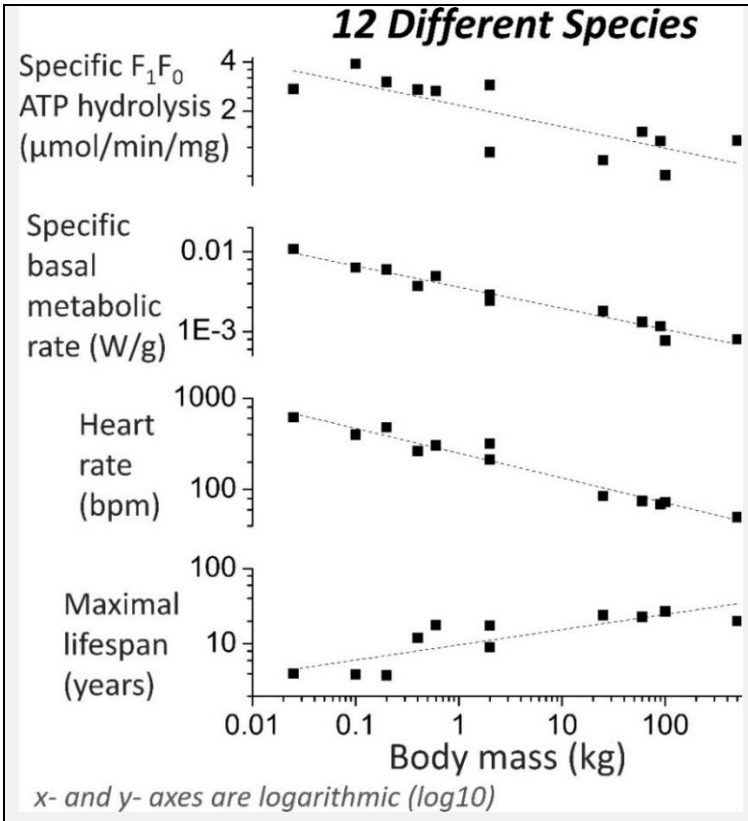

Figure 2 - 1st (top) panel shows a negative correlation between species body mass and specific F_1F_0 ATP hydrolysis (mg is of mitochondrial protein). 2nd panel shows a negative correlation between species body mass and specific basal metabolic rate. 3rd panel shows a negative correlation between species body mass and heart rate (bpm is beats per minute). 4th panel shows a positive correlation between species body mass and maximum lifespan.

Shown best fit lines to the plots of Figure 2 are of the form:

$\log_{10}(y) = \log_{10}(a) + b \cdot \log_{10}(x)$, where b is gradient:

	$\log_{10}(a)$	b		Adjusted R^2
1st panel	0.33791 (±0.04411)	-0.13213 (±0.03077)		0.61323
2nd panel	-2.44192 (±0.02381)	-0.26591 (±0.01661)	≈ *-0.25*	0.95872
3rd panel	2.39875 (±0.02593)	-0.27123 (±0.01808)	≈ *-0.25*	0.95318
4th panel	0.98595 (±0.06233)	0.20246 (±0.04528)	≈*+0.25*	0.65512

Pearson correlation coefficient (R), and associated p-values (one-tailed, because each alternative hypothesis is directional), for the log-log data of Figure 2:

		$\log_{10}$(y1)	$\log_{10}$(y2)	$\log_{10}$(y3)	$\log_{10}$(y4)
R	$\log_{10}$(body mass)	-0.80523	0.98105	-0.97849	0.83043
p		0.000788	0.0000000093	0.000000017	0.0007755

Where y1=specific F_1F_0 ATP hydrolysis, y2=specific basal metabolic rate, y3=heart rate, and y4=maximal lifespan.

Figure 3 recasts some of the data of Figure 2 (omitting body mass data).

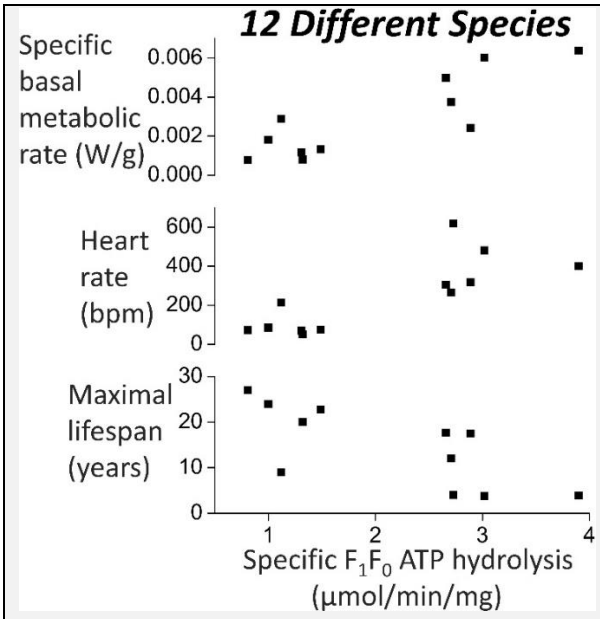

Figure 3 - 1st (top) panel shows, across species, a positive correlation between specific F_1F_0 ATP hydrolysis (mg is of mitochondrial protein) and specific basal metabolic rate. 2nd panel shows, across species, a positive correlation between specific F_1F_0 ATP hydrolysis and heart rate. 3rd panel shows, across species, a negative correlation between specific F_1F_0 ATP hydrolysis and maximal lifespan. Herein proposed, the 1st panel correlation drives the 2nd and 3rd panel correlations.

For the data used to produce Figure 3, the following table presents Pearson correlation (R) coefficients, and associated p-values (one-tailed, because each alternative hypothesis is directional), for its inter-relations:

Pearson correlation coefficient (R)				
	Specific basal metabolic rate	Heart rate	Maximal lifespan	
Specific F1F0 ATP hydrolysis	0.7016	0.8007	-0.7192	
	Specific basal metabolic rate	0.9476	-0.8144	
		Heart rate	-0.8572	
p-value (one-tailed)				
	Specific basal metabolic rate	Heart rate	Maximal lifespan	
Specific F1F0 ATP hydrolysis	0.0054965	0.0008765	0.0063065	
	Specific basal metabolic rate	0.0000015	0.001136	
		Heart rate	0.0003725	
Asymptotically exact harmonic mean p-value for combining independent/dependent tests				
Of all the p-values above (in this present table) = 0.000008933458 = **0.000009**				
Fisher's combined probability test				
Using p-values for [Specific F1F0 ATP hydrolysis vs. Maximal lifespan] (=0.0063065) &				
[Heart rate vs. Specific basal metabolic rate] (=0.0000015) = 0.0000002				

The p-values are small, despite the small values of *n*, in testament to the high *R* values. The asymptotically exact harmonic mean p-value was calculated according to the method of [7] (its post-published corrected method, as corrected on 7 October 2019). All the p-values are smaller than 0.05, and so all are *significant*.

Local inhibition of F_1F_0 ATP hydrolysis

I postulate that if F_1F_0 ATP hydrolysis is inhibited locally in a subject, i.e. only in a body region, then there is no appreciable body temperature drop. Not even in the affected body region, because of heat transfer (especially via blood flow) from other body regions. Indeed, supporting, [8] has shown the safety of local inhibition of F_1F_0 ATP hydrolysis *in vivo*. Wherein, in forebrain neurons of mice, they reduced the amount of F_1F_0 ATP hydrolysis by

~35%. By increasing IF1 protein amount by 300%. Wherein the extra IF1 protein was actually human IF1 protein, with a single amino acid substitution that increases its inhibitory potency against F_1F_0 ATP hydrolysis at pH 8. These mice were "normal in appearance, home-cage behaviour, reproduction, and longevity up to 1-year follow-up".

[9] showed the *in vivo* safety of locally decreasing F_1F_0 ATP hydrolysis, by locally increasing IF1 protein amount, in mouse liver (especially in perivenous hepatocytes): locally, extra IF1 protein decreased F_1F_0 ATP hydrolysis by 40% and decreased State 3 respiration rate by 44%. Wherein these mice had "no differences in weight, life span and cage behavior when compared to controls after one year of follow up".

[10] showed the *in vivo* safety of locally decreasing F_1F_0 ATP hydrolysis, by locally increasing IF1 protein amount, in mouse intestine: locally, this extra (human) IF1 protein decreased the F_1F_0 ATP hydrolysis capability by 35%, which decreased the oligomycin sensitive respiration rate by 60%. All safely.

Inhibiting F_1F_0 ATP hydrolysis decreases [ROS]

Data herein suggests that metabolic rate confers life, but that some correlate to it causes aging, which ultimately takes life away. This correlate might be Reactive Oxygen Species (ROS) [11-13]. Produced by electrons leaking from the respiratory chain during oxidative phosphorylation. If so, one would expect inhibition of F_1F_0 ATP hydrolysis to reduce the rate of ROS generation. This is experimentally observed. In *reinterpreted* data of [8].

[8] interpret their data as showing that increased IF1 protein amount, and decreased F_1F_0 ATP hydrolysis, *increases* [ROS]. But this is in error. What their data actually shows is that increased IF1 protein amount, and decreased F_1F_0 ATP hydrolysis, *decreases* [ROS]. [8] transgenically increased IF1 protein amount, which decreased F_1F_0 ATP hydrolysis, in the forebrain neurons of mice. This manipulation furnished these cells with a lower respiration rate (lower O_2 consumption rate). And a more hyperpolarized membrane potential across their mitochondrial inner membrane (Ψ_{IM}). Because of the latter (rendering a more negative mitochondrial matrix), these cells accumulate more positively charged ROS (superoxide) reporting MitoSOX^{TM} probe. Which means they have greater ROS signal. Which [8] mistakenly take at its face value, interpreting this as meaning greater [ROS]. However, once

the Ψ_{IM} disparity is factored in, which is a contribution of the present paper, then one can see that these cells actually have *less* [ROS].

[8] assay Ψ_{IM} by assaying TMRM accumulation. And assay [ROS] by MitoSOX probe fluorescence. But they don't realize that MitoSOX, like TMRM, is also a Delocalized Lipophilic Cation (DLC). And so its accumulation in the mitochondrial matrix is dependent upon Ψ_{IM}. Indeed, to an even greater degree than TMRM:

Basic pKa (MACRO, static, T=310 K) computationally predicted from structure using MarvinSketch (ChemAxon)

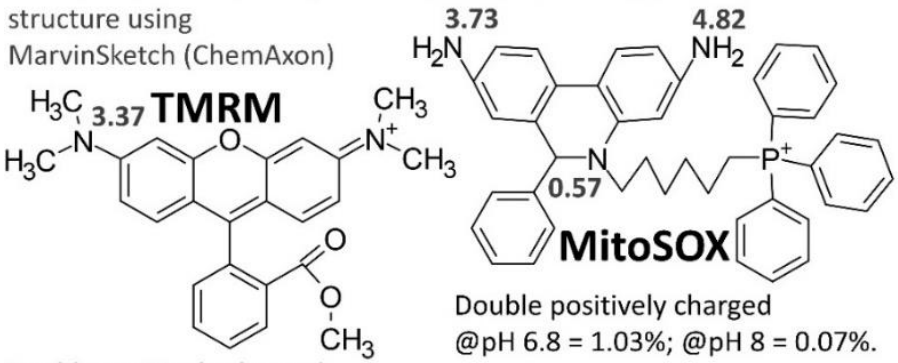

Double positively charged
@pH 6.8 = 0.04%; @pH 8 = 0%.
[matrix] = (99.96*10^(-140/-61.5))
+ (0.04*10^(-140/-46.1))
= **18,934**

Double positively charged
@pH 6.8 = 1.03%; @pH 8 = 0.07%.
[matrix] = (98.97*10^(-140/-61.5))
+ (0.96*10^(-140/-46.1))
+ (0.07*10^(-140/-30.7))
= **22,292**

Disparity between TMRM and MitoSOX accumulation in matrix increases with Ψ_{IM}

Ratio = 22,292/18,934 = 1.18 (Ψ_{IM} = -140 mV)
= 1.34 (Ψ_{IM} = -160 mV)
= 1.68 (Ψ_{IM} = -180 mV)
= 2.38 (Ψ_{IM} = -200 mV)

Nernst equation:
$$[matrix] = [IMS] \cdot 10^{\left(\frac{\Psi_{IM}}{-G}\right)}$$
G=1000*2.3026*(RT/zF);
where 1000 is a dimensionality factor to work in mV,
R = gas constant (8.31 J·mol^{-1}), T = temperature (K), z = species charge,
F = Faraday constant (96,485 C·mol^{-1}). G = 61.5 (cation), 30.7 (di-cation),
-61.5 (anion), -30.7 (di-anion) at T = 310 K = 37°C.
Use G = (61.5+30.7)/2 = 46.1 for a species that is +2 on one side,
and +1 on other side, of membrane.
matrix = mitochondrial matrix, IMS = mitochondrial intermembrane space, IM = mitochondrial inner membrane,
Ψ_{IM} = voltage across IM = -140 mV, pH of IMS = 6.8 (but might be as low as 6), pH of matrix = 8.

References for voltage across IM [14], pH of IMS [15-16], and pH of mitochondrial matrix [17]. Constraint in the User Interface (UI) of MarvinSketch meant that pH 6.8, rather than 6.88 or 6.9 [15], was used for the IMS. But pH 6.8 is within the observed range, wherein [15] reports 6.88±0.09.

Figure 4 herein, using data from [8], shows

(a) the disparity in TMRM accumulation (Ψ_{IM}) between cells that have elevated IF1 protein and those that don't; and

(b) by my calculation, the predicted disparity in MitoSOX fluorescence signal that this disparity in Ψ_{IM} should cause; and

(c) the actually observed disparity in MitoSOX fluorescence signal.

Wherein the observed is 66% less than what is predicted by the disparity in Ψ_{IM}. So, then the cells with elevated IF1 protein (and thence decreased F_1F_0 ATP hydrolysis) must have 66% lower [ROS].

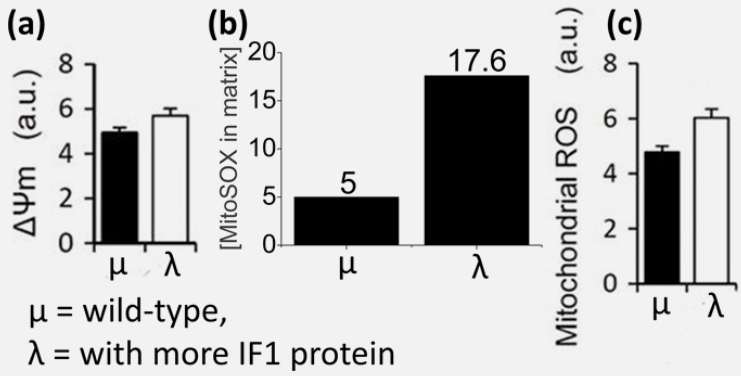

Figure 4 - Compared to wild-type mouse cells (μ), transgenic mouse cells, with more IF1 protein (λ), have a lower Reactive Oxygen Species (ROS) concentration. **(a)** Experimental data [8]: membrane potential across the inner mitochondrial membrane, Ψ_{IM} (or Ψ_M), as measured by TMRM accumulation. A typical value for Ψ_{IM} in normal mitochondria is -140 mV [14]. If we equate the 5 a.u. value for μ with -140 mV. Then the 6 a.u. value of λ is -168 mV. So, transgenic mouse cells, with more IF1 protein, have a more hyperpolarized membrane potential than wild-type cells. **(b)** Calculated data: predicted differential in MitoSOX accumulation in the mitochondrial matrix because of the different Ψ_{IM} values. **(c)** Experimental data [8]: Reported [ROS] by MitoSOX fluorescence. The MitoSOX fluorescence of transgenic mouse cells, with more IF1 protein, is 6 a.u. But wherein, because of their more hyperpolarized Ψ_{IM}, the MitoSOX fluorescence is expected to be greater than this, at 17.6 a.u. The fact that they have less MitoSOX fluorescence than this expected amount shows that they must have less [ROS]: ({17.6-6}/17.6)*100 = 66%. So, [ROS] is 66% lower in transgenic mouse cells, with more IF1 protein, than wild-type.

Some past approaches in the literature have tried to decrease [ROS] by increasing ROS mitigation [18-20]. By administering an anti-oxidant compound(s). Wherein I suggest that the potential in this ROS mitigation approach is constrained. Because when administering an anti-oxidant compound into a biological system, there are inherently so many more biological molecules (some of which are incredibly large e.g. DNA) than administered anti-oxidant molecules. That a ROS is always more likely to collide with a biological molecule, causing damage, rather than collide with an exogenously introduced anti-oxidant molecule, and be mitigated. For an exogenous anti-oxidant to efficaciously outcompete at scale, for ROS collision, with the *huge* number of biological molecules, so much anti-oxidant compound would have to be administered that toxicity is likely. Moreover, some anti-oxidants, e.g. vitamin C (ascorbic acid, ascorbate), may be pro-oxidants at higher concentrations [21] (vitamin C mitigates ROS species by reduction [electron donation]. But this means that it can also reduce Fe^{3+} to Fe^{2+}, priming the Fenton reaction to produce, from H_2O_2, arguably the worst ROS species of all, the hydroxyl radical, $^{\bullet}OH$, {Fenton reaction: $H_2O_2+Fe^{2+}\rightarrow {}^{\bullet}OH+OH^{-}+Fe^{3+}$, thereafter OH^{-} collects a proton to become H_2O}. Wherein the latter harmful action may outweigh the benefit of the former action at higher vitamin C concentrations).

In summary, ROS mitigation (even in its best case) is a very constrained, sub-optimal, approach.

By contrast, the present paper proposes a different approach to decreasing [ROS]. By decreasing ROS generation. Wherein, as observed in the data herein, **decreasing ROS generation can dramatically decrease [ROS]**.

[ROS] increases with body age [22-23]. Indeed, hair greying/whitening is reportedly because of increased [H_2O_2] (i.e. hair is bleached by the hydrogen peroxide) [24]. So, decreasing the [ROS] of an old animal, if only to the [ROS] of a young animal, is interesting. Moreover, keeping the [ROS] of a young animal at the same level throughout its life.

<u>Reinterpretation of data distinctively aligns with structural/crystallographic data</u>

[8-10] interpret increased IF1 protein amount decreasing respiration rate in mice as evidence that IF1 protein directly inhibits F_1F_0 ATP synthesis. I think this is mistaken. Newly revealed herein (*moreover in my corresponding patent applications, e.g.* [3]), in mice (especially; and in other mammals), substantial F_1F_0 ATP hydrolysis is occurring under normal conditions (e.g. refer Figure 1 herein). Hydrolysing a fraction of the synthesized ATP, meaning more

ATP needs to be synthesized. Which sets oxidative phosphorylation (OXPHOS) at high rate, to generate heat. Increased [IF1 protein] inhibits F_1F_0 ATP hydrolysis more, so less ATP needs to be made by F_1F_0 ATP synthesis, thence less OXPHOS is required, and less O_2 is consumed. So, more IF1 protein *does* decrease F_1F_0 ATP synthesis. But this is by inhibiting F_1F_0 ATP hydrolysis. *Not* by inhibiting F_1F_0 ATP synthesis. This reinterpretation, of the data of [8-10], distinctively aligns with the following (interpretation of) structural data.

ATP synthase comprises a molecular rotor that rotates one way when performing ATP synthesis. And the opposite way when performing ATP hydrolysis. A 2.1-Å crystal structure of bovine F_1-ATPase inhibited by an IF1 monomer fragment (residues 1-60 of the 84 residue long bovine IF1 protein, with 6 histidines {affinity tag for purification} added to its C-terminal end) has been interpreted (by Sir John Walker, Nobel Prize in Chemistry [1997], won for structural elucidation of ATP synthase) to suggest that IF1 can only block the rotation in one direction (that associated with ATP hydrolysis). And that IF1 is forced off by rotation in the other direction (that associated with ATP synthesis): "the reversal of rotation of the central stalk in the ATP synthase leads to the reactivation of the enzyme and the expulsion of the inhibitor protein", "IF1, the natural inhibitor protein found in mitochondria, prevents the hydrolysis, but not the synthesis of ATP by the ATP synthase" [25]. "[IF1] is a unidirectional inhibitor and does not inhibit ATP synthesis", "reversal of the direction of rotation of the rotor evidently destabilizes the interactions of IF1 with the F_1-domain of the inhibited enzyme leading to its eventual ejection from the inhibited catalytic interface" [26]. "Reversal, but not forward rotation, is prevented by an intrinsically unfolded inhibitor protein, IF1, which inserts itself in the machine and stops reverse rotation", "[IF1] inhibits the ATP hydrolytic activity of the intact mitochondrial F_1F_0-ATPase, but not its ability to synthesize ATP in the presence of a proton motive force", "IF1 is a unidirectional inhibitor of ATP hydrolysis only", "one characteristic feature of IF1 is that it is a unidirectional inhibitor of ATP hydrolysis without direct effect on ATP synthesis. "Once a proton motive force in the appropriate sense is applied to the rotor of the inhibited complex, its direction of rotation will reverse, and bound IF1 will be ejected from its inhibitory site at the $\alpha_{DP}\beta_{DP}$-catalytic interface", "IF1 is a unidirectional inhibitor of ATP hydrolysis that has no direct effect on ATP synthesis by F_1F_0-ATPase" [27].

Across different species, greater specific F_1F_0 ATP hydrolysis correlates with more mitochondrial ROS detected

This section correlates the variables listed down the left-hand-side of the table below (their data is presented in a table in the Methods section) to data from [28]. [28] consolidates superoxide ($O_2^{\bullet-}$) and H_2O_2 measurements from a number of different species, across a number of different studies. The superoxide measurements tend to be from Sub-Mitochondrial Particles (SMPs), the H_2O_2 measurements from isolated mitochondria. Herein, both these measurements can be termed "mitochondrial ROS" measurements. Utilizing the mitochondrial ROS data from [28]:

Pearson correlation coefficient (R)								
	[SUPEROXIDE] DETECTED (nmol superoxide/minute/mg of protein)							
	A	B	C	D	E	F		
Specific F1F0 ATP hydrolysis	0.7711	0.6714	0.7724	0.7815	0.7995	0.7937		
Specific basal metabolic rate	0.7489	0.9415	0.8734	0.9449	0.7904	0.7891		
Heart rate	0.8573	0.9667	0.8327	0.9241	0.786	0.779		
Maximal lifespan	-0.7362	-0.7372	-0.6732	-0.7322	-0.7114	-0.6662		
	[H2O2] DETECTED (nmol H2O2/minute/mg of protein)							
	B	C	D	G	H	I	J	K
Specific F1F0 ATP hydrolysis	0.865	0.8675	0.8226	0.712	0.7665	0.719	0.703	0.7945
Specific basal metabolic rate	0.8288	0.525	0.6127	0.5542	0.6065	0.5804	0.6945	0.6866
Heart rate	0.813	0.5486	0.627	0.5808	0.7646	0.621	0.6553	0.7057
Maximal lifespan	-0.8191	-0.7059	-0.7755	-0.7878	-0.8073	-0.8246	-0.6642	-0.7533

In the table, please note that the lower section (for H_2O_2) has a different selection of capital letter headings than the upper section (for superoxide). Because it wasn't possible to calculate columns H, I, J, K for superoxide, and columns A, E, F for H_2O_2, from the data available in [28] (or the primary papers it pulls data from). Below is a key to the table above. Within it, primary source papers are referred to as they are in Tables 1 and 2 of [28]. In this key, *n* is the number of species that overlap with the species that I have specific F_1F_0 ATP hydrolysis data for (from [29]). And thence the number of species included to generate the Pearson correlation coefficients in that particular (capital letter headed) column. The highest value of *n* is 8, wherein this consists of cow, pig, rabbit, pigeon, guinea pig, rat, hamster, and mouse. The data in [28] from "Sohal et al. 1993b" (as [28] refers to it) was excluded. Because its values are over 1,000 times different from the values of the other studies. That primary paper aside, all the other mitochondrial ROS data in [28], for species I have specific F_1F_0 ATP hydrolysis data for (from [29]), was included to make the table above. If a primary source paper's data, sourced from [28], had more than 4 species overlapping with the species I have specific F_1F_0 ATP hydrolysis data for, Pearson correlation coefficients were calculated. For primary source papers with 4 or less species of overlap, their data is only incorporated into

the means. In total, via [28], mitochondrial ROS data from 7 different primary papers is used, from 3 different organs (liver, kidney, heart), from 3 different research groups, from studies separated by up to 18 years (by publication date).

A = Liver, "Sohal et al. 1989"; n=5
B = Kidney, "Ku et al. 1993"; n=7 (n=6 for H202 assay)
C = Heart, "Ku et al. 1993"; n=7
D = mean of B and C; n=7
E = mean of A, B, C; n=7
F = mean of E and [kidney and heart, "Ku and Sohal 1993"]; n=8
G = mean of D and [kidney and heart, "Ku and Sohal 1993"]; n=8
H = Liver, "Sohal et al. 1990)"; n=6
I = mean of G and H; n=8
J = mean of I and "Lambert et al. 2007"; n=8
K = mean of J, "Herrero and Barja 1997", "Herrero and Barja 1998"; n=8

Using the mean of *all* the superoxide data, across all the used studies, is column F; using the mean of *all* the H_2O_2 data, across all the used studies, is column K. To report p-values (one-tailed, because each alternative hypothesis is directional) for these columns:

p-value (one-tailed)		
	Superoxide	H2O2
	F	K
Specific F1F0 ATP hydrolysis	0.009347	0.0092445
Specific basal metabolic rate	0.009949	0.0300005
Heart rate	0.011355	0.0252435
Maximal lifespan	0.035629	0.015467

These p-values are small, despite the small value of *n* (8) for each, in testament to the high *R* values. All these p-values are smaller than 0.05. So all are *significant*.

Reporting from the table: the greater the specific F_1F_0 ATP hydrolysis, the more mitochondrial ROS detected. The greater the specific basal metabolic rate, the more mitochondrial ROS detected. The greater the heart rate, the more mitochondrial ROS detected. The greater the maximal lifespan, the less mitochondrial ROS detected.

[28] only reports, and so the table above only uses, data from isolated mitochondria and SMPs. What is the situation in a more complete system? In whole cells respiring glucose? [30] shows that, in *ex vivo* brain slices, respiring glucose, ROS (superoxide) production increases with age. And that the gradient of this increase is steeper in shorter living species. “The rate of age-related increases of superoxide dependent chemiluminescence was inversely

related to the maximum lifespan of the animals". At least for the species they looked at. Wherein there aren't enough shared species to calculate a Pearson correlation coefficient with the data herein unfortunately. In the present study, an implemented rule is that the Pearson correlation coefficient isn't employed for any cases that there aren't at least 5 pairs (x,y) of data.

Across different species, greater specific F_1F_0 ATP hydrolysis correlates with more ROS damage detected

The following table correlates the variables listed along its top (their data is presented in a table in the Methods section) to data from [31]. Showing Pearson correlation (R) coefficients (and p-values, one-tailed because each alternative hypothesis is directional) to data from [31], which reports, from a number of different species, the urinary excretion of (probable) repair products of oxidative DNA damage: 8-oxo-7,8-dihydroguanine (8-oxoGua), 8-oxo-7,8-dihydro-2'-deoxyguanosine (8-oxodG), and 5-(hydroxymethyl)uracil (5-HMUra).

		Specific F1F0 ATP hydrolysis	Specific basal metabolic rate	Heart rate	Maximal lifespan	log10(body mass)
R	**8-OxoGua**	**0.8455**	**0.9019**	**0.9488**	**-0.972**	**-0.9889**
p		0.0169805	0.0069815	0.001933	0.002801	0.000092
R	**8-OxodG**	**0.838**	**0.9955**	**0.9626**	**-0.7675**	**-0.9289**
p		0.01862	0.000015	0.001036	0.064891	0.0037015
R	**5-HMUra**	**0.7053**	**0.9545**	**0.8704**	**-0.6204**	**-0.8665**
p		0.0587375	0.001529	0.012053	0.13209	0.012772
R	**MEAN**	**0.8223**	**0.9779**	**0.9609**	**-0.8453**	**-0.9775**
p		0.02228	0.0003635	0.001132	0.035661	0.000377
	Unit: nmol/mmol creatinine					

A rationale of [31] appears to be that bigger species have more cells. Thence these species have more DNA, and they produce more creatinine. So [31] reasons that the disparity in DNA amount can be washed out of the data by dividing its values by the amount of creatinine. With this standardization, smaller species are observed to have higher values of (probable) DNA repair products in their (per unit of) urine. Reflecting greater specific DNA repair. Presumably reflecting greater specific ROS damage of DNA. Perhaps reflecting greater specific [ROS] more directly, if these oxidized products can be produced by ROS interaction with the corresponding free substrates (guanine, deoxyguanosine, uracil), which aren't incorporated into DNA/RNA.

Oxidative damage to DNA increases with age [32-33]. In [31], the "biological age" of the individuals from the different species was constant (around 20% of maximal lifespan for each species) *except* for pig (4% of maximal lifespan). Removing pig data didn't change the direction of any of the correlations, or majorly change any of their R values (data not shown; three biggest changes in R value, upon removal of pig data, were 0.0546, 0.0402, 0.0213; without pig data, correlations to maximal lifespan couldn't be computed because of insufficient number of data points [atop of omission of human data for maximal lifespan correlations, by rationale given in the Methods section]).

In the table (most immediately) above, all the correlations to the mean of data are *significant* (p-value < 0.05).

The following table correlates the variables listed along its top (their data is presented in a table in the Methods section) to data from [34]. Showing Pearson correlation (R) coefficients (and p-values, one-tailed because each alternative hypothesis is directional) to data from [34], which reports, from a number of different species, upon the amount of a ROS damage product, 8-oxo-7,8-dihydro-2'-deoxyguanosine (8-oxodG) (standardized to the amount of deoxyguanosine, dG; per 10^5 dG), in mitochondrial DNA (mtDNA).

	8-oxodG/10^5dG in mtDNA	Specific F1F0 ATP hydrolysis	Specific basal metabolic rate	Heart rate	Maximal lifespan	log10(body mass)
R	**Brain**	**0.885**	**0.8837**	**0.9246**	**-0.7369**	**0.7531**
p		0.022999	0.0233855	0.012286	0.07772	0.070845
R	**Heart**	**0.7335**	**0.9509**	**0.9642**	**-0.7438**	**-0.9575**
p		0.030316	0.0004995	0.000229	0.02764	0.0003495
R	**MEAN**	**0.8212**	**0.9738**	**0.9867**	**-0.8533**	**-0.9157**
p		0.044142	0.0025355	0.000919	0.03297	0.0145035

The mean only includes species for which *both* brain and heart data is in the data set. Data was extracted from graphs in [34] using WebPlotDigitizer, https://apps.automeris.io/wpd/. [34] optimized more for a constant chronological, rather than "biological", age. All the individuals, from the different species, were around one to two years old: "the mean age of the animals was 8 months (mice), 11 months (rat), 1.4 years (guinea pig), 1.5 years (rabbit), 1 year (pig), and 1.5–2.5 years (sheep, cow, and horse)" [34].

In the table (most immediately) above, all the correlations to the mean of data are *significant* (p-value < 0.05).

The following table correlates the variables listed along its top (their data is presented in a table in the Methods section) to data from [35]. Showing Pearson correlation (R) coefficients (and p-values, one-tailed because each alternative hypothesis is directional) to data from [35], which reports, from a number of different species, upon the amount of a ROS damage product, malondialdehyde (MDA), formed by lipid peroxidation.

		Specific F1F0 ATP hydrolysis	Specific basal metabolic rate	Heart rate	Maximal lifespan	log10(body mass)
R	**LP**	**0.8976**	**0.9221**	**0.909**	**-0.8075**	**-0.8191**
p		0.0030475	0.001559	0.002283	0.01403	0.0120945
	LP = *in vivo* Lipid Peroxidation (mmol MDA/g tissue)					

Data was extracted from Fig. 5 in [35] using (aforementioned) WebPlotDigitizer. "All animals used were young adults with an age within 15–30% of their MLSP" [35], wherein MLSP is maximum lifespan.

In the table (most immediately) above, all the correlations are *significant* (p-value < 0.05).

<u>Numerical prediction observed</u>

Kleiber's law is that an animal's basal metabolic rate scales to $M^{0.75}$, where M is the animal's mass [36-37]. Thence an animal's specific basal metabolic rate scales to $M^{0.75}/M = M^{-0.25}$. Therefore the log-log plot of body mass (x-axis), and specific basal metabolic rate (y-axis), has a gradient of -0.25. Indeed, this is observed in the 2nd panel of Figure 2 herein (refer to the corresponding table of its best fit line equations). Moreover, its 3rd and 4th panels also conform to "quarter-power scaling". In which its heart rate and maximal lifespan data both scale to body mass with the same exponents as (is typical) in the literature. $M^{-0.25}$ and $M^{0.25}$ respectively [38-39]. However, in Figure 2 herein, it is notable that specific F_1F_0 ATP hydrolysis, which I suggest is a drive to specific basal metabolic rate (which scales to $M^{-0.25}$), does *not* have the -0.25 exponent itself. Its exponent is instead -0.13213 (±0.03077). This suggests that something might be missing. Specific F_1F_0 ATP hydrolysis data in prior figures, e.g. in Figure 2, is actually from Sub-Mitochondrial Particles [SMPs] (data from [29]). In which all the intricate internal structure of mitochondria is lost. I suggest that this is what is missing in the exponent. In intact mitochondria, across different species, [40] reports that [mitochondrial inner membrane surface area/mitochondrial matrix volume] ($cm^2/\mu l$) scales to $M^{-0.102}$.

Selecting data from [40], for species that I have specific F_1F_0 ATP hydrolysis data for (from SMPs, from [29]), the product, *g*, of [specific F_1F_0 ATP hydrolysis (from SMPs)], multiplied by [mitochondrial inner membrane surface area/mitochondrial matrix volume], scales to **precisely** $M^{-0.25}$. As shown in Figure 5.

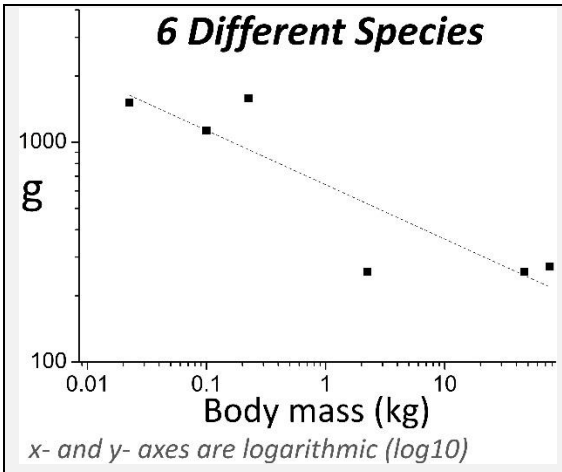

Figure 5 - On the y-axis, *g* is

$$g = h \cdot (s/v)$$

wherein *h* is specific F_1F_0 ATP hydrolysis in Sub-Mitochondrial Particles [SMPs] (µmol/min/mg; mg is of mitochondrial protein), *s* is mitochondrial inner membrane surface area (cm^2), *v* is mitochondrial matrix volume (µl). Data for *h* is from [29] (and has been used in prior figures herein, e.g. Figure 2). Data for *s* and *v* is from [40]. In this figure, each species' body mass value is the mean of pooled body mass values, for the particular species, from [29] and [40].

Across species, *g* decreases with body mass (M), with an **exponent of -0.25**.

The best fit line in Figure 5 is:

$\log_{10}(y) = \log_{10}(a) + b \cdot \log_{10}(x)$, where *b* is gradient:

$\log_{10}(a)$	*b*	Adjusted R^2
2.80659 (±0.08226)	-0.24725 (±0.06192) ≈ ***-0.25***	0.74928

Pearson correlation coefficient (R), and its p-value (one-tailed, because the alternative hypothesis is directional), for the log-log data of Figure 5:

		$\log_{10}(g)$

R	$\log_{10}$(body mass)	-0.8941
p		0.0081

I suggest that *g*, defined in the Figure 5 legend, can be (abstractly) interpreted as being specific F_1F_0 ATP hydrolysis in mitochondria (μmol/min/mg·cm^2/μl). So, whereas *h* is specific F_1F_0 ATP hydrolysis in Sub-Mitochondrial Particles [SMPs] *in vitro*. *g* is (interpreted to correspond to) specific F_1F_0 ATP hydrolysis in intact mitochondria *in vivo*. Wherein *g* and *h* are interrelated by the equation in the legend of Figure 5. However, I don't force this interpretation. And so herein, I refer to *g* as merely *g*. Rather than as specific F_1F_0 ATP hydrolysis in mitochondria. *h* can be interpreted as being the inverse of IF1 protein activity (IF1 protein inhibits F_1F_0 ATP hydrolysis).

More mitochondrial inner membrane surface area, per mitochondrial matrix volume, is to say the mitochondrial inner membrane has more and/or larger invaginations (cristae). Sacrificing mitochondrial matrix volume for greater mitochondrial inner membrane surface area. This greater surface area of the mitochondrial inner membrane means there is more proton leak across it. Furthermore, cristae locally increase proton concentration on the intermembrane side of the mitochondrial inner membrane, which increases the Ohmic (or supra-Ohmic) drive for proton leak, wherein more and/or bigger cristae increases this more. A cristae is bigger by longer protrusion into the mitochondrial matrix.

As aforementioned, Figure 5 shows that specific F_1F_0 ATP hydrolysis combines with mitochondrial inner membrane surface area (per mitochondrial matrix volume) to confer, *precisely*, the expected -0.25 exponent. That this relation is because of proton leak is suggested by specific F_1F_0 ATP hydrolysis combining with the rate of proton leak to confer, within the margin of slope error, a -0.25 exponent also. As shown in Figure 6.
In overlapping support, [40] uses data from more species than are represented in Figure 6, and finds body mass and proton leak related with an exponent of -0.129 (±0.049). Which, when added to the aforementioned exponent relating body mass and specific F_1F_0 ATP hydrolysis (-0.13213±0.03077), yields an exponent of -0.26, with -0.25 within its margin of error.

Pearson correlation coefficient (R), and its p-value (one-tailed, because the alternative hypothesis is directional), between rate of proton leak ([nmol of H^+]/min/mg protein) across the inner mitochondrial membrane {when the membrane potential across it is -170 mV, with ATP synthase blocked by oligomycin} (l), and (s/v), where s is mitochondrial inner membrane surface area (cm^2), and v is mitochondrial matrix volume (µl): data from [40]:

		(s/v)
R	l	0.861
p		0.014

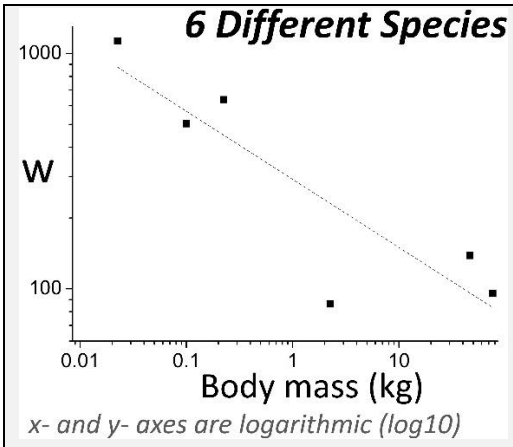

Figure 6 - On the y-axis, w is

$$w = h \cdot l$$

wherein h is specific F_1F_0 ATP hydrolysis in Sub-Mitochondrial Particles [SMPs] (µmol/min/mg; mg is of mitochondrial protein), l is proton leak rate across the inner mitochondrial membrane, when the membrane potential across it is -170 mV, and ATP synthase is blocked by oligomycin ([nmol of H^+]/min/mg protein). Data for h is from [29] (and has been used in prior figures herein, e.g. Figure 2). Data for l is from [40]. In this figure, each species' body mass value is the mean of pooled body mass values, for the particular species, from [29] and [40].

Across species, w decreases with body mass (M), with (within the margin of slope error) an exponent of -0.25.

The best fit line in Figure 6 is:

$\log_{10}(y) = \log_{10}(a) + b \cdot \log_{10}(x)$, where b is gradient:

$\log_{10}(a)$	b	Adjusted R^2

2.46545 (±0.10233)	-0.28943 (±0.07704) ≈ *-0.25*	0.72399

Pearson correlation coefficient (R), and its p-value (one-tailed, because the alternative hypothesis is directional), for the log-log data of Figure 6:

		$\log_{10}$(w)
R	$\log_{10}$(body mass)	-0.8827
p		0.0099

Pearson correlation coefficients (R), and their p-values (one-tailed, because each alternative hypothesis is directional), between *h, g* and *w* (variables as defined in the legends of Figures 5 and 6):

		g	*w*
R	*h*	0.8323	0.6779
p		0.020	0.069
R		*g*	0.9036
p			0.0067

Pearson correlation (R) coefficients, and their p-values (one-tailed, because each alternative hypothesis is directional):

		Specific basal metabolic rate	Heart rate	Maximal lifespan
R	***h***	**0.7016**	**0.8007**	**-0.7192**
p		0.0054965	0.000877	0.006307
R	***g***	**0.8816**	**0.9466**	**-0.7942**
p		0.010099	0.002101	0.029586
R	***w***	**0.9691**	**0.9442**	**-0.6952**
p		0.0007085	0.002292	0.062598

The correlations with *h*, where *h* is specific F_1F_0 ATP hydrolysis (from [29]), are as presented in an earlier table. Its correlations are calculated with more species, and so a higher value of *n*, than the correlations to *g* and *w*. And thence its correlations have a smaller p-value for any given value of R.

Looking at R values only, the correlations of *g* are superior to those of *h*. Those of *w* are superior to those of *g*. Except for the correlation to maximal lifespan.
When *h* is correlated to the same, smaller data set as *g* and *w*, its correlation to maximal lifespan doesn't worsen but improves (-0.7842), and its correlation to specific basal metabolic rate and heart rate is 0.7318 and 0.7706 respectively.

Comparing the table below, to the table most immediately above, one can see that the correlations of each of *g* and *w*, are *much* superior to those of (*s*/*v*) and *l* (variables as defined in legends of Figures 5 and 6). To specific basal metabolic rate, heart rate, and maximal lifespan (data for these variables is presented in a table in the Methods section). R is the Pearson correlation coefficient and p-values are one-tailed, because each alternative hypothesis is directional. Incidentally, proton leak, *l*, negatively correlates with maximal lifespan (at least across species, for these species). Although not significantly so.

		h	Specific basal metabolic rate	Heart rate	Maximal lifespan
(*s* /*v*)	R	0.4445	0.7588	0.8193	-0.5301
	p	0.188581	0.040125	0.023015	0.1396655
l	R	0.4159	0.8794	0.8283	-0.496
	p	0.20606	0.01047	0.020845	0.158506

Considered in totality, the data of this present Results section (encompassing Figures 5 and 6) suggests that it might be the combination of F_1F_0 ATP hydrolysis ***and*** proton leak, which sets specific basal metabolic rate (setting heart rate), which dictates maximal lifespan.

Why might F_1F_0 ATP hydrolysis, and proton leak, *both* be important?
Oxidative phosphorylation synthesizes ATP. F_1F_0 ATP hydrolysis hydrolyses a fraction of this ATP. At a level constrained by IF1 protein activity. Wherein smaller, shorter living species have less specific IF1 protein activity. This F_1F_0 ATP hydrolysis pumps protons out of the mitochondrial matrix, across the inner mitochondrial membrane, into the mitochondrial intermembrane space. A fraction of these protons return to the mitochondrial matrix via proton leak. Wherein smaller, shorter living species have greater proton leak because of a greater mitochondrial inner membrane surface area (per volume of mitochondrial matrix). And because of their greater rate of F_1F_0 ATP hydrolysis, pumping more protons per unit time into the mitochondrial intermembrane space. A fraction of the ATP synthase proton conduits in the mitochondrial inner membrane, actively pumping protons energetically "uphill", instead of passing protons energetically "downhill", can explain how so much proton leak can

occur. Why so many protons cross the mitochondrial inner membrane at a point of higher resistance. Dissipating their potential energy as heat. Rather than just passing through the lower resistance conduit, ATP synthase, which can capture (a fraction of) their potential energy loss in the chemical energy of ATP. *{But these ATP synthase complexes are available for "forward", proton passing, ATP synthesizing (instead of "reverse", ATP consuming, proton pumping) action if cellular ATP demand increases}*.

This proton leaking is especially pronounced when there is particularly high [ATP] in the mitochondrial matrix, which happens when cellular energy demand is low. Elegantly, when the cell is hydrolysing much ATP to perform much useful work, inherently generating heat as a by-product (2nd Law of Thermodynamics), [ATP] in the mitochondrial matrix is lower and F_1F_0 ATP hydrolysis, and proton leak, is lower. But when the cell isn't performing much work, [ATP] in the mitochondrial matrix is higher and so F_1F_0 ATP hydrolysis, and proton leak, is higher. Which generates heat to keep the body at 37°C. So, when useful work can generate heat, the spurious processes are less. But when not, they are more. For emphasis, this is recast in the next paragraph.

When the body is resting and so isn't performing much work, F_1F_0 ATP hydrolysis (and its drive to F_1F_0 ATP synthesis and metabolic rate) confers endogenous heat production. But when the body is active and performing appreciable work, ATP is consumed to do this work (inherently generating heat as a by-product, 2nd Law of Thermodynamics), and so there is less ATP available to F_1F_0 ATP hydrolysis, which is reduced as a result. So when performing work, which inherently generates heat, the futile (no work) process to generate heat is decreased, affording more energy to actually perform work, and reducing the chance that the body will overheat. So, in the resting state, heat generation is (fractionally) by a futile process, until more work is required, after which the heat generation by the actual performing of work substitutes for a reduction in heat generation by the futile process. Elegant.

Quarter-power scaling

It is interesting to contemplate that the observed quarter-power scaling, between novel variable, *w*, and body mass, might be the fundamental drive to the quarter-power scaling observed (e.g. in Figure 2 herein) between body mass and each of specific basal metabolic rate (-0.25), heart rate (-0.25), and maximal lifespan (+0.25). Indeed, the basis might be at the cellular or sub-cellular level because the specific metabolic rate of liver slices, sourced from

different sized species, adheres to quarter-power scaling (-0.25) *in vitro* [41]. Curiously, *w* has a geometric component, via its proton leak rate, which is a function of inner mitochondrial membrane surface area, which is a *non-Euclidean* shape. Because of its invaginations (sacrifices some volume for greater surface area). A longstanding mystery is why, across species, where M is adult body mass, basal metabolic rate scales with $M^{0.75}$ (Kleiber's law), instead of $M^{0.67}$, which is what is expected on the basis of how surface area scales with volume for a *Euclidean* object [38]. "One cannot but wonder why the power formula, in general, and the mass exponents of 3/4, 1/4 and -1/4, in particular, are so effective in describing biological phenomenon" [38].

Equation for maximal lifespan in terms of specific F_1F_0 ATP hydrolysis

Recasting afore-presented experimental data, Figure 7 shows (across different species) specific F_1F_0 ATP hydrolysis, specific basal metabolic rate, and heart rate for different values of maximal lifespan.

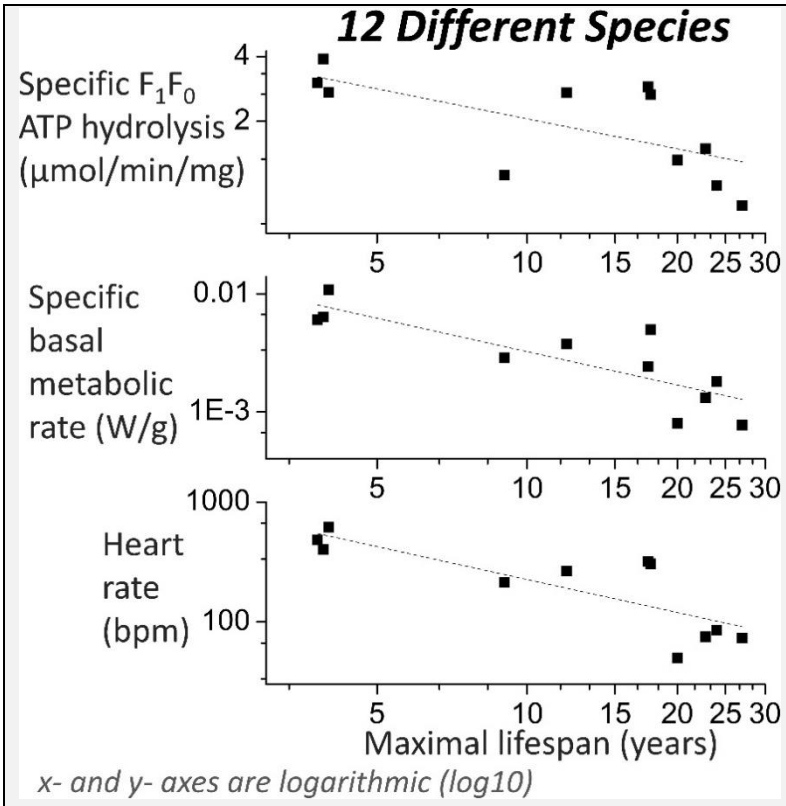

Figure 7 - Across different species, specific F_1F_0 ATP hydrolysis, specific basal metabolic rate, and heart rate for different values of maximal lifespan.

Shown best fit lines in Figure 7 are of the form:

$\log_{10}(y) = \log_{10}(a) + b \cdot \log_{10}(x)$, where b is gradient:

	$\log_{10}(a)$	b	Adjusted R^2
1st panel	0.77685 (±0.19253)	-0.46465 (±0.17242)	0.3851
2nd panel	-1.5502 (±0.22922)	-0.93884 (±0.20528)	0.66575
3rd panel	3.26704 (±0.247)	-0.91411 (±0.2212)	0.61654

Rearranging the plot equation from the 1st panel in Figure 7, gives an equation for maximal lifespan (*years*), x, in terms of specific F_1F_0 ATP hydrolysis (*μmol/min/mg*), y:

$$x = 10^{(\{\log_{10}(y) - 0.77685\}/-0.46465)}$$

Mediation analysis

I performed mediation analysis, summarized in Figure 8, in the JASP software (version 0.14.1; https://jasp-stats.org/; developed by a team at the University of Amsterdam; it runs atop of R {https://www.r-project.org/}). Selecting a bootstrap method. Called "Percentile" in JASP, which corresponds to "Percentile bootstrap (PC)" in [42]. Run with 10,000 replications (ten times greater than the default number of replications = 1,000). Note that for the data inputted, I multiplied all the specific basal metabolic rate values by 10,000 (rescaled this variable) to prevent "numerical underflow" in the underlying computations performed by lavaan [43], an R package for Structural Equation Modelling [SEM], which JASP runs for SEM (mediation analysis). Such re-scaling of an input variable(s) for SEM is a good and common practice. Because it is preferable for the different input variables to have a similar order of scale. And it is absolutely needed in this case because the variable with very small numbers (specific basal metabolic rate in W/g) causes even smaller numbers to occur in the internal computations (e.g. in the computations/manipulations of variances, covariances, Hessian, gradients etc.). Causing "numerical underflow". An alternative method to prevent this "numerical underflow" is to select the option of "Standardized estimates" in JASP. To standardize (mean = 0, standard deviation = 1) all the variables before estimation. But this method is arguably inferior. Because it is manipulating each variable with a quantity, the standard deviation, which is *estimated*, with an error. Instead of manipulating a single variable with a constant, which is *precisely known* (10,000). Regardless, the results from this alternative method, utilizing "Standardized estimates", are presented at the end of this section. From which the same conclusions are drawn.

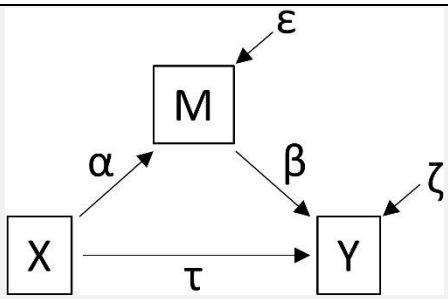

Figure 8 - An indirect effect (mediation) exists when an independent variable (X) acts upon a dependent variable (Y) through an intervening/mediating variable (M). Represented by two regression equations [42]:

$$M = b_M + (\alpha \cdot X) + \varepsilon$$

$$Y = b_Y + (\beta \cdot M) + (\tau \cdot X) + \zeta$$

b_M and b_Y are regression intercepts. ε and ζ are random disturbance terms. α, β and τ are regression coefficients.

Indirect effect (*effect of X upon Y, via M*) = **α·β**.

Direct effect = τ.

Total effect (*of X upon Y*) = (α·β) + τ.

For the table below, (*with the data of these variables as presented in a table in the Methods section*), *X* is specific F_1F_0 ATP hydrolysis, *M* is specific basal metabolic rate (*10,000), and *Y* is maximal lifespan.

			95% Confidence Interval (CI)	
α	β	**Indirect effect (α·β)**	Lower	Upper
20	-0.17	-3.452	-9.512	-1.201
		Direct effect (τ)	Lower	Upper
		-2.554	-6.266	4.124

Evidence for an effect is when zero (0) is not within the range of the 95% confidence interval. The data in the table suggests that there is no direct effect between specific F_1F_0 ATP hydrolysis and maximal lifespan. That the effect of specific F_1F_0 ATP hydrolysis upon maximal lifespan is solely indirect, via specific basal metabolic rate.

Figure 9 presents the proposed model of mediation. Mediation data supporting its [specific F_1F_0 ATP hydrolysis → specific basal metabolic rate → maximal lifespan] arm has already

been presented. Mediation data supporting its [specific F_1F_0 ATP hydrolysis → specific basal metabolic rate → heart rate] arm is below. (*With the data of these variables as presented in a table in the Methods section*), where *X* is specific F_1F_0 ATP hydrolysis, *M* is specific basal metabolic rate (*10,000), and *Y* is heart rate.

			95% Confidence Interval (CI)	
α	β	**Indirect effect (α·β)**	Lower	Upper
20	4.6	94.363	22.578	191.3
		Direct effect (τ)	Lower	Upper
		48.372	-35.584	109.96

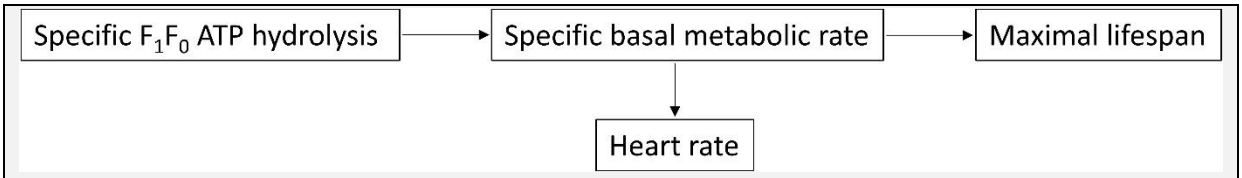

Figure 9 - Mediation model. Supported by the mediation analysis herein. In this model, specific F_1F_0 ATP hydrolysis sets heart rate, and maximal lifespan, via setting specific basal metabolic rate.

The mediation analysis, when instead using "Standardized estimates", is presented in the table below. In this case, the specific basal metabolic rate values are *not* multiplied by 10,000. For each arm of the mediation model (afore-presented in Figure 9): as before, there is no zero (0) within the 95% confidence interval for the indirect effect. But there is for the direct effect. Indicating that, for each arm, there *is* an indirect effect (via the Mediator variable [specific basal metabolic rate]), and *no* direct effect. This corresponds with the mediation analysis results presented earlier. Further supporting the mediation model of Figure 9.

			95% Confidence Interval (CI)				
Specific F1F0 ATP hydrolysis → Specific basal metabolic rate → Maximal lifespan							
α	β	Indirect effect (α·β)	Lower	Upper			
0.66	-0.61	-0.402	-1.096	-0.137			
		Direct effect (τ)	Lower	Upper			
		-0.297	-0.759	0.485			
Specific F1F0 ATP hydrolysis → Specific basal metabolic rate → Heart rate							
α	β	Indirect effect (α·β)	Lower	Upper			
0.66	0.76	0.506	0.12	1.007			
		Direct effect (τ)	Lower	Upper			
		0.259	-0.186	0.589			

Interventional evidence for causality in the mediation model

Mediation analysis in the previous section showed that the data is consistent with a model in which specific F_1F_0 ATP hydrolysis dictates maximal lifespan, via dictating specific basal metabolic rate. Specific F_1F_0 ATP hydrolysis → specific basal metabolic rate → maximal lifespan.

Evidence for causality between specific F_1F_0 ATP hydrolysis and specific basal metabolic rate is that an interventional decrease in F_1F_0 ATP hydrolysis causes a decrease in metabolic rate (O_2 consumption). As presented herein, in the earlier Results section components titled "Local inhibition of F_1F_0 ATP hydrolysis" and "Inhibiting F_1F_0 ATP hydrolysis decreases [ROS]". For example, to quote therefrom: "extra IF1 protein decreased F_1F_0 ATP hydrolysis by 40% and decreased State 3 respiration rate by 44%". Moreover, in the "New experimental results" section earlier herein, drug inhibiting F_1F_0 ATP hydrolysis decreased metabolic heat generation, causing body temperature drop in mice (*when* body > ambient temperature). In Figure 1.

Evidence for causality between specific basal metabolic rate and maximum lifespan is that a decrease in metabolic rate can extend lifespan. As presented in the work of [44-45], where mice with lower metabolic heat generation (consuming less O_2/kg/hour than control mice), and lower body temperature (0.3 to 0.5°C reduction), have an extended lifespan (increased median lifespan, by 12% in males, and 20% in females). This lower metabolic rate was conferred by overexpressing uncoupling protein UCP2 in hypcretin neurons of their hypothalamus. Selectively making this brain region hotter, fooling it into thinking the rest of the body is warmer than it is, so that it directs less heat generation.

Future

However, although there is the aforementioned interventional evidence for causality between (*i*) specific F_1F_0 ATP hydrolysis and specific metabolic rate, and (*ii*) between specific metabolic rate and lifespan. Plain, rather than interpolated, interventional evidence for causality between specific F_1F_0 ATP hydrolysis and lifespan is absent. At least to date. A future aim is a mouse lifespan (or surrogate endpoint/biomarker [46]) study. With the mice administered a F_1F_0 ATP hydrolysis inhibiting drug, e.g. from my US patent application [3].

New experimental results

Anti-cancer

Figures 10 and 11 show results from the NCI-60 one-dose *in vitro* assay. Performed by the National Cancer Institute (NCI, USA). With compounds I submitted. This protocol tests the effect, if any, of a single test compound (10 µM) on the growth/survivability of 60 different cancer cell lines, originated from 9 different tissues, as compared to the no compound control [47]. A tested compound's activity can range from negative % (cancer growth promotion), to 0% (no activity), to 100% (complete cancer growth inhibition), to 200% (all starting cancer cells are dead). NCI-60 tests are performed at a controlled temperature of 37°C. For 48 hours.

More specifically, Figures 10 and 11 show that compounds which potently inhibit F_1F_0 ATP hydrolysis exert potent anti-cancer activity. Figure 10 shows the *in vitro* anti-cancer activity of separated stereoisomers 6a and 6b. Figure 10A shows their structure. 6a is the *R* stereoisomer in high enantiomeric excess (>97% ee). 6b is the *S* stereoisomer in high enantiomeric excess (>97% ee; administered to mice in Figure 1). Figure 10B shows the anti-cancer activity of 6a (10 µM). Figure 10C shows the anti-cancer activity of 6b (10 µM). As specified in Figure 10A, 6b potently inhibits F_1F_0 ATP hydrolysis (EC_{50} F_1F_0 ATP hydrolysis = 0.018 µM in a Sub-Mitochondrial Particle {SMP} assay [3]). Whilst 6a does not (EC_{50} F_1F_0 ATP hydrolysis > 100 µM in the SMP assay [3]). In other words, the *S* stereoisomer potently inhibits F_1F_0 ATP hydrolysis, and the *R* stereoisomer does not. But the anti-cancer activity of 6a and 6b is similar in Figures 10B and 10C. Because, to interpret, they both undergo racemization in a biological system. Which erodes their enantiomeric excess during the 48 hours duration of the NCI-60 anti-cancer tests. So, they both converge towards/upon being the racemate, 19a (EC_{50} F_1F_0 ATP hydrolysis = 0.033 µM in the SMP assay [3], Figure 10A). Such that both samples ultimately contain a substantial proportion of *S* stereoisomer. And so both exert anti-cancer activity by inhibiting F_1F_0 ATP hydrolysis. But racemization is not instantaneous, and so the 6b sample confers greater *S* stereoisomer exposure ("area under the curve") to the cancer cells than the 6a sample. And thence confers greater anti-cancer activity: 66% vs. 57% mean (67% vs. 59% median) cancer growth inhibition, across all 60 cancer cell lines.

Observable in aforementioned Figure 10a, opposite stereoisomers, 6a and 6b, have hydrogen on their chiral carbon. Figure 11 discloses the anti-cancer activity of stereoisomers 7a and 7b. These have the same structure as 6a and 6b, except that they have deuterium (enrichment) instead of hydrogen on their chiral carbon (>99% molar percent deuterium incorporation at

their chiral carbon). Their structure is shown in Figure 11A. 7a is the *R* stereoisomer in high enantiomeric excess (>97% ee). 7b is the *S* stereoisomer in high enantiomeric excess (>97% ee). Figure 11B shows the anti-cancer activity of 7a (10 µM). Figure 11C shows the anti-cancer activity of 7b (10 µM). This anti-cancer data is also from the National Cancer Institute's standardized NCI-60 testing protocol. So, directly comparable to the aforementioned anti-cancer data for 6a and 6b. To summarize all the NCI-60 data, the mean and median % cancer growth inhibition conferred (by 10 µM) is shown in the table below:

	6a	6b	(6b-6a)	7a	7b	(7b-7a)	(7b-7a)/(6b-6a)
Mean	57.3	66.15	8.85	52.35	72.81	20.46	2.3
Median	58.62	66.9	8.28	52.09	74.51	22.42	2.7

7b exerts greater anti-cancer activity than 6b. 7a exerts less anti-cancer activity than 6a. Thence the difference between the anti-cancer activity of 7b and 7a is greater than that between 6b and 6a. To interpret, this is because, whereas 6a and 6b have hydrogen (H) attached to the chiral carbon, 7a and 7b have deuterium (D, ^{2}H) attached to the chiral carbon. Deuterium slows the racemization rate by a Kinetic Isotope Effect (KIE [48]; C-^{2}H bond is stronger than a C-H bond). So, because of a slower racemization rate, 7b maintains its enantiomeric excess (of *S*) better than 6b. Conferring 7b greater anti-cancer activity than 6b. Because of a slower racemization rate, 7a maintains its enantiomeric excess (of *R*) better than 6a. Conferring 7a less anti-cancer activity than 6a. The disparity in anti-cancer activity between 7b and 7a is 2-3 times greater than that between 6b and 6a. Which is the correct order of magnitude for a KIE (>1 and ≤10 [49], greater if tunnelling is very mechanistically relevant [50]).

If the *S* stereoisomer has anti-cancer activity, and the *R* stereoisomer does not, hypothesizing their enantiomerization in a biological system, the mean of 6a and 6b anti-cancer activity should equal the anti-cancer activity of the 6a/6b racemate. If this racemate was tested. Similarly, the mean of 7a and 7b anti-cancer activity should equal the anti-cancer activity of the 7a/7b racemate. If this racemate was tested. Supportively, the mean of 6a and 6b median anti-cancer activity is equal to the mean of 7a and 7b median anti-cancer activity: numbers below are drawn from the earlier table:

{(58.62+66.9)/2} = 62.76 = 63%, ≈ {(52.09+74.51)/2} = 63.3 = 63%

(*The mean of 6a and 6b mean anti-cancer activity is nearly equal to the mean of 7a and 7b mean anti-cancer activity: {(57.3+66.15)/2} = 61.73 = 62%, ≈ {(52.35+72.81)/2} = 62.58 = 63%*).

The following features of the data have already been herein addressed/explained, wherein each following sample name refers to the median of its anti-cancer activity (sourced from earlier table): (7a+7b)/2=(6a+6b)/2, 7b>7a, 6b>6a, 7b>6b, 7a<6a. In NCI-60 compound testing, anti-cancer activity can range from 0% (no activity) to 100% (complete cancer growth inhibition) to 200% (all starting cancer cells are dead). So, the possible range is 0-200% (*if* the assumption is made that no administered compound will promote cancer growth, and so *if* the possibility of increased cancer growth upon compound administration is dismissed). To do some supporting theoretical analysis, using A, B, C, D, wherein each of these letters can independently be any integer in the range 0-200, the chance, by chance, of all of the following being true at the same time: (A+B)/2=(C+D)/2 (equivalently A+B=C+D), A>B, C>D, A>C, B<D, is 0.04% (125 times smaller than 5%, the most common significance threshold used by those of the art; its corresponding decimal p-value is 0.0004, which is <0.05). If A, B, C, D can be fractional also, and not only integers, the chance is even smaller, much smaller (not shown). The chance, by chance, of all of the following being true at the same time (delimited to integers): (A+B)/2=(C+D)/2=63, A>B, C>D, A>C, B<D, is 0.00025% (corresponding decimal p-value is 0.0000025, which is <0.05).

The anti-cancer activity of 6a, 6b, 7a, 7b are all highly correlated (in the table below, p-values are one-tailed because each alternative hypothesis is directional). Because they tend to have greater, or lesser, anti-cancer activity against the same of the 60 cancer cell lines. This, by the rationale/basis of [51], indicates that they are exerting anti-cancer activity by the same molecular mechanism. Indeed, to interpret the data herein, by selectively inhibiting F_1F_0 ATP hydrolysis.

Pearson Correlation Coefficient (R):					
	6a	6b	7a	7b	
6a	1				
6b	0.7991	1			
7a	0.7693	0.5205	1		
7b	0.6614	0.6451	0.8049	1	
N=60 for all samples; P-value (one-tailed):					
	6a	6b	7a	7b	
6a	/				
6b	9.85E-15	/			
7a	3.48E-13	1.01E-05	/		
7b	4.39E-09	1.32E-08	4.60E-15	/	
Fisher's combined probability test					
Using p-values for [6a vs. 7a] and [6b vs. 7b]					
			3.48E-13	1.32E-08	
p-value = **2.20E-19** = 0.0000000000000000002					

So, Figures 10 and 11 show that compounds which potently inhibit F_1F_0 ATP hydrolysis exert potent anti-cancer activity. I predicted this result before it was observed. By rational design. Because I reasoned that the abnormally glycolytic metabolism of cancers (Warburg effect [52]), especially used by the most dangerous thereof [53-57], hinges upon abnormally high rates of F_1F_0 ATP hydrolysis. Consuming glycolytic ATP (imported into mitochondria by the Adenine Nucleotide Transporter, driven by higher [ATP], and lower [ADP], in the cytoplasm than in the mitochondrial matrix). Releasing glycolysis from ATP negative feedback inhibition (ATP allosterically exerts negative feedback inhibition upon the glycolytic enzymes phosphofructokinase and pyruvate kinase [58]). Yielding higher glycolytic rate. Thence more glycolytic intermediates are available to be shunted into biosynthesis (enabling faster cancer cell proliferation). And conferring more NADPH produced by the pentose phosphate pathway, enabling more Reactive Oxygen Species (ROS) mitigation. By the NADPH dependent glutathione, and NADPH dependent thioredoxin, ROS mitigation systems. And less ROS are produced because oxidative phosphorylation {OXPHOS} is disfavoured by the high proton motive force (pmf, comprising high {more hyperpolarized} Ψ_{IM} [59]) across the mitochondrial inner membrane created by F_1F_0 ATP hydrolysis. So, [ROS] is lower. Enabling enduring information fidelity of DNA and thereby "limitless replicative potential" (i.e. immortality, which is distinctive trait of cancer [60], which normal somatic cells don't share; {I propose} mutational load of cancer primarily acquired before, on the path to, cancer). A F_1F_0 ATP hydrolysis inhibiting drug inhibits this cancer metabolic

program, conferring anti-cancer activity. Whilst (prospectively) helping, instead of harming, normal cells *in vivo*. Increasing their metabolic efficiency, so less chemical energy of food is dissipated as heat (Figure 1). Thereby (*if* the ambient temperature, and/or bodily insulation, substitutes for lower metabolic heat production) possibly combating cachexia/wasting. Which is observed in many advanced/terminal cancer patients, and is often the cause of their death [61]. Moreover, *in vivo*, to hypothesize, cachexia/wasting might be additionally combated by the compound conferred decrease in glycolytic rate of cancer cells. Decreasing their glucose influx and lactate efflux. Thence decreasing the energetically expensive conversion of lactate to glucose by the Cori cycle of the liver. Which costs 6 ATP for every lactate to glucose converted [58]. Elevated blood [lactate] correlates with worse cancer prognosis [62]. In this way, the anti-cancer benefit *in vivo* is expected to be greater than that shown herein *in vitro*. Especially in the case of cancer cells in a solid (hypoxic/anoxic) tumour, which might singly rely upon F_1F_0 ATP hydrolysis to maintain pmf (Ψ_{IM}). Where loss of Ψ_{IM} is a well-known trigger for apoptosis [63]. The *in vitro* studies herein cannot report this (hypothesized) effect because they are conducted at atmospheric pO_2 (at the elevation of the National Cancer Institute in Maryland, USA). Tumour hypoxia correlates with poor patient prognosis [64-69]. Tumour hypoxia is associated with radio- [70-71] and chemo- [72-73] resistant cancer.

In further supporting data, I've shown anti-cancer activity, in NCI-60 testing, by other compounds, of completely different scaffolds, which also selectively inhibit F_1F_0 ATP hydrolysis. For example, please see the 45 pages of experimental data in my US patent application [3] (*following my earlier application* [74]). My work, predominantly in the patent (rather than scholarly) literature, reports a new molecular target for exerting anti-cancer activity. F_1F_0 ATP hydrolysis. And novel drugs acting upon that target.

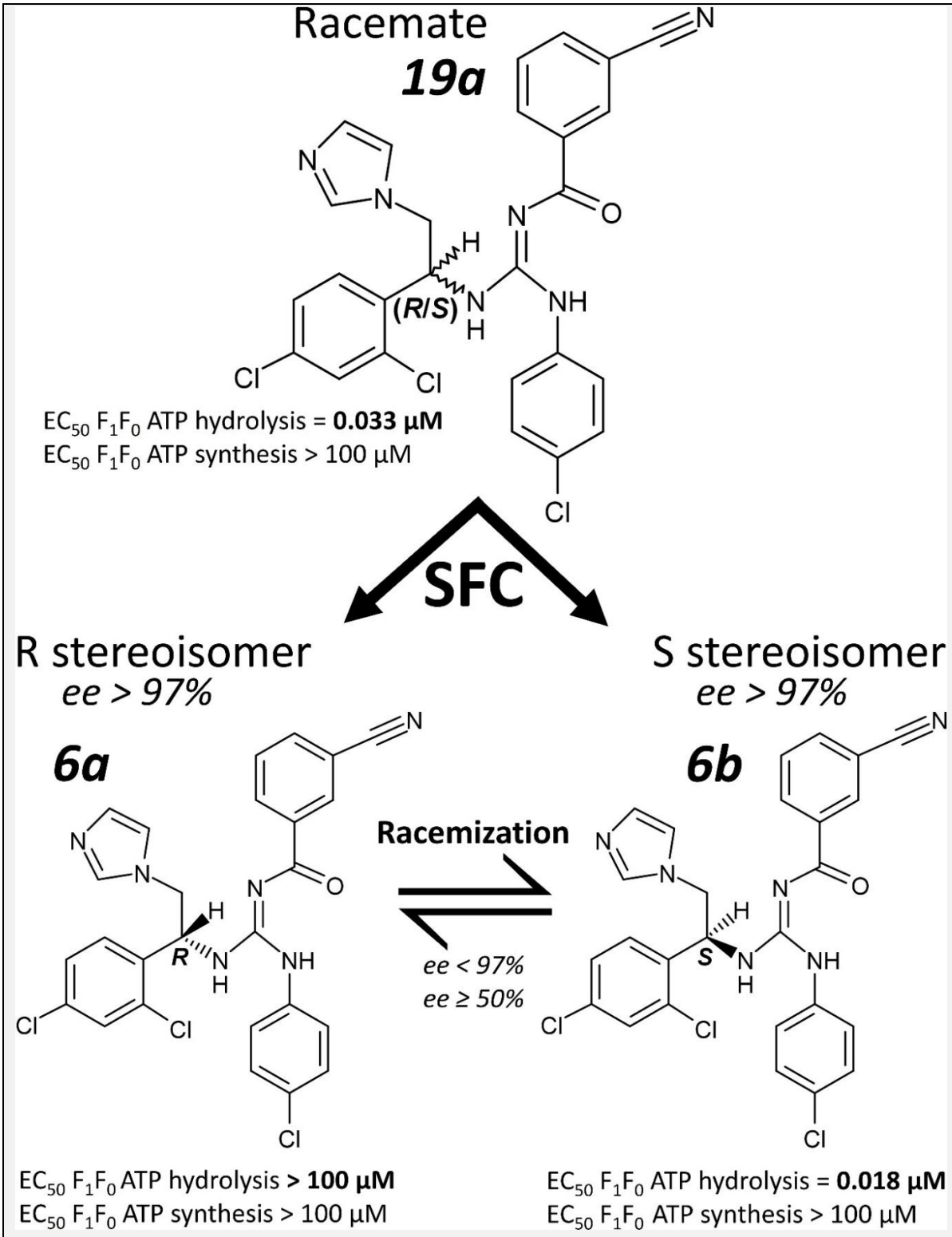

Figure 10A - Structure of racemate, 19a, and its separated stereoisomers (separated stereoisomer fractions) 6a and 6b. SFC is chiral supercritical fluid chromatography, ee is enantiomeric excess. EC_{50} values are from a Sub-Mitochondrial Particle (SMP) assay.

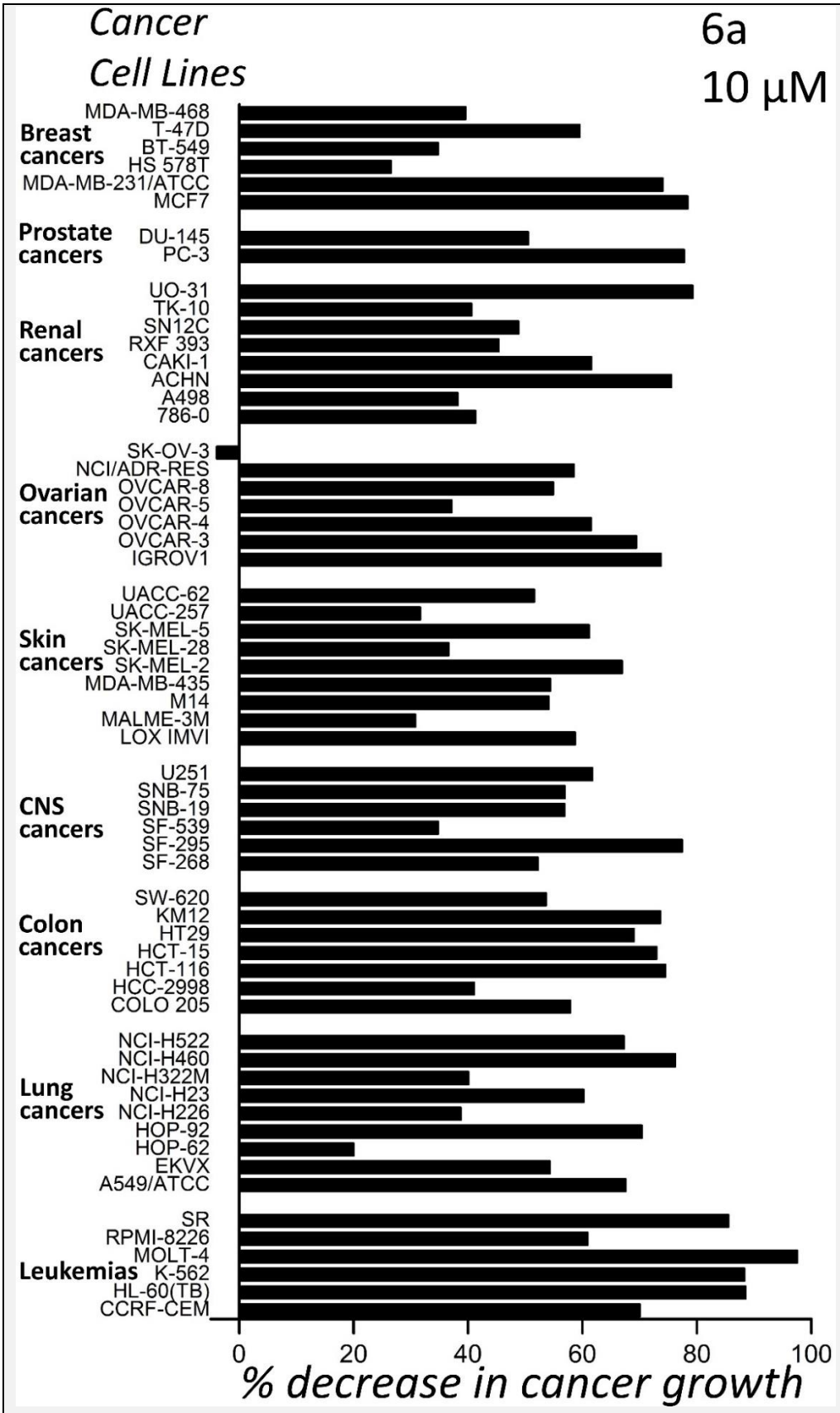

Figure 10B - Anti-cancer activity of compound 6a (10 µM) in NCI-60 testing.

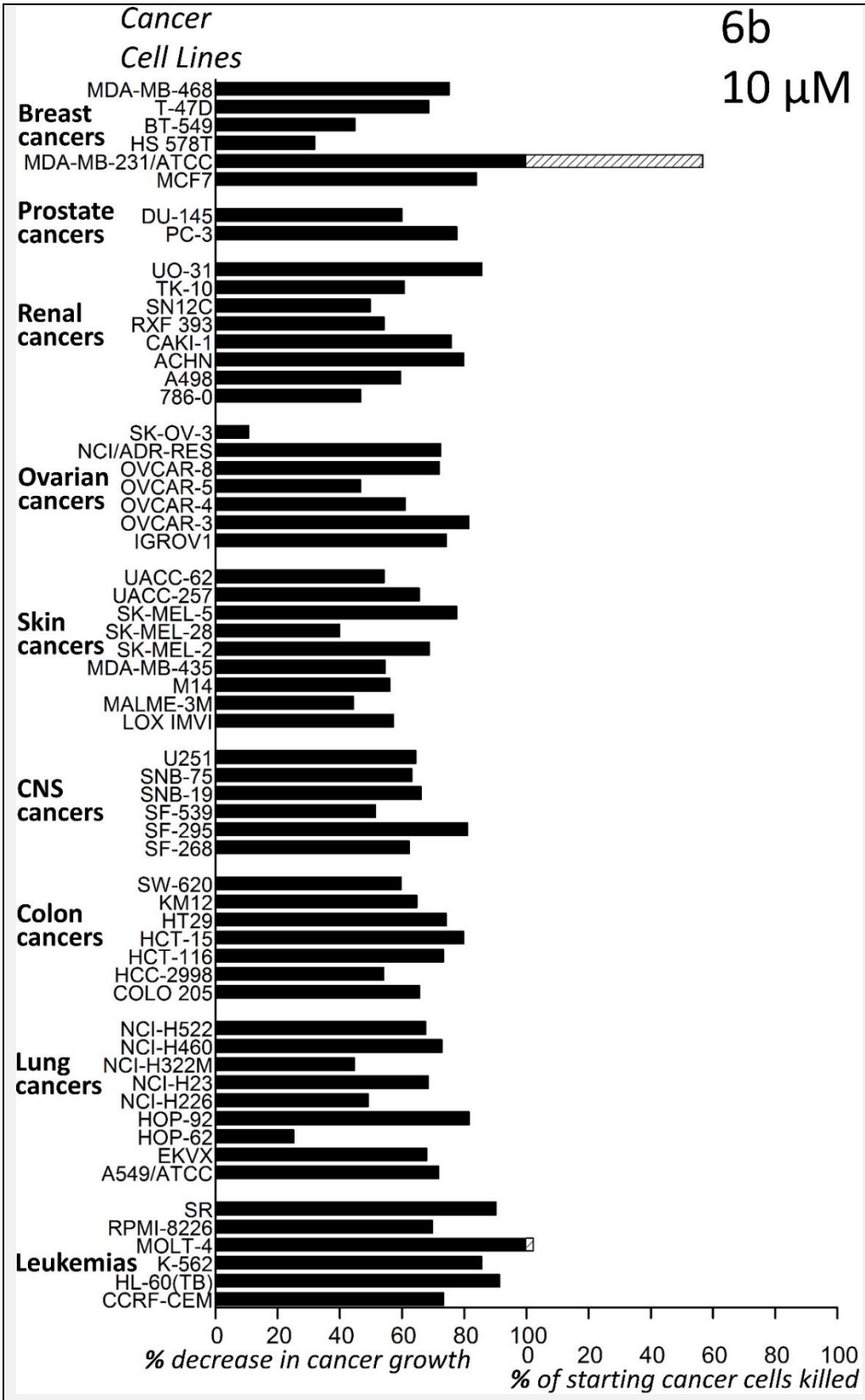

Figure 10C - Anti-cancer activity of compound 6b (10 µM) in NCI-60 testing.

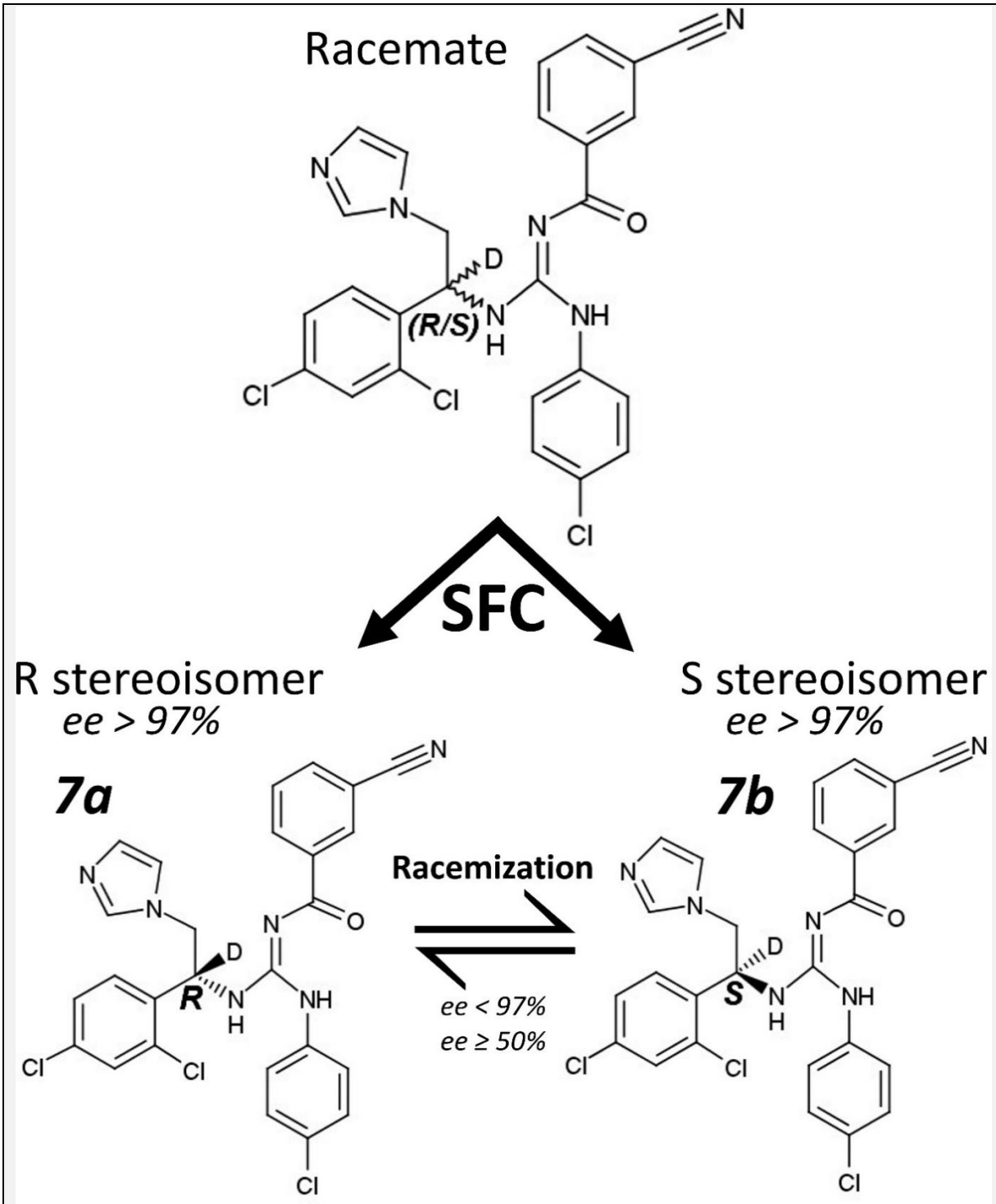

Figure 11A - Structure of separated stereoisomers (separated stereoisomer fractions) 7a and 7b. SFC is chiral supercritical fluid chromatography, ee is enantiomeric excess. D is deuterium (^{2}H).

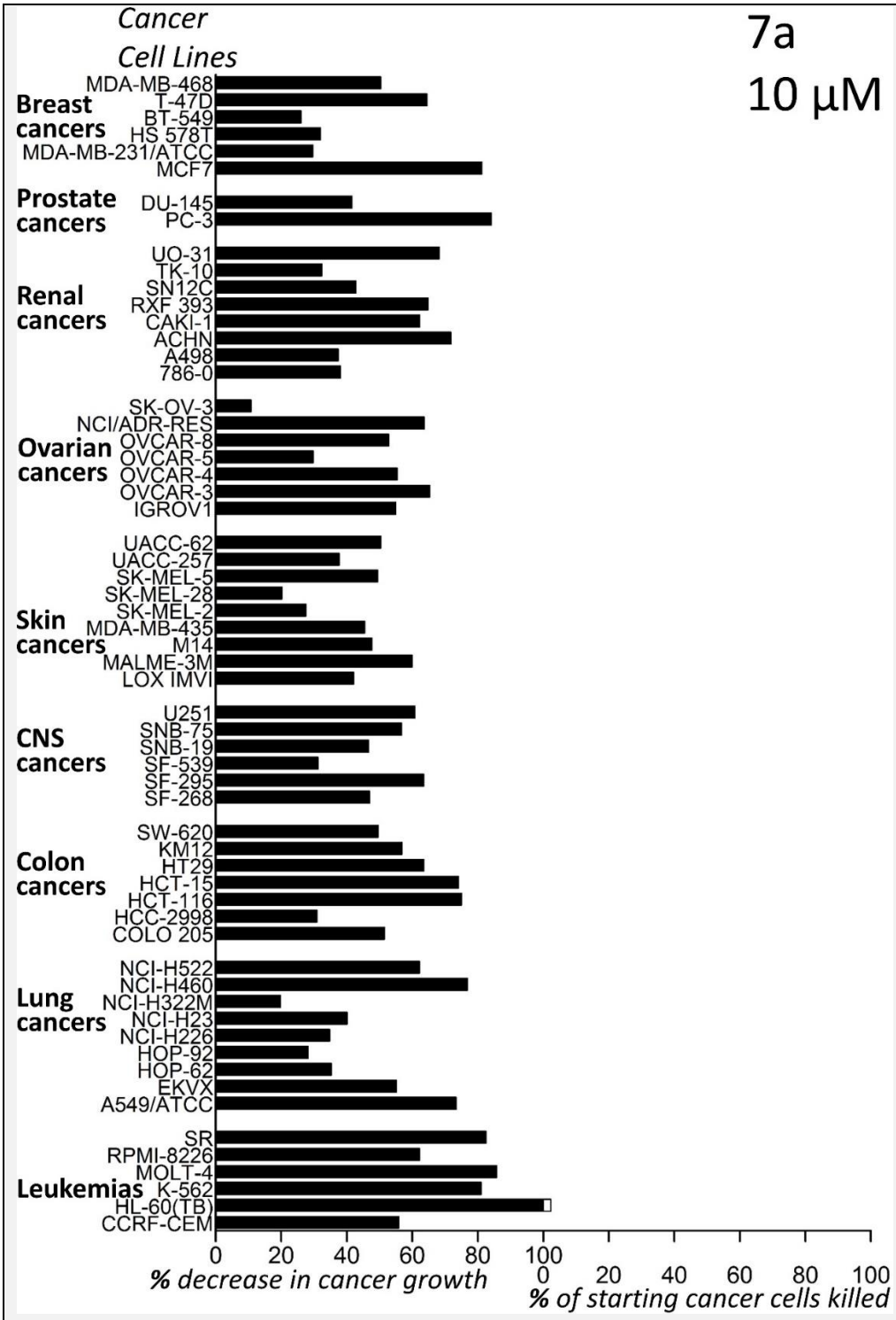

Figure 11B - Anti-cancer activity of compound 7a (10 µM) in NCI-60 testing.

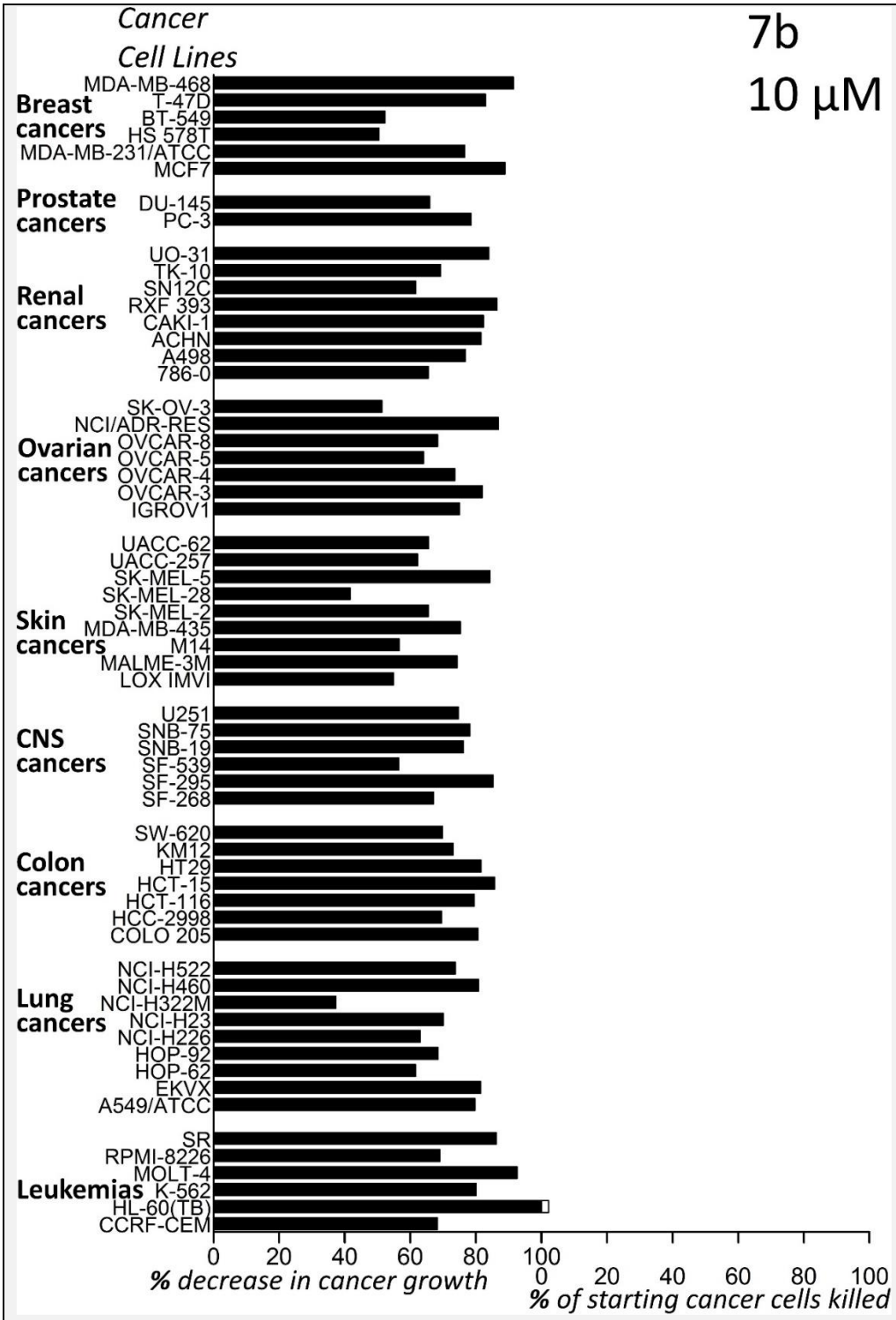

Figure 11C - Anti-cancer activity of compound 7b (10 µM) in NCI-60 testing.

It is notable that F_1F_0 ATP hydrolysis inhibiting compounds, hypothesized to slow aging herein (Discussion section), have anti-cancer activity (Figures 10 and 11). Because a worry/critique of trying to slow aging is the argument that, because cancer is immortal [60], conferring slower aging/immortality upon a normal cell is making it closer to being cancer.

Such that even if an anti-aging approach could be found, because of it inextricably increasing the cancer risk, lifespan wouldn't be very much extended, if at all. Conferring a practical block/limit to appreciable lifespan extension. For example, this is a concern, in at least some people's minds, with expression of telomerase (in normal somatic cells) approaches [75-77]. However, by contrast, inhibiting F_1F_0 ATP hydrolysis actively exerts potent anti-cancer activity (Figures 10 and 11). So, distinctively, it is a drive against, and not to, cancer. Arguably, anti-cancer activity is a highly desirable, if not a mandatory, trait of a longevity drug. Indeed, rapamycin (also known as sirolimus), an mTOR inhibiting drug, which can slow aging and extend lifespan in mice, has anti-cancer activity also [78]. In NCI-60 one-dose (10 µM) testing, it confers mean and median % cancer growth inhibition of 56.22% and 55.45% respectively (NSC 226080 in [79]). Temsirolimus, a prodrug of rapamycin (metabolized to rapamycin in the body), is approved by the U.S. Food and Drug Administration (FDA), and the European Medicines Agency (EMA), for the treatment of Renal Cell Carcinoma (RCC) [80].

At least some present cancer treatments, e.g. radiotherapy, (probably because their Mechanism of Action {MOA} is, at least in part, to increase Reactive Oxygen Species, ROS [70-73]) accelerate aging in normal cells. Thence (presumably because aging/age is a major risk factor for cancer [81]) increasing subsequent cancer risk [384-385]. I propose F_1F_0 ATP hydrolysis inhibitor compounds do the inverse. Still conferring anti-cancer therapy (Figures 10 and 11; partly, by aforementioned rationale, via increasing [ROS] in cancer cells). But whilst slowing aging in normal cells (by reducing their intracellular [ROS], Figure 4), which reduces the subsequent/secondary cancer risk.

To theorize, inhibiting F_1F_0 ATP hydrolysis slows both heavily glycolytic (cancer) and predominantly oxidative (normal cell) metabolisms. The former *increases* intracellular [ROS] in cancer cells. The latter *decreases* intracellular [ROS] in normal cells.

DISCUSSION

<u>F_1F_0 ATP hydrolysis is a major determinant of metabolic rate</u>

A key contribution of this present paper (*and my corresponding patent applications, e.g. [3]*) is the new finding, from new experimental data, that specific F_1F_0 ATP hydrolysis is a major determinant of specific basal metabolic rate. Although [8-10] show that greater IF1 protein activity slows metabolic rate, they interpret that this is because of IF1 protein directly inhibiting F_1F_0 ATP synthesis. I instead assert that IF1 protein does <u>*not*</u> directly inhibit F_1F_0

ATP synthesis. And that greater IF1 protein activity slows metabolic rate by greater inhibition of F_1F_0 ATP hydrolysis. Where, newly reported herein (*and in sister patent applications*), F_1F_0 ATP hydrolysis is prevalent *in vivo*, conferring metabolic heat generation. Evidenced by Figure 1 herein.

New correlations discovered

Across species (at least across the species set studied), less specific F_1F_0 ATP hydrolysis *significantly* correlates with greater maximal lifespan. Where mediation analysis indicates that this correlation is mediated by specific basal metabolic rate. Wherein interventional (mouse) experiments indicate causality between less F_1F_0 ATP hydrolysis and slower metabolic rate, and causality between slower metabolic rate and longer lifespan. Interventional (mouse) experiments indicate causality between less F_1F_0 ATP hydrolysis and less Reactive Oxygen Species (ROS) generation. Across species (at least across the species set studied), less specific F_1F_0 ATP hydrolysis correlates with less mitochondrial ROS detected. And less ROS damage. To DNA, mitochondrial DNA (mtDNA), and to cellular/membrane lipids.

Why do different species age at different rates, and have different maximal lifespans?

My interpretation of the data herein is that (at least partially) the basis to different maximal lifespans, in different mammal species (*which can vary over many orders of magnitude*), is different specific F_1F_0 ATP hydrolysis rates. Set by different specific IF1 protein activities.

This interpretation makes experimentally testable predictions.

Predicted

Metabolic rate enables life, but (*at least seemingly*) a correlate(s) to it causes aging, which ultimately takes it away. As I've newly shown, much of mammalian metabolic rate is, via F_1F_0 ATP hydrolysis, to convert the chemical energy of food into heat energy, to keep the body temperature at 37°C (e.g. because action potential characteristics, such as conduction velocity, are temperature dependent [84-89], and 37°C enables fast action/reaction). To extrapolate/predict, if exogenous heat energy keeps the body at 37°C, e.g. via an ambient temperature of 37°C, endogenously generated heat energy can afford to be less, metabolic rate can be less, and aging can be slower. Wherein slower metabolic rate can (as demonstrated in Figure 1) be conferred by a F_1F_0 ATP hydrolysis inhibitor compound. Some examples of which are in my US patent application [3], e.g. novel compound:

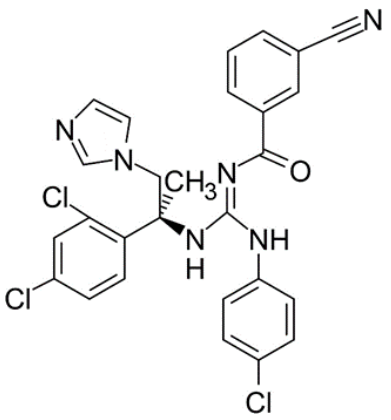

To elaborate upon this prediction: *systemic* administration of a F_1F_0 ATP hydrolysis inhibiting drug, *systemically* inhibiting F_1F_0 ATP hydrolysis, so *systemically* reducing metabolic rate, increases lifespan. *If* the ambient temperature to the subject, and/or the subject's bodily insulation, is increased. To offset their decreased metabolic heat production. Wherein, notably, if the ambient temperature is 37°C, no metabolic heat production is required for the body to be at 37°C. So, no matter the decrease in metabolic heat production, the ambient temperature never need be in excess of 37°C. The ambient temperature to the subject, and/or their bodily insulation, only needs to be greater when they have an effective amount of drug in their system. Which, optionally, can be timed to be only/predominantly at night, whilst they sleep. If the pharmacokinetics of the selected F_1F_0 ATP hydrolysis inhibiting drug permits. As an aside, reduced metabolic heat production in a subject is arguably a feature, and not a bug, in many hotter parts of the world. Because it can, by increasing the body's thermoneutral temperature (*above and below which, greater metabolic rate is required to maintain the body at 37°C*), presumably increase thermal comfort in such climates. For example, in Singapore or Thailand. A sizeable percentage of the world's population lives in hot climates. Or in seasonally hot climates.

<u>Two (2) predicted prospects</u>

[1] ***Systemically*** administer a F_1F_0 ATP hydrolysis inhibitor compound, to slow aging in the entirety of the body, but wherein the subject's ambient temperature and/or bodily insulation needs to be controlled accordingly. {*This can be done at night for example, whilst the subject sleeps. And/or in a controlled environment building/complex/vehicle. And/or in a hot climate country. And/or utilizing more clothing*}.

[2] ***Locally*** administer a F_1F_0 ATP hydrolysis inhibitor compound, to slow aging in just part(s) of the body, but wherein there are no thermoregulatory issues to be concerned with. Because of heat transfer, especially via blood flow, from other body regions. Local inhibition of F_1F_0 ATP hydrolysis has already proven safe in mice (Results section titled "Local inhibition of F_1F_0 ATP hydrolysis").

For example, *local* administration, to skin of the human face (e.g. around the eyes). For example, of a functional human IF1 protein fragment (e.g. its residues 42-58 [90-93]). Concatenated, to its N-terminal end, is a Mitochondrial Import Sequence (MIS), as used by the complete IF1 protein. And concatenated, to its N-terminal end, is a Cell Penetrating Peptide (CPP) sequence. Once inside the cell, endogenous protein machinery in the mitochondrial matrix cleaves off the MIS (and inherently the {more N-terminal} CPP sequence with it). A string of seven arginine residues is a very effective CPP sequence [94]. Wherein this is an amino acid sequence that occurs naturally within the human body. In a number of different proteins findable by a BLAST [95] search. So, this candidate cosmetic agent is a concatenation of amino acid sequences that naturally occur within the human body. Many cosmetics, especially the premium brands, contain amino acid sequences (peptides) these days.

<u>Local administration conferring systemic benefit?</u>

There is a thesis that neurodegenerative diseases, such as Alzheimer's (which can cause dementia) and Parkinson's disease, correlate with aging because they are caused by aging. Indeed, caused by the oxidative stress of aging [96-113]. "Mitochondrial dysfunction and oxidative stress occur early in all major neurodegenerative diseases, and there is strong evidence that this dysfunction has a causal role in disease pathogenesis" [96]. More broadly, many further diseases have an incredibly (e.g. exponentially) increased risk of incidence with age. And can be said to be diseases of aging. Many, if not all, diseases of aging might be caused by a body part(s) aging, and declining in function, faster than the rest of the body. So, such diseases might be prevented/ameliorated by locally slowing the aging of that body part(s). So that it better matches the aging rate of the rest of the body. Or is even slower. This can better match "healthspan" to lifespan. For example, dopamine neurons in the pars compacta, in the substantia nigra, decline in number by 5-10% per decade, presumably by dying, which is a predisposing drive to Parkinson's disease [114-116]. Extrapolating from (predicting upon) the data herein: specifically reducing F_1F_0 ATP hydrolysis in these neurons will reduce their aging rate. Wherein their resulting reduction in metabolic heat production

will be offset by heat transfer from other cell types and body regions, especially via blood flow. Another postulated use case is topical administration of a F_1F_0 ATP hydrolysis inhibitor compound to the eye(s), to avert/treat/slow Age-related Macular Degeneration (AMD). Wherein there is presently no treatment for dry AMD, which more than 150 million people have now. Its incidence is projected to increase to nearly 300 million people by 2040 [117].

Some further medical applications?

As taught herein (e.g. refer to the Results section titled "New experimental results", which encompasses Figure 1), a systemically administered F_1F_0 ATP hydrolysis inhibitor drug can reduce body temperature to a value controlled by the intersection of drug dosage and ambient temperature. Even at maximum possible effect, the drug cannot make body temperature fall below, only towards/to, ambient temperature. So, at high (systemically administered) drug dose, body temperature can be controlled by controlling ambient temperature.

This might have many medical applications. For example, emergency grade hyp*er*thermia is an extremely dangerous aspect to many Emergency Room (ER) admissions, e.g. in some trauma patients. And there are many medical conditions in which the body can get too (dangerously) hot, e.g. fever, sepsis, malignant hyperthermia, neuroleptic malignant syndrome, hypermetabolism etc. It may also enable controlled hyp*o*thermia for a medical/surgical/protective purpose (called "Targeted Temperature Management, TTM", "therapeutic hypothermia", or "protective hypothermia"), for which there are many applications, e.g. neuroprotection after a stroke, cardioprotection after a heart attack, deep hypothermic circulatory arrest for surgery (e.g. brain surgery, e.g. brain tumour removal), slowing adverse chemical reactions/bleeding/bacterial growth in the body after poisoning/injury (e.g. gun-shot wound), conferring longer than the "golden hour" to get an injured soldier to a field hospital etc.

Postscript

Much herein has already published, via (some of) my patent applications already publishing (e.g. variants of Figures 1 and 10 published, as Figures 15 and 8 respectively, in my patent application [3], e.g. variants of Figures 2 and 11 published, as Figures 24 and 10, in my patent applications [118-119]). But this present paper is its first report in the scholarly literature. A very recent preprint has further confirmed one of the assertions of this present paper, and its patent application predecessors (e.g. [118-119]), that (to quote it) "IF1 is required to prevent the onset of ATP hydrolysis under OXPHOS conditions", "IF1 is

essential under OXPHOS conditions to prevent reverse ATP synthase activity", "our data clearly show that IF1 is necessary to block ATP hydrolysis under OXPHOS conditions", "to prevent futile ATP synthesis/hydrolysis cycles by reverse ATP synthase activity and ATP hydrolysis, IF1 is essential even and especially under OXPHOS conditions", "IF1 is beneficial for ATP production even under OXPHOS conditions", "ATP levels were lower in IF1-KO cells under OXPHOS conditions", "clearly, this data demonstrates the importance of IF1 to block futile ATP hydrolysis under OXPHOS conditions" [120].

METHODS (*with supplementary information, data & analysis*)

Some definitions: "specific", by convention, can refer to "per unit mass", which is a convention used often herein. "Maximal lifespan" of a species is the longest lifespan ever recorded for a member of that species.

Synthesis of 6a and 6b (*6b administered to mice in Figure 1; anti-cancer data in Figure 10*)

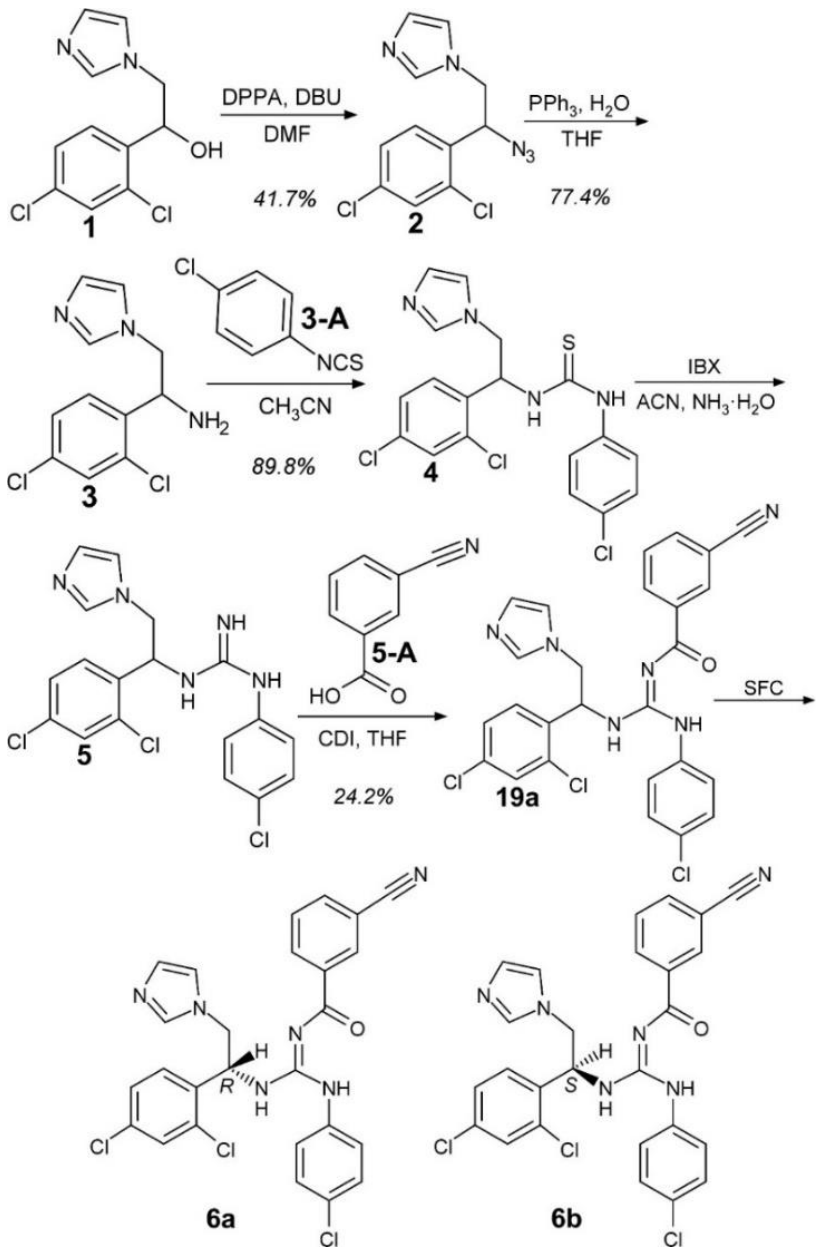

6a {enantiomeric excess (ee) ≥97%}: Liquid Chromatography-Mass Spectrometry (LC-MS): Liquid Chromatography (LC) Retention Time (RT) = 2.516 minutes, Mass spectrometry (MS; electrospray ionization, positive mode): *m/z* 537.1 $[M+H]^+$, 559.1 $[M+Na]^+$, 269.1 $[M+2H]^{2+}$.

^{1}H NMR (400 MHz, DMSO-*d6*) δ (ppm) 11.43 (s, 1H), 8.30 (s, 1H), 8.21 (d, J = 7.9 Hz, 1H), 7.93 (d, J = 7.8 Hz, 2H), 7.67 – 7.56 (m, 3H), 7.50 (t, J = 6.5 Hz, 4H), 7.20 (s, 1H), 7.09 (d, J = 8.2 Hz, 2H), 6.97 (s, 1H), 5.96 (s, 1H), 4.34 (s, 1H), 4.19 (s, 1H). {*NMR probe temperature = 298.15 K*}.

6b {enantiomeric excess (ee) ≥97%}: Liquid Chromatography-Mass Spectrometry (LC-MS): Liquid Chromatography (LC) Retention Time (RT) = 2.516 minutes, Mass Spectrometry

(MS; electrospray ionization, positive mode): *m/z* 537.1 $[M+H]^+$, 559.1 $[M+Na]^+$, 269.1 $[M+2H]^{2+}$.

^{1}H NMR (400 MHz, DMSO-*d6*) δ (ppm) 11.43 (s, 1H), 8.30 (s, 1H), 8.21 (d, J = 7.9 Hz, 1H), 7.93 (d, J = 7.8 Hz, 2H), 7.68 – 7.56 (m, 3H), 7.56 – 7.46 (m, 4H), 7.20 (s, 1H), 7.09 (d, J = 8.1 Hz, 2H), 6.97 (s, 1H), 5.96 (s, 1H), 4.33 (s, 1H), 4.19 (s, 1H). {*NMR probe temperature = 298.15 K*}.

The presented Nuclear Magnetic Resonance (NMR) peaks are from using the "Auto Assignment" algorithm in MestReNova version 12 software (Mestrelab Research, Santiago de Compostela, Spain). Which picks peaks in an inputted NMR spectrum, influenced by an inputted structure, which was structure 19a in the reaction scheme above.

<u>Performed synthesis of 6a and 6b in detail</u>

In this section, numbers in square brackets are CAS numbers.

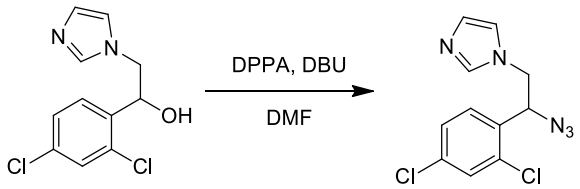

1 **2**

1. Charged Compound 1 [24155-42-8] (10.0 g, 1.00 X by weight) and DPPA [26386-88-9] (10.7 g, 1.07 X by weight) in DMF [68-12-2] (50 mL, 5.00 X by volume).
2. Charged DBU [6674-22-2] (5.90 g, 0.59 X by weight) into the mixture, under nitrogen atmosphere at 0°C, then stirred for about 15 minutes.
3. After that, took the reaction mixture to 20-30°C and stirred for 24 hours.
4. Thin-Layer Chromatography (TLC; DCM/MeOH = 10/1, R_f = 0.6) showed raw material remained, LC-MS (Starting Material [SM]: RT = 0.729 minutes, Product: RT = 0.822 minutes) indicated reaction mixture had desired product.
5. The reaction mixture was extracted with EtOAc (100 mL x 3).
6. The combined organic phase was washed with aq.NaCl (100 mL), dried with Na_2SO_4, filtered and concentrated in vacuum to get the residue.
7. The residue was purified by column chromatography (DCM/MeOH = 1/0 to 100/1).
8. Compound 2 (4.82 g, 41.7%, 95% purity) was obtained as a yellow oil, which was confirmed by ^{H}NMR and HPLC (Retention Time (RT) = 1.919 minutes).

Compound 2: ^{1}H NMR ($CDCl_3$, 400 MHz) δ (ppm) 7.47 (d, J = 2.2 Hz, 1H), 7.41 (s, 1H), 7.33 - 7.28 (m, 1H), 7.26 - 7.23 (m, 1H), 7.06 (s, 1H), 6.92 (s, 1H), 5.26 (m,1H), 4.23 (m, 1H), 4.02 (m, 1H).

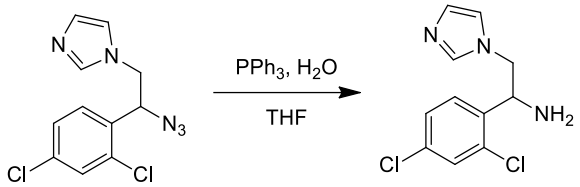

2 **3**

1. Charged Compound 2 (3.00 g, 1.00 X by weight) and PPh_3 [603-35-0] (8.40 g, 2.80 X by weight) in H_2O (1 mL, 0.33 X by volume) and THF [109-99-9] (10 mL, 3.33 X by volume).
2. Stirred at 70°C for 24 hours.
3. Checked the reaction by LC-MS (SM: RT = 0.822 minutes, Product: RT = 0.299 minutes), it showed that Compound 2 was consumed completely, and that the desired mass was detected.
4. The reaction mixture was concentrated under reduced pressure to remove THF.
5. The reaction mixture was added with H_2O (30 mL), adjusted pH to 3 with con.HCl and washed with EtOAc (30 mL).
6. After that, collected water phase, adjusted pH to 13 with 1N aq.NaOH, then exacted with EtOAc (30 mL x 2).
7. The combined organic phase was washed with aq.NaCl (30 mL), dried with Na_2SO_4, filtered, and concentrated in vacuum to obtain the product.
8. Compound 3 (2.23 g, 77.4%, 94.5% purity) was obtained as a yellow liquid, which was confirmed by ^{H}NMR and HPLC (Retention Time = 0.658 minutes).

Compound 3: ^{1}H NMR ($CDCl_3$, 400 MHz) δ (ppm) 7.48 - 7.37 (m, 3H), 7.30 - 7.26 (m, 1H), 7.06 (s, 1H), 6.91 (s, 1H), 4.72 (m, 1H), 4.21 (m, 1H), 3.91 (m, 1H).

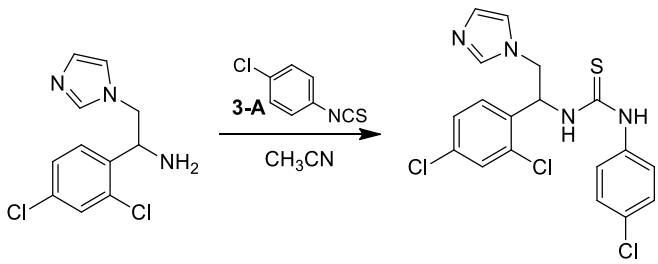

3 **4**

1. Charged Compound 3 (2.00 g, 1.00 X by weight) and Compound 3-A [2131-55-7] (1.30 g, 0.65 X by weight) in CH_3CN [75-05-8] (30 mL, 15.00 X by volume).
2. Stirred at 20-30°C for 12 hours.
3. Checked the reaction by TLC (DCM/MeOH = 10/1, R_f = 0.7) and LC-MS (SM: RT = 0.299 minutes, Product: RT = 0.949 minutes), desired product was detected, TLC indicated Compound 3 was consumed completely.
4. The reaction mixture was concentrated under reduced pressure to remove CH_3CN to obtain the residue.
5. The residue was purified by column chromatography (DCM/MeOH = 1/0 to 50/1).
6. Compound 4 (2.95 g, 89.8%, 99.7% purity) was obtained as a white solid, which was confirmed by ^{H}NMR and HPLC (Retention Time = 2.521 minutes).
Compound 4: ^{1}H NMR (DMSO-*d6*, 400 MHz) δ (ppm) 9.81 (s, 1H), 8.54 (d, J = 7.5 Hz, 1H), 7.64 (s, 1H), 7.55 (s, 1H), 7.53 - 7.48 (m, 1H), 7.45 - 7.41 (m, 1H), 7.38 (d, J = 8.6 Hz, 2H), 7.28 (d, J=8.4 Hz, 2H), 7.11 (s, 1H), 6.94 (s, 1H), 6.03 (s, 1H), 4.46 - 4.34 (m, 1H), 4.31 - 4.22 (m, 1H).

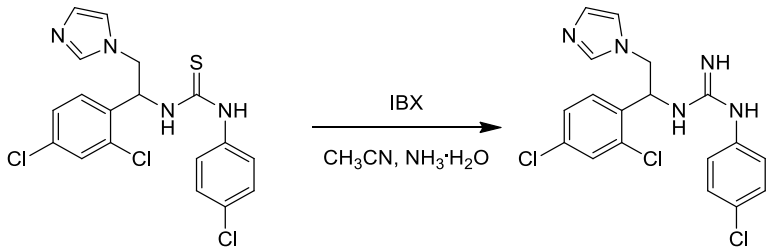

4 **5**

1. Charged Compound 4 (1.63 g, 1.00 X by weight) and IBX [61717-82-6] (1.18 g, 0.75 X by weight) in CH_3CN [75-05-8] (16 mL, 10.00 X by volume) and $NH_3.H_2O$ [1336-21-6] (8 mL, 5.00 X by volume).
2. Stirred at 20-30°C for 18 hours.
3. Checked the reaction by LC-MS (SM: RT = 0.949 minutes, Product: RT = 1.050 minutes) and HPLC (SM: RT = 2.535 minutes, Product: RT = 1.757 minutes), desired product was detected.
4. The reaction mixture was extracted with EtOAc (20 mL x 3).
5. The combined organic phase was washed with aq.NaCl (20 mL), dried with Na_2SO_4, filtered and concentrated *in vacuo* to obtain the crude product (1.0 g, white solid), which was used into next step directly.

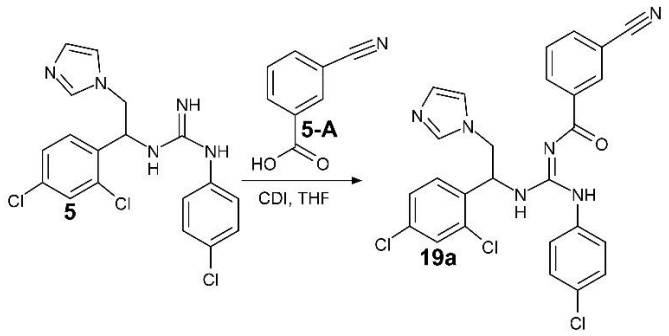

1. Charged Compound 5-A [1877-72-1] (0.36 g, 0.36 X by weight) and CDI [530-62-1] (0.40 g, 0.36 X by weight) in THF [109-99-9] (20 mL, 20.00 X by volume), stirred at 20-30°C for 3 hours.
2. Charged Compound 5 into the reaction mixture, stirred at 20-30°C for 14 hours.
3. Checked the reaction by LC-MS (SM: RT = 1.050 minutes, Product: RT = 1.347 minutes) and TLC (DCM/MeOH = 10/1, R_f = 0.75), desired mass was detected. TLC indicated the raw material was consumed completely.
4. The reaction mixture was concentrated under reduced pressure to remove THF.
5. The reaction mixture was extracted with EtOAc (20 mL x 3)
6. The combined organic phase was washed with aq.NaCl (20 mL), dried with Na_2SO_4, filtered and concentrated *in vacuo* to obtain the residue.
7. The residue was purified by column chromatography (DCM/MeOH = 1/0 to 100/1) and chiral SFC {column: AD (250 mm*50 mm, 10 µm); mobile phase: [0.1%NH_3H_2O IPA]; B%: 28%-28%, 3.5 minutes} separating the stereoisomers of Compound 19a: 6b (0.17 g, SFC RT = 2.35 minutes) was obtained as a white solid, 6a (0.15 g, SFC RT = 2.69 minutes) was obtained as a white solid.

Abbreviations used: Ph=phenyl, MeOH=methanol, CDI=1,1'-carbonyldiimidazole, DCM=dichloromethane, DBU=1,8-diazabicyclo[5,4,0]undec-7-ene, DMF=N,N-dimethylformamide, DPPA=diphenylphosphoryl azide, EtOAc=ethyl acetate, IBX=2-iodoxybenzoic acid, IPA=isopropanol, R_f=retention value, RT=retention time, THF=tetrahydrofuran, TLC=thin-layer chromatography, SM=starting material, SFC=chiral supercritical fluid chromatography, LC-MS=Liquid Chromatography Mass Spectrometry, HPLC=High-performance liquid chromatography, NMR=Nuclear magnetic resonance, aq.=aqueous, con.=concentrated, MeCN=methyl cyanide (acetonitrile), DMSO=dimethyl sulfoxide.

<u>Spectral data for 6b</u>

Its expected/calculated *m/z*, from its structure (Figure 1), using the "exact molecular weight" calculator in MarvinSketch software (Chemaxon, Budapest, Hungary), which uses the mass of the *most prevalent* isotope of each element in the molecule:
537.08 $[M+H]^+$, 559.06 $[M+Na]^+$, 269.04 $[M+2H]^{2+}$, 575.03 $[M+K]^+$).

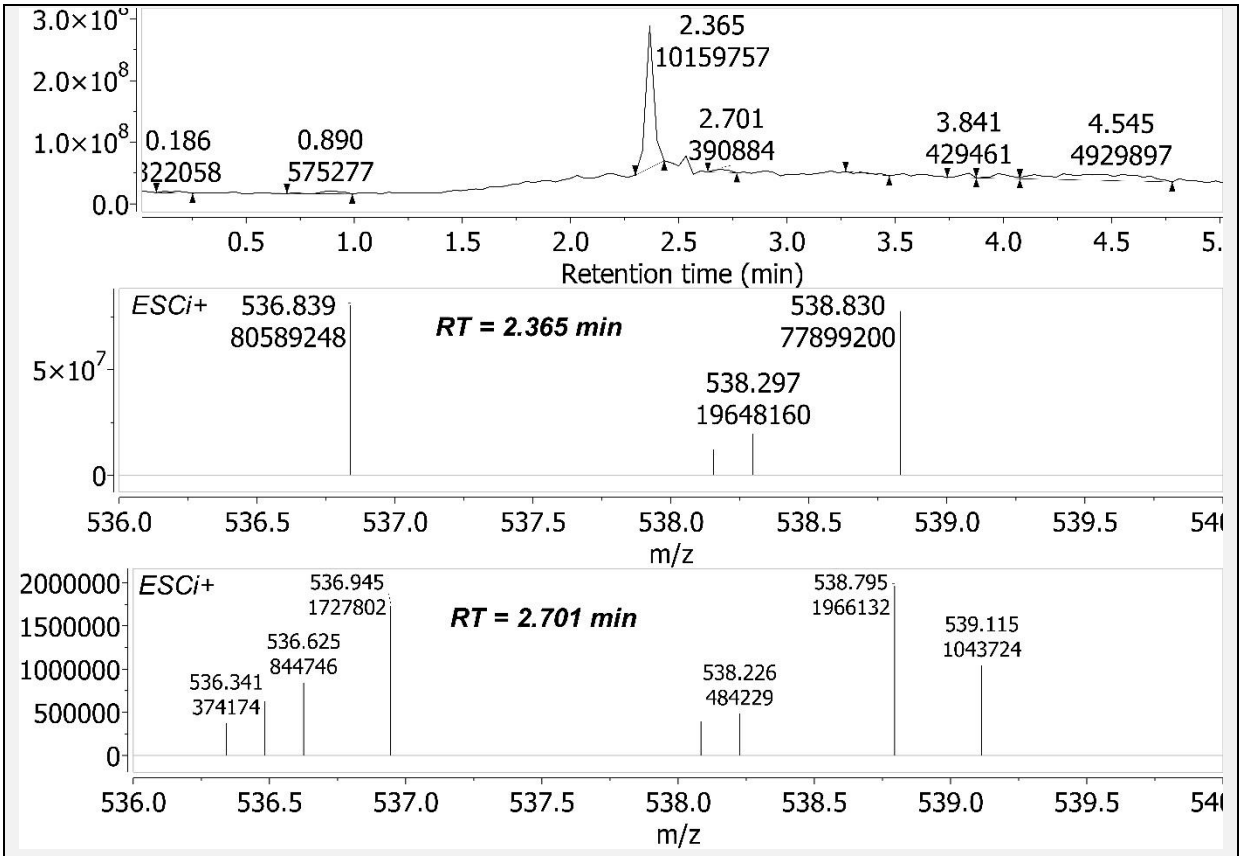

Figure 12 - Chiral Supercritical Fluid Chromotography Mass Spectrum (chiral SFC-MS) of 6b sample. *Upper panel*: Chiral-SFC annotated with Retention Time (RT, minutes), and area under peak. *S* stereoisomer is found in the [RT=2.365] peak. *Middle panel*: Component of the Mass Spectrum (MS) of the [RT=2.365] peak. Therein is *m/z* 536.839 $[M+H]^+$ (*0.19 removed from Expected. Better concordance in subsequent spectra*). Y-axis presents intensity. ESCi™ is multi-mode ionization (PCT/US03/16892), which switches at very high speed between Electrospray Ionization (ESI) and Atmospheric Pressure Chemical Ionization (APCI) ionization methods. ESCi+ refers to using ESCi in its positive ionization mode. Polarity positive. *Bottom panel*: Component of the Mass Spectrum (MS) of the [RT=2.701] peak.

Using this present figure, *S* stereoisomer excess (%) in this sample = (80589248/(80589248+1727802))*100 = 97.9%; enantiomeric excess (ee, %) = (97.9-50)*2 = 95.8%. Calculating the ee directly, rather than via the stereoisomer excess, ee =

((80589248-1727802)/(80589248+1727802))*100 = 95.8%. Working back from this ee to the stereoisomer excess: (95.8/2)+50 = 97.9%.

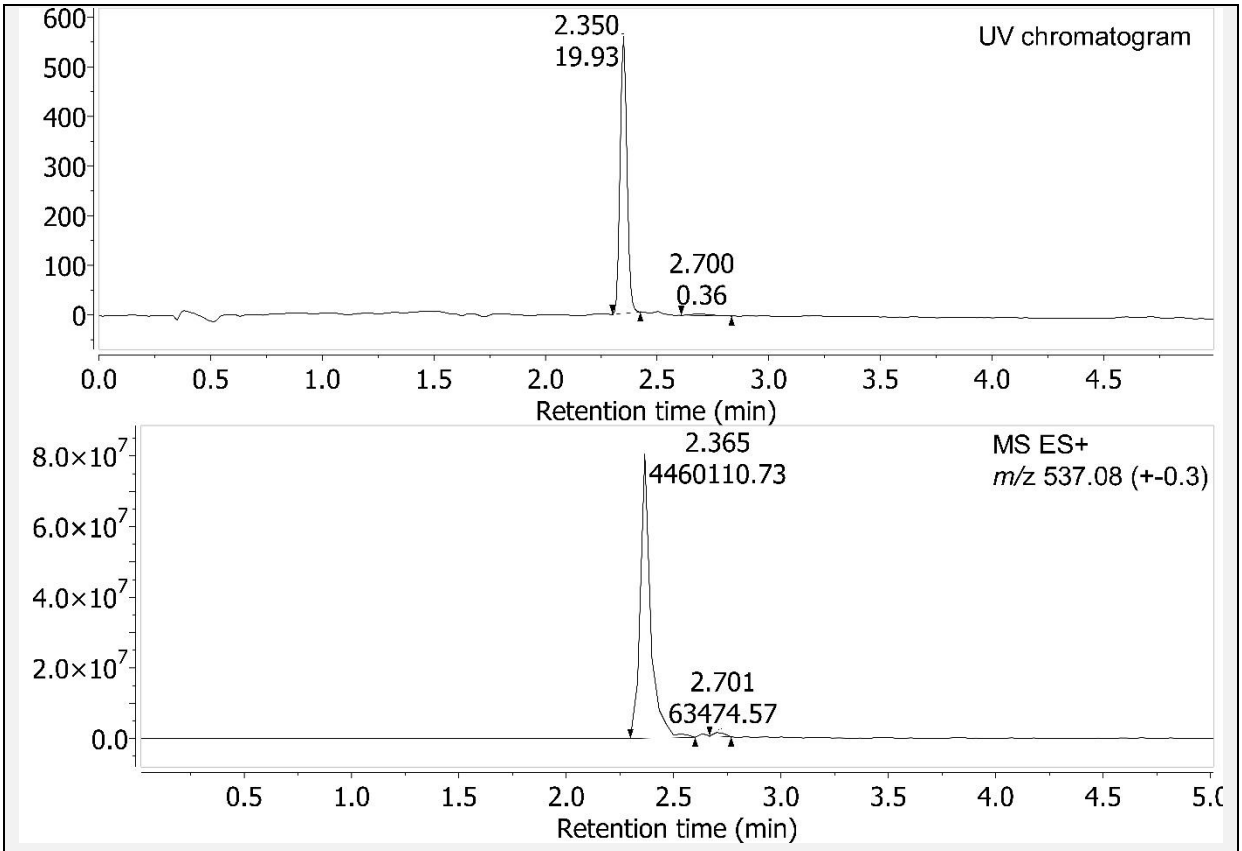

Figure 13 – Chiral Supercritical Fluid Chromotography (chiral-SFC) of 6b sample. Using the UV Chromatogram component, *S* stereoisomer excess (%) in this 6b sample = (19.93/(19.93+0.36))*100 = 98.23%; enantiomeric excess (ee) = (98.23-50)*2 = 96.46%.

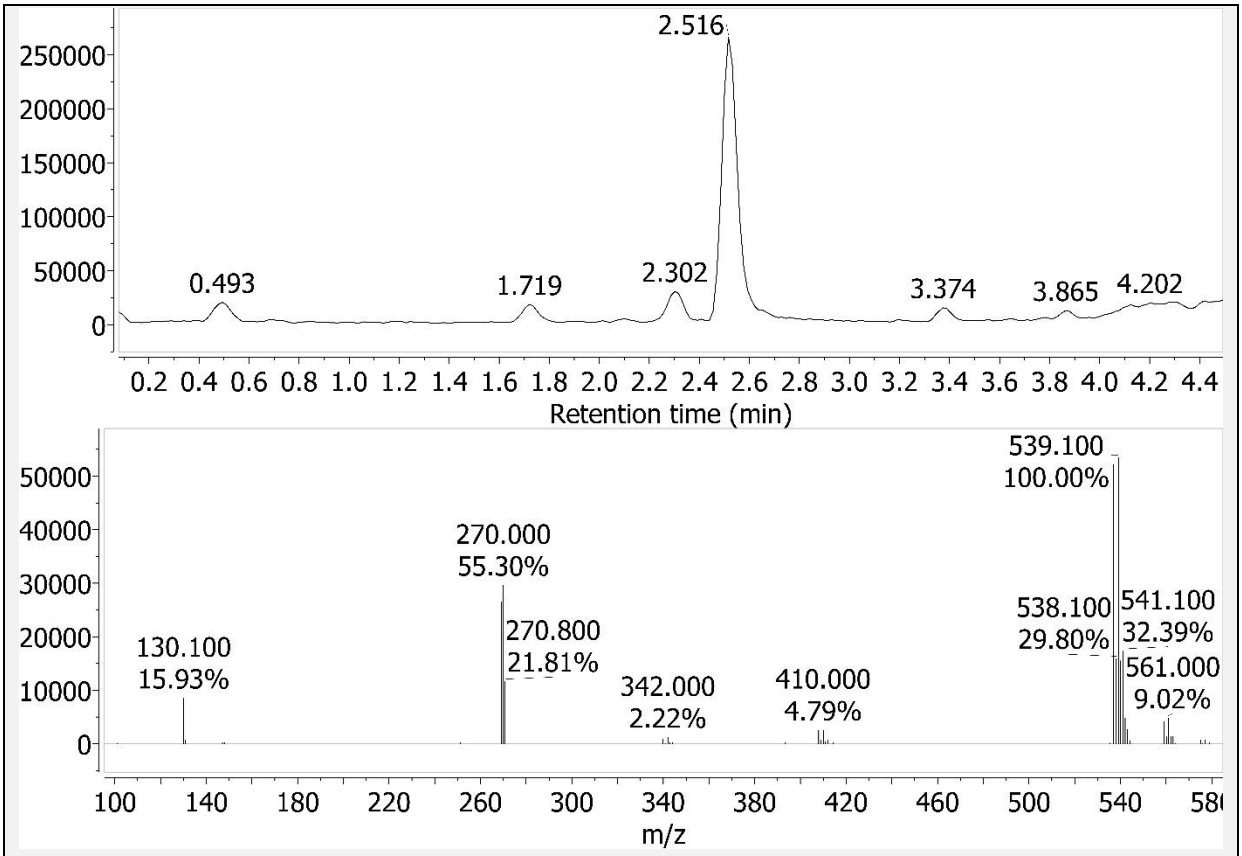

Figure 14 - Liquid Chromatography–Mass Spectrometry (LC-MS) spectrum for 6b sample. *Upper panel*: Liquid Chromatography (LC) Retention Time (RT) = 2.516 minutes. *Lower panel*: Mass Spectrum (MS) of the [RT peak=2.516]. Shows positively charged species: "Ionization mode = API-ES" and "Polarity = Positive". Wherein API is "Atmospheric Pressure Ionization". And ES is Electrospray. Percentages are relative abundance.

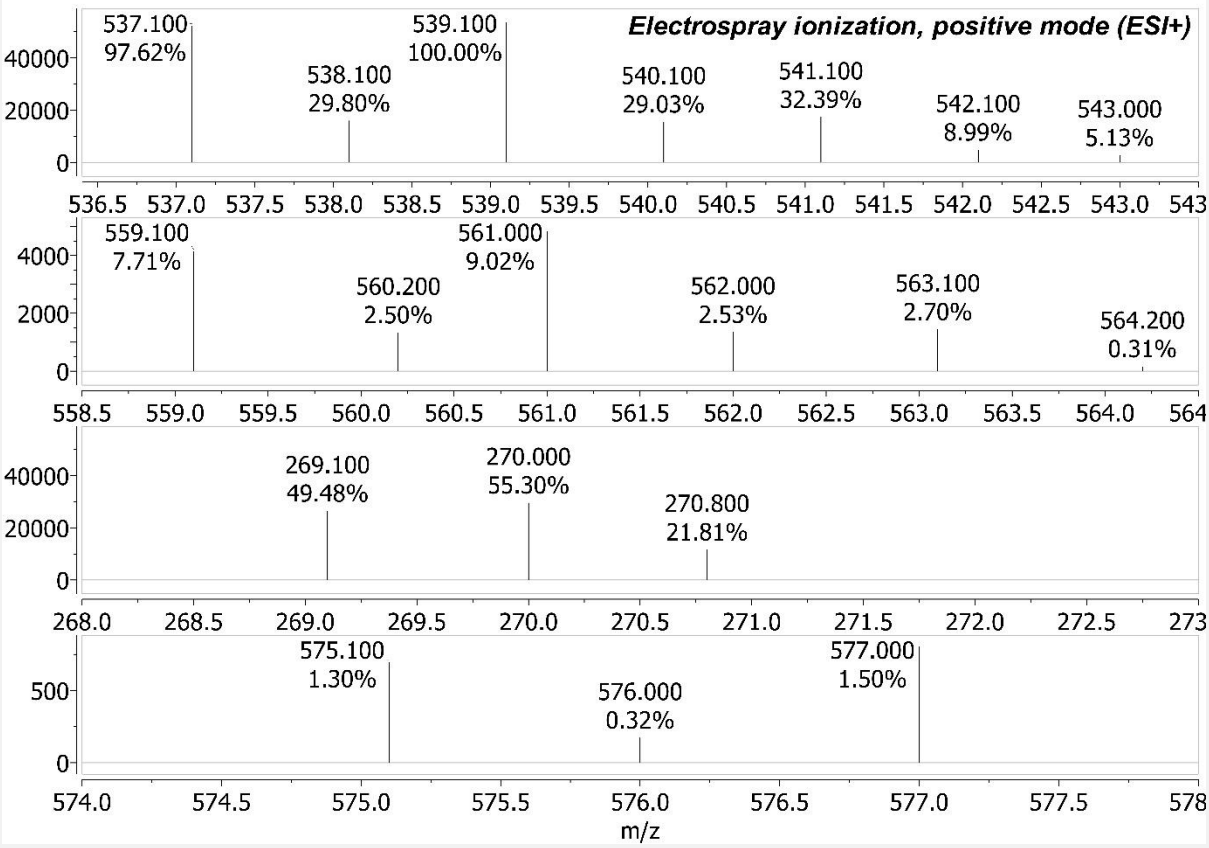

Figure 15 – Some Mass Spectrum (MS) components of Figure 14. *Upper panel*: *m/z* 537.1 $[M+H]^+$. *2nd panel*: *m/z* 559.1 $[M+Na]^+$. *3rd panel*: *m/z* 269.1 $[M+2H]^{2+}$. *Bottom panel*: *m/z* 575.1 $[M+K]^+$. All these Observed *m/z* are within 0.07 of Expected.

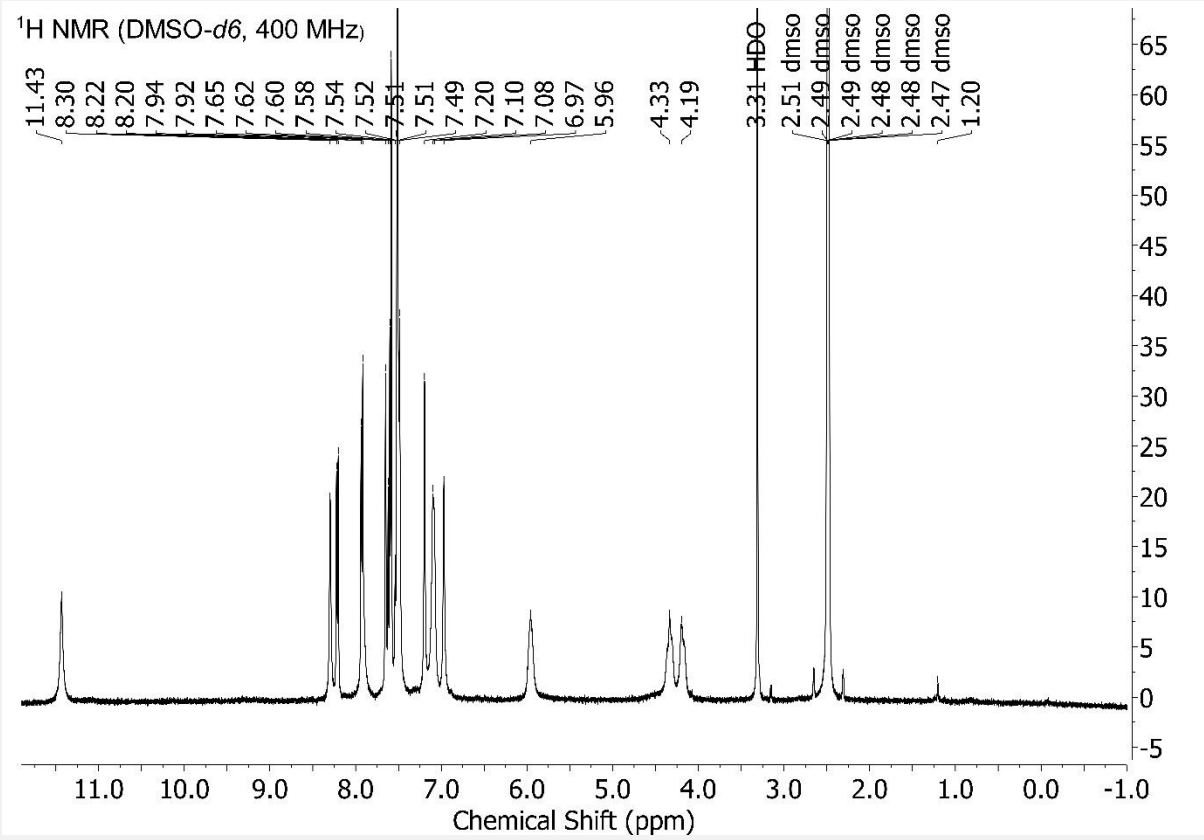

Figure 16 - ^{1}H NMR {*NMR probe temperature = 298.15 K*} for 6b sample. Scaled to the highest compound peak. Peaks identified by the "Auto peak picking" algorithm (based on Global Spectral Deconvolution, GSD) of MestReNova version 12 software. With default program settings used. And no chemical structure used/inputted to guide/constrain this peak picking.

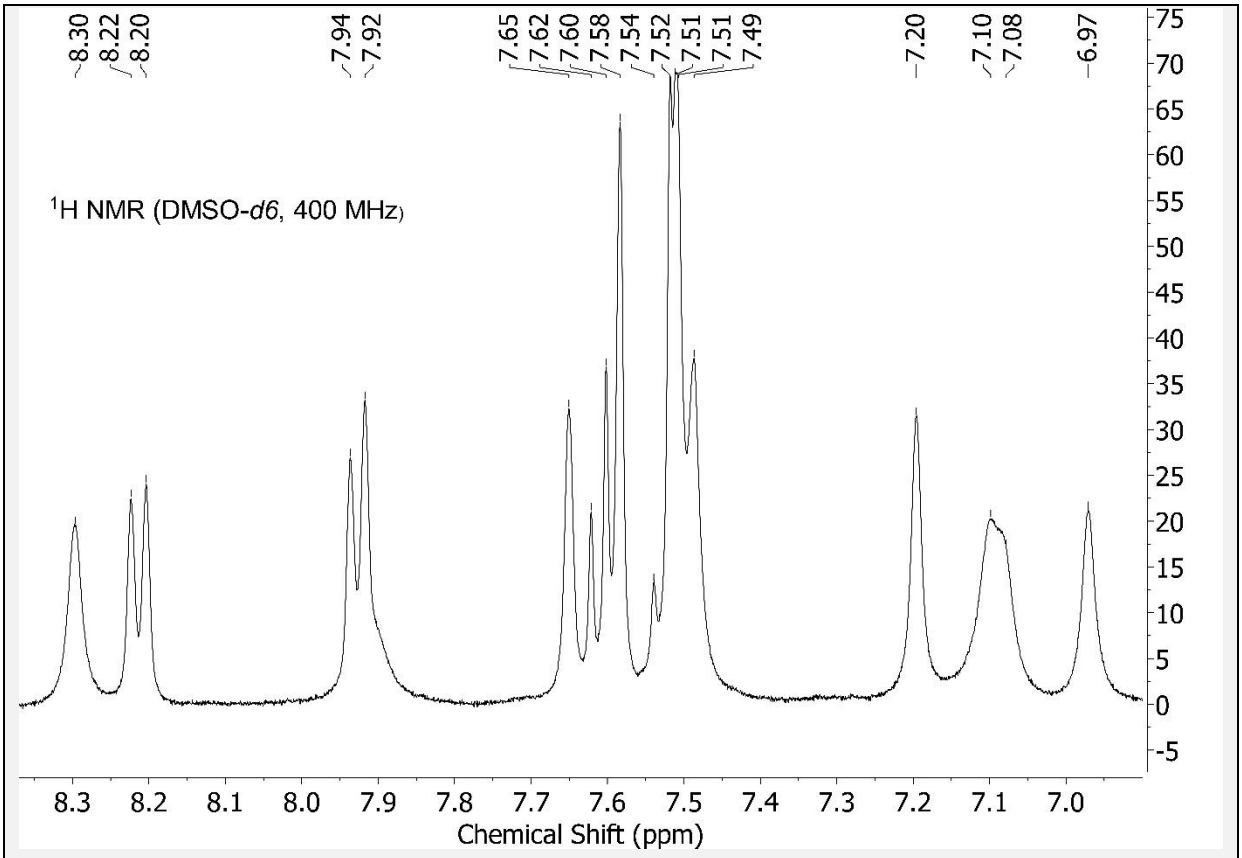

Figure 17 - Aromatic region of Figure 16 expanded.

Spectral data for 6a

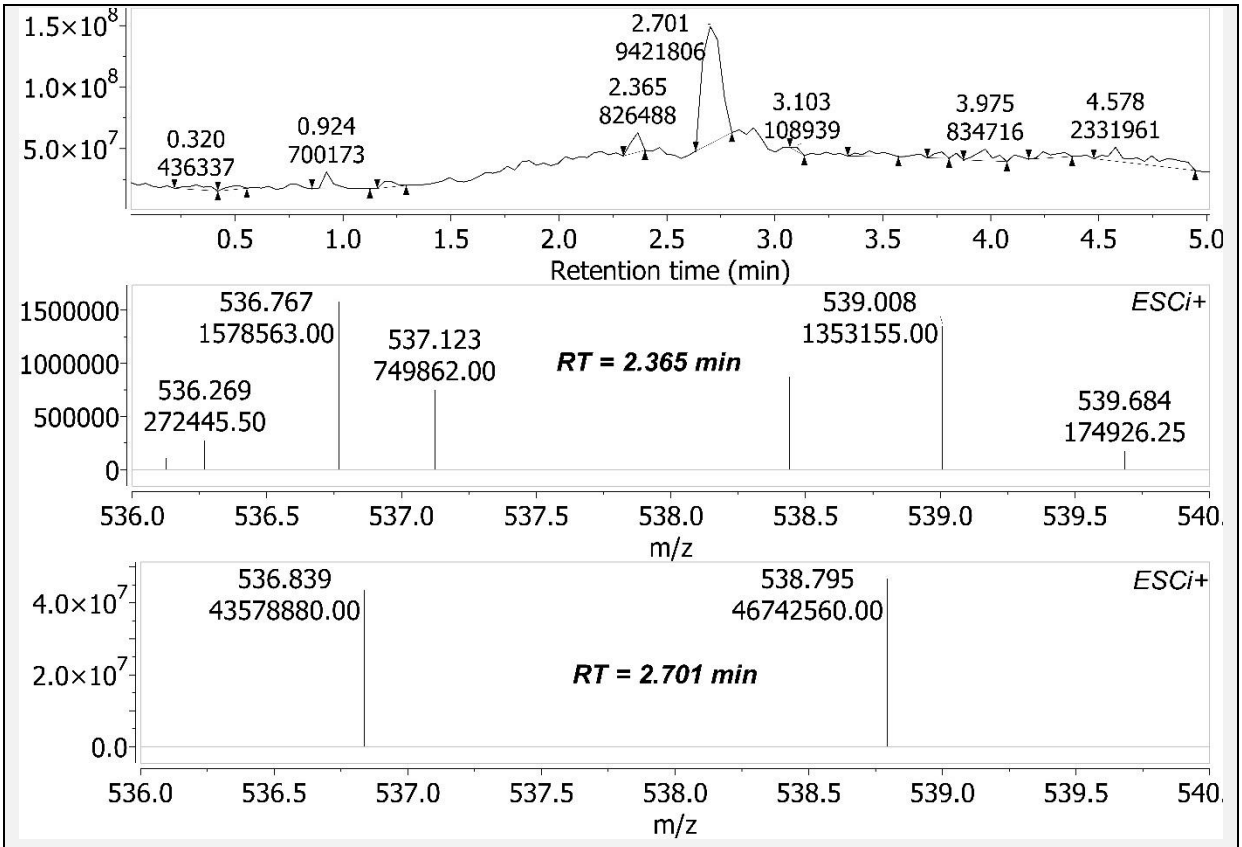

Figure 18 - Chiral SFC-MS of 6a sample. *Upper panel*: Chiral-SFC annotated with Retention Time (RT, minutes), and area under peak. *R* stereoisomer is found in the [RT=2.701] peak. *Middle panel*: Component of the Mass Spectrum (MS) of the [RT=2.365] peak. *Bottom panel*: Component of the Mass Spectrum (MS) of the [RT=2.701] peak. Therein is *m/z* 536.839 $[M+H]^+$ (*0.19 removed from Expected. Better concordance in subsequent spectra*). Using this present figure, *R* stereoisomer excess (%) in this sample = (435788880/(435788880+1578563))*100 = 99.64%; enantiomeric excess (ee) = (99.64-50)*2 = 99.28%.

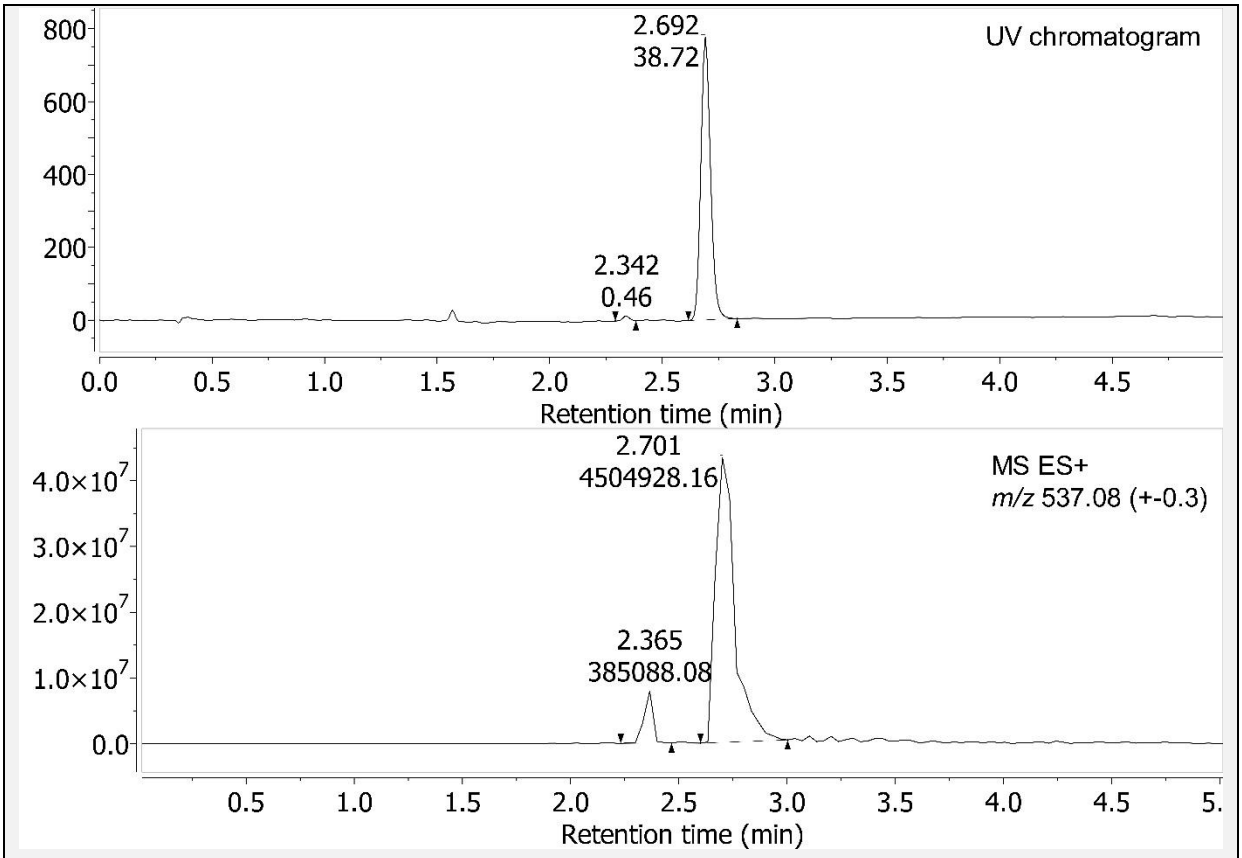

Figure 19 – Chiral-SFC of 6a sample. Using the UV Chromatogram component, *R* stereoisomer excess (%) in this 6a sample = (38.72/(38.72+0.46))*100 = 98.83%; enantiomeric excess (ee) = (98.83-50)*2 = 97.66%.

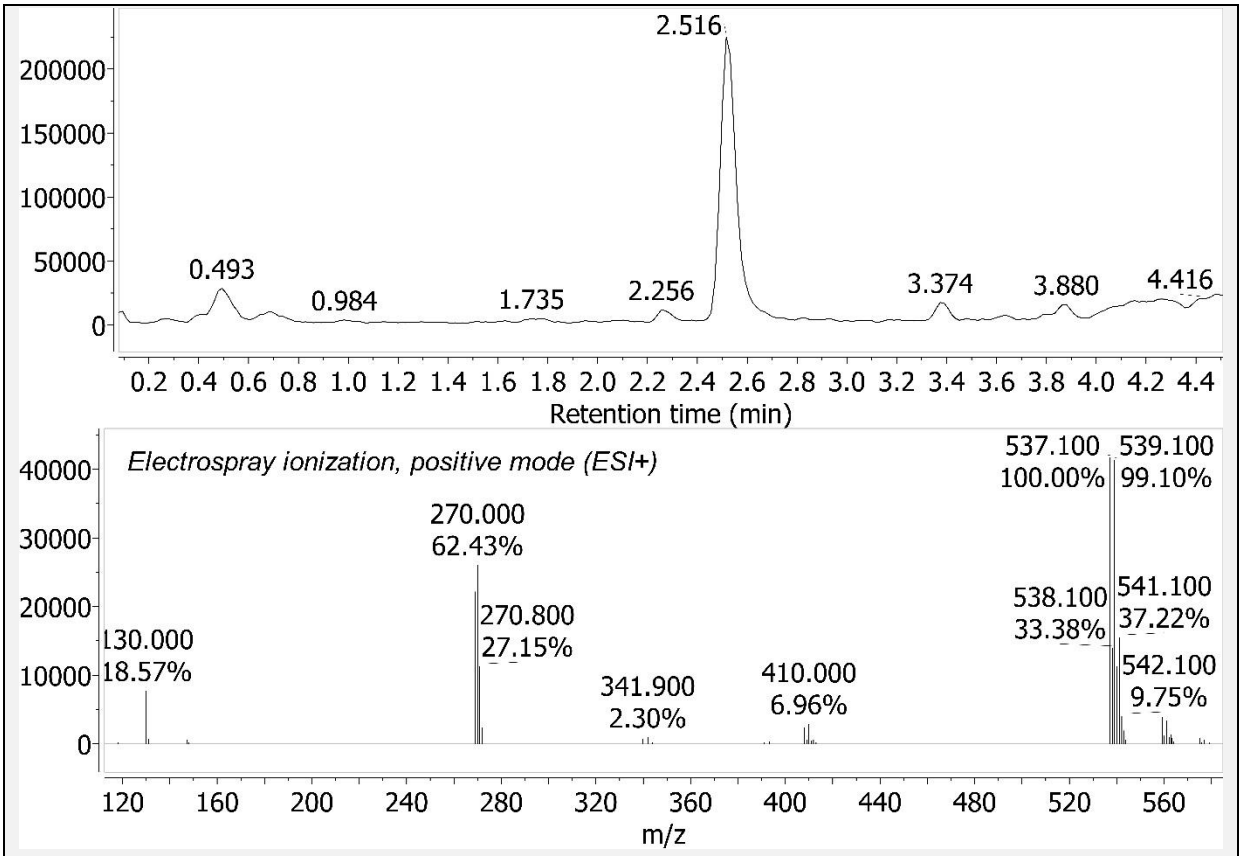

Figure 20 – LC-MS spectrum for 6a sample. *Upper panel*: Liquid Chromatography (LC) Retention Time (RT) = 2.516 minutes. *Lower panel*: Mass Spectrum (MS) of the [RT peak=2.516].

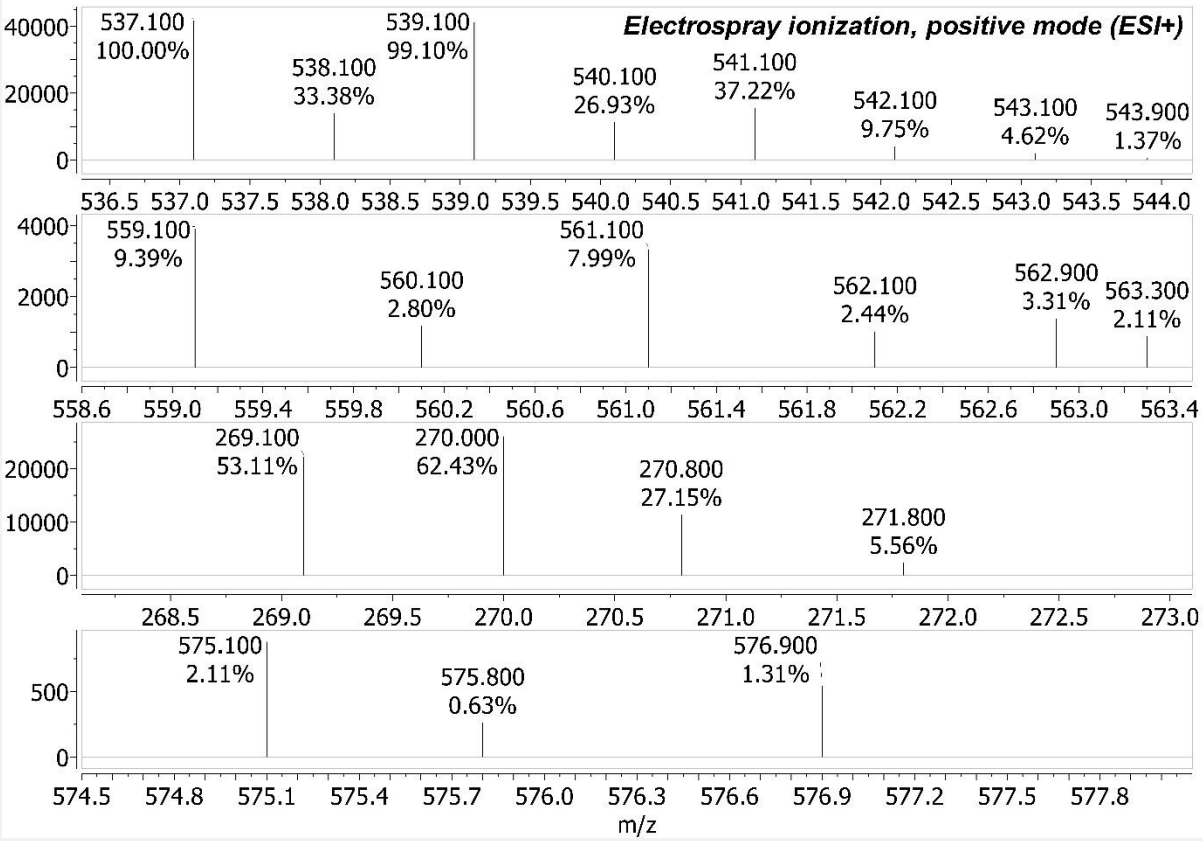

Figure 21 – Some Mass Spectrum (MS) components of Figure 20. *Upper panel*: *m/z* 537.1 $[M+H]^+$. *2nd panel*: *m/z* 559.1 $[M+Na]^+$. *3rd panel*: *m/z* 269.1 $[M+2H]^{2+}$. *Bottom panel*: *m/z* 575.1 $[M+K]^+$. All these Observed *m/z* are within 0.07 of Expected.

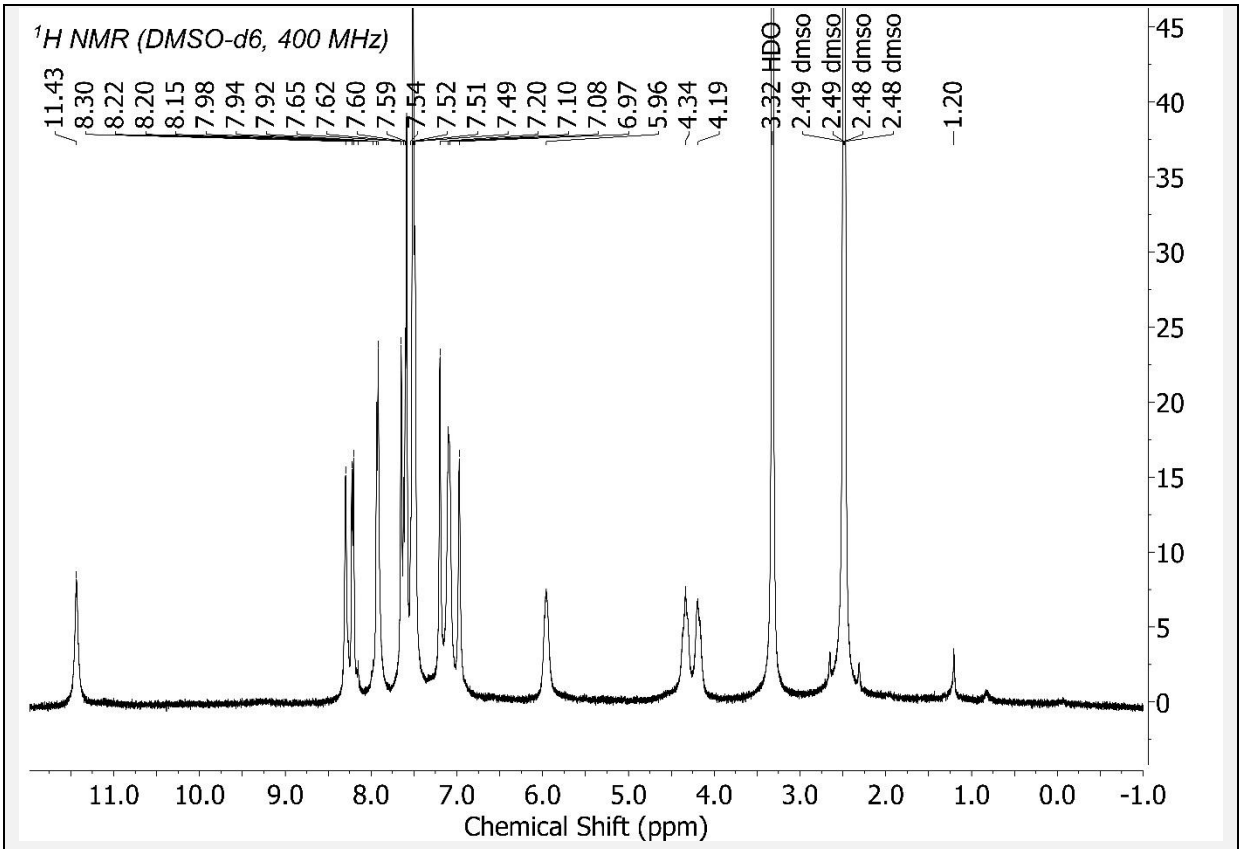

Figure 22 – ^{1}H NMR {*NMR probe temperature = 298.15 K*} for 6a sample. Scaled to the highest compound peak. Peaks identified by the "Auto peak picking" algorithm (based on Global Spectral Deconvolution, GSD) of MestReNova version 12 software. With default program settings used. And no chemical structure used/inputted to guide/constrain this peak picking.

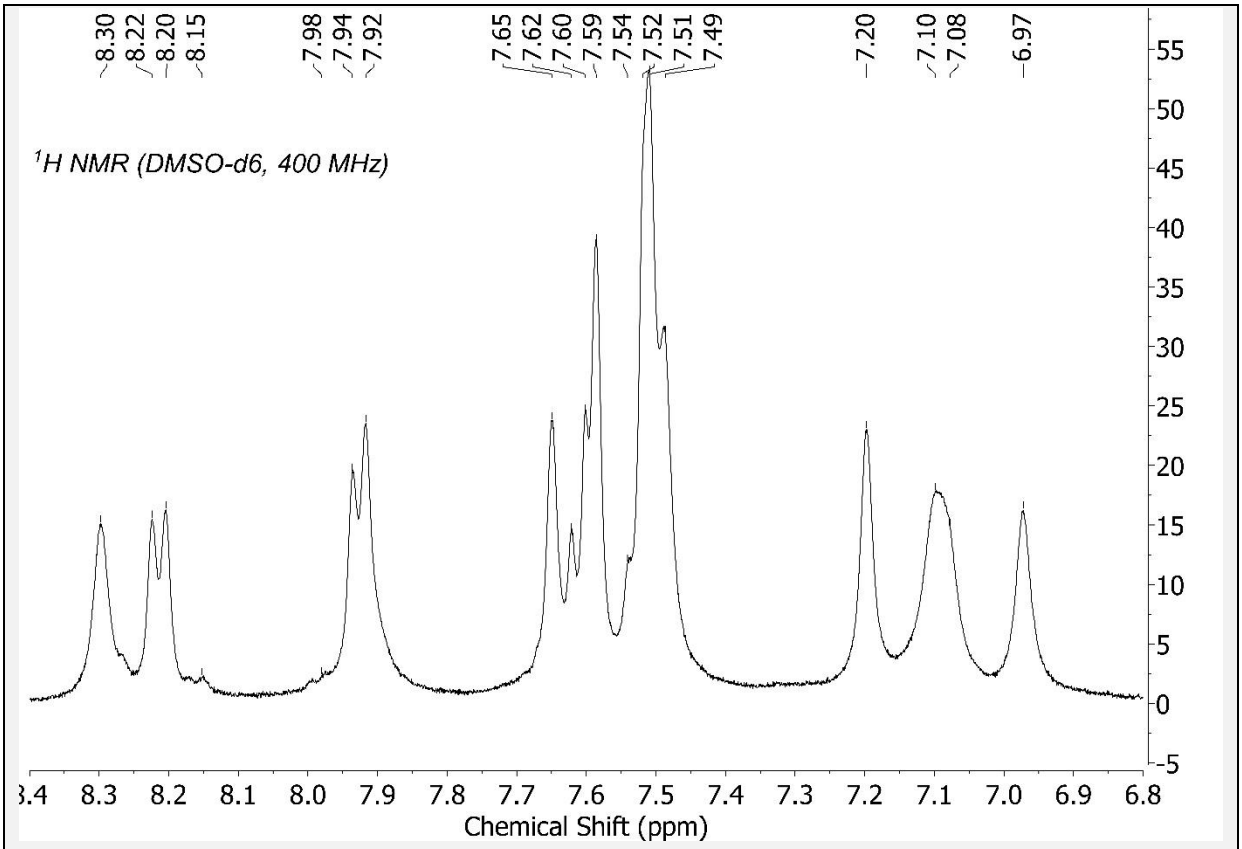

Figure 23 - Aromatic region of Figure 22 expanded.

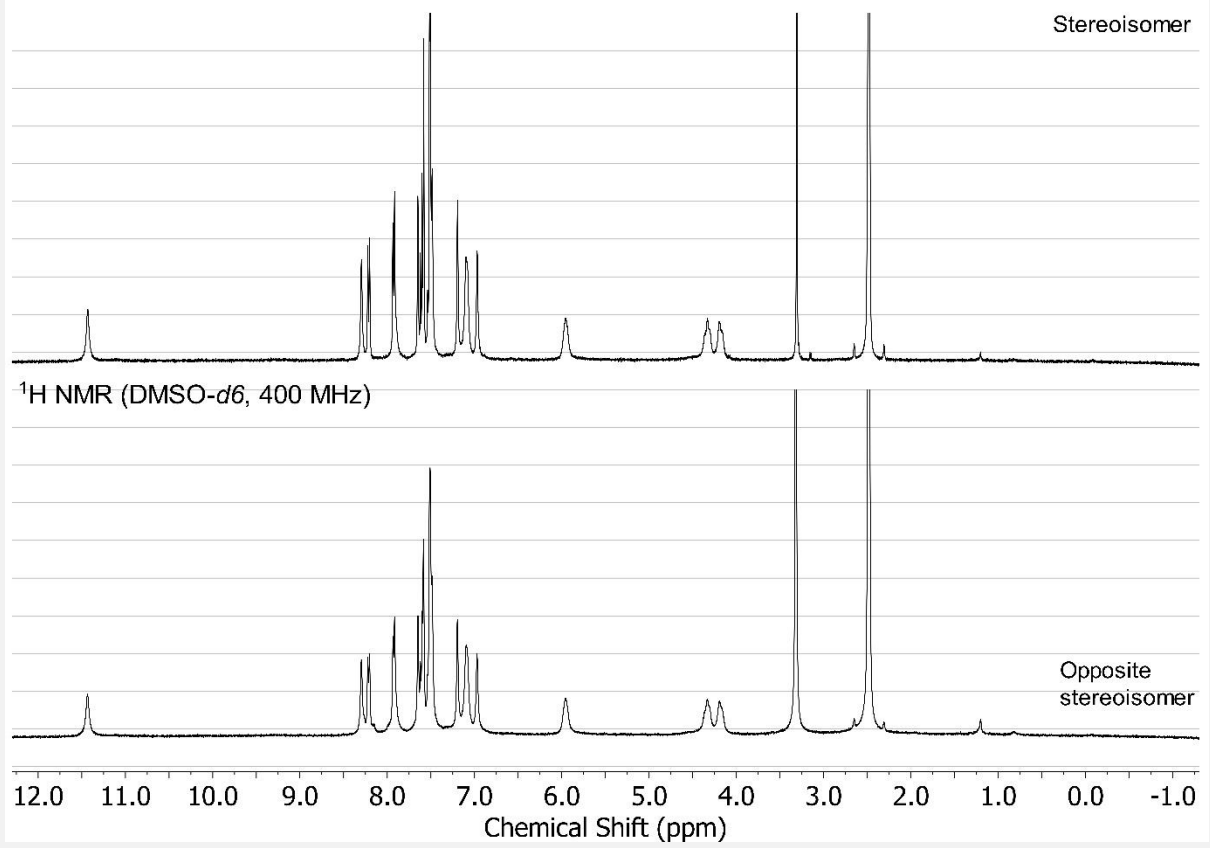

Figure 24 - 6b data in upper panel, 6a data in lower panel.

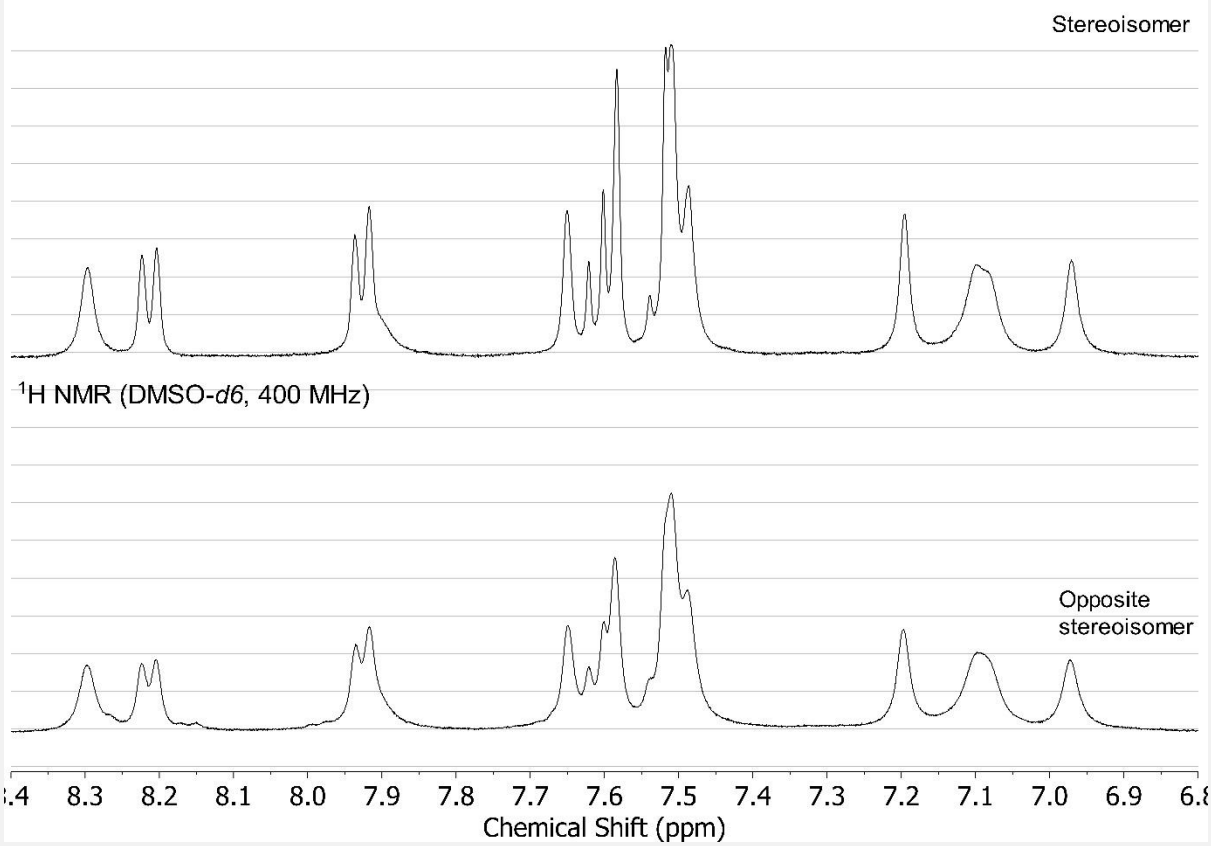

Figure 25 - Aromatic region: 6b data in upper panel, 6a data in lower panel.

6b drug administered to mice (*generating Figure 1*)

Four female C57BL/6 strain mice (*Mus Musculus*) were sourced from Shanghai Lingchang Bio-Technology Co. Ltd. They were 12-14 weeks old on the day of the rectal temperature recording experiment. Their care and use was in strict accordance with the regulations of the Association for Assessment and Accreditation of Laboratory Animal Care (AAALAC). Some details of their care: *ad libitum* Co^{60} irradiation sterilized dry granule food, reverse osmosis autoclaved drinking water, corn cob bedding, polysulfone individually ventilated cage (IVC, containing up to 5 animals): 325 mm*210 mm*180 mm, 12 hour light/dark cycle, 40-70% humidity, 20-26°C room temperature.

StudyDirector™ software (Studylog Systems, Inc. CA, USA) was used to allocate/randomize control/treatment groups. Mice were marked by ear coding (notch).

When recording rectal temperature, care was taken to ensure constant depth of probe insertion across different recordings. Time was afforded for rectal probe temperature to equilibrate with rectal temperature. And time was afforded between recordings for probe

temperature to reset. The rectal temperature recording experiment was started between 8 and 9 am.

Intravenous (IV) administration (tail vein): dosing volume per weight of drug = 10 µl/g, solution (not suspension). Sterilised (0.22 µm filter), vortexed vehicle = 12.5% solutol, 12.5% ethanol, 75% water. IV solutions freshly prepared before injection.

The two mice intravenously injected with 20 and 40 mg/kg drug doses both exhibited hypoactivity and tachypnea. Which are both signs of hypothermia [121], coinciding with their rectal temperature drop to below 30°C. 210 minutes (3.5 hours) after the intravenous injection of 20 mg/kg, that mouse died ("choked when drinking water" was the reported observation by the experimenter. Reason/how is unknown. Possibly the ingested water {at room temperature} reduced the mouse's body temperature further towards room temperature). The mouse injected with 40 mg/kg was found dead the next day. The mouse injected with 2 mg/kg survived, and was sacrificed 54 days later. 24 hours post the IV injection, its rectal temperature was 39.99°C, compared to 39.48°C in the control (vehicle administered) mouse. So, the (intravenous) Maximal Tolerated Dose (MTD) in mice is definitely greater than 2 mg/kg, and possibly less than 20 mg/kg. Demonstrated, it is an active, potent drug *in vivo*. A prediction is that the MTD would be greater if the ambient temperature was safely higher. For example, it would be higher if the ambient temperature was instead 30°C. Even higher if it was 34°C, and higher still if 37°C. *See # below*.

A (unfortunate, but mice sparing) confounding issue is that in the 43 days preceding the rectal temperature recording experiment (which was conducted on day 44) the mice were used in a different experiment. A dose escalation study of a different chemical entity. Of the same chemical formula, but the opposite stereoisomer thereof (*R*), in enantiomeric excess (≥97%): 6a in the synthesis scheme presented earlier. Which, unlike 6b, does *not* inhibit F_1F_0 ATP hydrolysis (6b EC_{50} F_1F_0 ATP hydrolysis = 0.018 µM, 6a EC_{50} F_1F_0 ATP hydrolysis > 100 µM [3]). This experiment sought the Maximal Tolerated Dose (MTD) in mice of 6a. Wherein the control mouse was always administered vehicle, and the three test mice were administered an escalating 6a dose amount every 3 days, ultimately reaching 40 mg/kg. The final dose of 6a was on day 39, wherein the highest dose given then was 2 mg/kg (ran out of 6a and so doses were low on that last day). So, the MTD was not successfully found for 6a. More details of these experiments can be found in my US patent application [3].

Incidentally, by way of comparison, in mice, the intravenous LD_{50} (dose that kills 50% of the cohort) for the FDA approved anti-depressants, clomipramine HCl and imipramine HCl, is 22

and 27 mg/kg respectively (Register of Toxic Effects of Chemical Substances, RTECS). Some human patients take these drugs daily, safely, for years.

 # Incidentally, it is widely underappreciated that laboratory mice should probably be kept at a higher than typical room temperature. Typical room temperature (~21°C) is thermoneutral for us humans (in clothes). But it isn't for mice. Whose thermoneutral temperature is instead ~32°C [122]. So, nearly all mouse studies in the literature are performed with cold stressed mice (!). To house mice at a higher than room temperature, their cages can be placed in plant growth incubators, e.g. as made by Thermo Fisher Scientific Inc. Or there are various veterinary incubator options, e.g. animal Intensive Care Unit (ICU) incubators, e.g. as made by Darwin Chambers Inc., Powers Scientific Inc, Brinsea Products Ltd, Lyon Technologies Inc. etc. Or the mice can be housed in water proof mouse cages submerged in fish tanks, which are heated by thermostatic electric fish tank heaters [123]. Or normal mouse cages can be heated with chemical reaction hand warmers [124-125]. Or the entire room that the mouse cages are in can simply be set at a higher temperature. The expense of this temperature management is probably less if the experiment is performed in an equatorial climate, e.g. in Singapore. There is likely a business opportunity/niche for a Contract Research Organization (CRO), possibly equatorially/tropically located (optionally subterranean, so buffered from the colder temperatures of storms), that can perform mice studies at a temperature closer to their thermoneutral temperature.

Generating Figure 2

For each species, the F_1F_0 ATP hydrolysis data herein is from Sub-Mitochondrial Particles (SMPs). Produced by sonicating mitochondria, which were isolated from ischemic heart tissue. Ischemia, by collapsing the proton motive force (pmf), causing a lower pH in the mitochondrial matrix, increases the active fraction of IF1 protein. Which comprises IF1 protein monomers and dimers, which *can* bind ATP synthase [2]. As opposed to IF1 protein tetramers, and higher oligomers, which cannot. Ischemia ensures that a large proportion of IF1 protein complexes with the membrane bound ATP synthase. Which means that more IF1 protein is retained/available after the subsequent SMP generation protocol. SMPs are inside-out (inverted). With the mitochondrial matrix side of the membrane, and so the ATP hydrolysing and IF1 binding modules of ATP synthase, on their outer face. So, IF1 protein is wanted on the outside, not on the inside, of the SMPs. Prior ischemia, which combines IF1 protein with the mitochondrial matrix side of ATP synthase, assists this. Moreover, (at least

some of) this activated IF1 protein fraction carries over into the start of the subsequent F_1F_0 ATP hydrolysis assay (conducted at pH 7.8, for 5 minutes). So best showcasing differences in IF1 protein activity between different species. Rendering them detectable by the resolution of this experiment. Where (to hypothesize) the differences in IF1 protein activity, driving differences in F_1F_0 ATP hydrolysis, comprise differences in IF1 protein amount (versus ATP synthase amount), IF1 protein inhibitory potency for F_1F_0 ATP hydrolysis, and IF1 protein tendency/self-affinity for tetramerization and higher oligomerization (self-sequesteration) at non-acidic pH. This F_1F_0 ATP hydrolysis data was sourced from [29] (column titled "Ischemic" in its Table 1), along with its heart rate and body mass data therein. Maximum lifespan data was sourced from the AnAge database [5]. Specific basal metabolic rate data herein, for each cited species, is the mean of values for that species sourced from AnAge [5] and the landmark papers by Max Kleiber in 1932 and 1947 [36-37], which set out Kleiber's Law. But the specific basal metabolic rate of rat value from [37] was omitted from this mean, because its value is not from an adult. Further incorporated into the mean of mouse is the value of 0.0092125 W/g (sourced at ambient [thermoneutral] temperature of 32°C, for C57 mouse strain) from [126]. Further incorporated into the mean of rat is the value of 0.005695 W/g (sourced at ambient [thermoneutral] temperature of 28°C) from [127]. For converting O_2 consumption into energy I used [1 ml O_2 = 20.1 Joules], which is a well-known conversion factor, e.g. as used by [122, 127].

Best fit lines were calculated by OriginPro 8 software (OriginLab Corporation, Northampton, MA, USA), using its "Fit Linear" functionality. Which uses linear regression, with least squares estimation.

Marrying data

In Figure 2, body mass data and data in the 1st (top) and 3rd panels is from [29], data in the 2nd and 4th panels is from the AnAge database [5] (*the 2nd panel incorporates further data from other sources, as specified above*). This data combination, and its interpretation here, is novel. There was some (enduring) margin for error in marrying these data sets because [29] uses imprecise terms such as sheep, hamster etc., wherein there are a number of different species in [5] that can fall into these categories. But a common sense alignment was applied in each case, by estimating which species [29] likely had easiest access to, so most likely used, and so most likely refers to. So, utilizing this estimation, the 12 species that Figure 2 herein refers to are: cow (domestic cattle, *Bos taurus*), mouse (house mouse, *Mus musculus*),

rat (brown rat, *Rattus norvegicus*), hamster (golden hamster, *Mesocricetus auratus*), guinea pig (*Cavia porcellus*), pigeon (common wood-pigeon, *Columba palumbus*), chicken (*Gallus gallus*), rabbit (European rabbit, *Oryctolagus cuniculus*), sheep (domestic sheep, *Ovis aries*), pig (*Sus scrofa domesticus*), dog (*Canis lupus familiaris*) and human (*Homo sapiens*). Although an acknowledged, reasonable possibility is that the pigeon species that [29] used was instead the rock pigeon (*Columba livia*). Which I discuss later on, in the section titled "Birds".

Data from [5] was sourced primarily in August 2018. Which is when the kernel (e.g. Figure 2) of this work was done.

Omitting human maximal lifespan

Herein, the maximum lifespan of human from [5] (122.5 years) isn't shown in any of the figures. Nor utilized in any of the calculations, e.g. not used in any of the Pearson (or Spearman's rank) correlation coefficient calculations to maximal lifespan. Because (arguably) this value isn't fairly comparable to the maximal lifespan values used. Because (*a*) modern medicine is disproportionally applied to humans, (*b*) many modern humans live in shelter and comfort (*and* with complete freedom and stimulation, unlike an animal in a zoo for example), and (*c*) the verifiable lifespan data set for humans is very much larger, with so many countries recording births and deaths (the bigger the data set, the greater the chance a higher maximum lifespan will be found). So, compared to the human number, which is drawn from a huge sample size, the other numbers, drawn from small sample sizes, are likely to be an underestimate of species maximal lifespan. Human could perhaps be more comparably incorporated by using a maximum lifespan record from a smaller human data set. To mirror the small data sets for the other species. Preferably wherein this data set comes from humans living in the past, e.g. from 1881 Germany, where life expectancy of men and women was 35.6 and 38.5 years respectively (Statistisches Bundesamt Deutschland, www.destatis.de). However, omission was chosen instead.

Chicken maximum lifespan

The AnAge database [5] states 30 years for the maximal lifespan of chicken (red junglefowl, *Gallus gallus*). *But* in the "Observations" section of this database entry, AnAge says that this "remains unproven. For comparative analyses the use of a more conservative value for maximum longevity, such as 15 or 20 years, is recommended". I split the difference, between 15 and 20, and use 17.5 years.

Raw (unlogged) data used to produce Figure 2

	Body mass	Specific F1F0 ATP hydrolysis	Specific basal metabolic rate	Heart rate	Maximum lifespan
Cow	500	1.32	0.000798458	50	20
Pig	100	0.81	0.000771	73	27
Human	90	1.31	0.001164574	69	Unused
Sheep	60	1.49	0.001319925	75	22.8
Dog	25	1	0.001804232	85	24
Rabbit	2	1.12	0.002887816	213	9
Chicken	2	2.89	0.002418352	318	17.5
Pigeon	0.6	2.66	0.004975053	305	17.7
Guinea Pig	0.4	2.71	0.003740752	265	12
Rat	0.2	3.02	0.00601463	481	3.8
Hamster	0.1	3.9	0.006377	400	3.9
Mouse	0.025	2.73	0.010858546	618	4

Specific F_1F_0 ATP hydrolysis (μmol/min/mg) data is from [29] (column titled "Ischemic" in its Table 1). Body mass (kg) and heart rate (bpm) data is also from [29] (Table 3 therein). Maximal lifespan (years) data is from [5]. Specific basal metabolic rate (W/g) data is the mean of data from [5], [36-37], [126], and [127]: a compilation of sources because no single source has data for all the investigated species. The mean specific basal metabolic rate data in the table above is calculated from its source papers as shown in the subsequent table, where [α] is [5], [β] is [36], [γ] is [37], [δ] is [126], and [ε] is [127]. The specific basal metabolic rate of rat value from [37] is omitted, because its value is not from an adult. With data from [126] and [127], for converting O_2 consumption into energy I used [1 ml O_2 = 20.1 Joules], which is a well-known conversion factor, e.g. as used by [122, 127].

	[α]	[β]	[γ]	[δ]	[ε]	Mean
Cow	0.000884	0.000759568	0.000751805			0.000798458
Pig	0.000771					0.000771
Human	0.001183	0.001195378	0.001115345			0.001164574
Sheep		0.001296472	0.001343377			0.001319925
Dog		0.001745968	0.001862497			0.001804232
Rabbit	0.003411		0.002364633			0.002887816
Chicken	0.002216	0.002620705				0.002418352
Pigeon		0.004975053				0.004975053
Guinea Pig	0.003333		0.004148504			0.003740752
Rat	0.006786	0.00556289	Omitted		0.005695	0.00601463
Hamster	0.006377					0.006377
Mouse	0.015056		0.008307139	0.0092125		0.010858546

Figures 3 and 7 use the same raw data as Figure 2, except without the body mass data.

My workings to get to the 0.0092125 W/g figure from [δ] [126]: from its Table 3, ignoring error bars, for the C57 mouse strain, at an ambient temperature of 32°C (which is the ambient temperature with the lowest O_2 consumption on this line of table. And so, out of the ambient temperatures tested at, this one is most likely closest to, or possibly even at, the C57 mouse's thermoneutral temperature. The thermoneutral temperature of mice is known to be at/around 32°C, e.g. refer Fig. 5 in [122]), O_2 consumption = 1.65 cc/g/hour, where "cc" is cubic centimetre (cm^3), (*to get into kg, which is the SI unit of mass*) *1,000 = 1,650 cm^3/kg/hour = (*because 1 cm^3 = 1 ml, and 1 ml O_2 consumption = 20.1 Joules* [122]) 33,165 J/kg/hour = (*because power = energy/time = J/s; 60*60 seconds in 1 hour*) 33,165/(60*60) = 9.2125 W/kg = 0.0092125 W/g.

My workings to get to the 0.005695 W/g figure from [ε] [127]: from the first line of its Table 1, which refers to BMR (=Basal Metabolic Rate), sourced at an ambient temperature of 28°C (at/around the thermoneutral temperature of a rat [127]), for the Simonsen (Sprague-Dawley derived) rat strain, O_2 consumption = 17 ml/kg/minute = (*because 1 ml O_2 consumption = 20.1 Joules* [122, 127]) 341.7 J/kg/minute = (*because power = energy/time = J/s; 60 seconds in 1 minute*) 341.7/60 = 5.695 W/kg = 0.005695 W/g. Which actually corresponds well with the value given for specific metabolic rate on the same line of the same table = 5.7 W/kg.

The conversion algorithm I used for data from [36] and [37]: starting with metabolic rate per day (Kcal) and body weight (kg): converted kcal to calories, converted calories to Joules, divided this by body weight (kg) to get in J/kg/day, (*because power = J/s*) divided by number of seconds in a day (24*60*60) to get in W/kg, then /1000 to get in W/g.

Data was drawn from Table 1 of Kleiber's 1932 paper [36]: from its "W Average weight, kilo-grams" and "Cals. per 24 hrs. per animal" columns. In my calculations, an error in this paper was corrected: the table actually reports kilocalories (kcal), not calories as it purports. This error is evident, for example, when comparing the data (e.g. for woman) of Kleiber's 1932 [36] and 1947 [37] papers (which report independent data sets: "No data were used that were already incorporated in the earlier study (1932)" [37]). The latter's Table 2, where the unit of its "Metabol. rate per day" column is correctly labelled kcal. The unit error is identified to be with the 1932, rather than the 1947 paper, because I know the order of magnitude of calories that a person needs per day, even if inactive, is thousands of

kilocalories. For example, from the National Health Service (NHS) website: "As a guide, an average man needs around 2,500 kcal (10,500 kJ) a day to maintain a healthy body weight. For an average woman, that figure is around 2,000 kcal (8,400 kJ) a day" [149].

Note, to relay a possibly confounding issue in the data sourced from [36]: quoting [36]: "The relatively low value of the hen may be in connection with the fact that the determinations had been made in darkness".

Note that, in at least some cases, a specific basal metabolic rate value sourced from [5] is a mean of values sourced from a number of different sources ("if more than one pair of values was available, the logarithmic average was used. If discrepancies were noticed between two or more pairs of values, then only the most recent pair was used" [128]). But none of these sources include any of [36], [37], [126], [127]. So, these are all independent data sources. At least for now. But these paper values may well get incorporated into the means of the [5] database, called the AnAge (Animal Ageing and Longevity) database, in the future.

Normality of data

Kolmogorov-Smirnov Test of Normality (D)		p-value	Verdict		
Specific F1F0 ATP hydrolysis	0.22906	0.48489	Normal		
Specific basal metabolic rate	0.17987	0.77037	Normal		
Heart rate	0.23315	0.46279	Normal		
Maximal lifespan	0.17922	0.81215	Normal		
Normal = data does not differ significantly from that which is normally distributed					

Spearman

Correlations were assessed using the Pearson correlation coefficient (R), which assays for a *linear* correlation (change in *x* associated with a *proportional* change in *y*). By contrast, Spearman's rank correlation coefficient (ρ) assays for a *monotonic* correlation (change in *x* associated with a proportional, *or non-proportional*, change in *y*). It using the ranked values for each variable rather than the raw data. For comparison, for the data used to produce Figure 3, the following table presents Spearman's rank correlation coefficients, and associated p-values (one-tailed, because each alternative hypothesis is directional), for its inter-relations:

Spearman's rank correlation coefficient (ρ)				
	Specific basal metabolic rate	Heart rate	Maximal lifespan	
Specific F1F0 ATP hydrolysis	0.75525	0.78322	-0.80909	
	Specific basal metabolic rate	0.93007	-0.86364	
		Heart rate	-0.82727	
p-value (one-tailed)				
	Specific basal metabolic rate	Heart rate	Maximal lifespan	
Specific F1F0 ATP hydrolysis	0.002254	0.001293	0.0012795	
	Specific basal metabolic rate	0.000006	0.000306	
		Heart rate	0.0008385	
Asymptotically exact harmonic mean p-value for combining independent/dependent tests				
Of all the p-values above (in this present table) = 0.00003467136 = **0.00003**				
Fisher's combined probability test				
Using p-values for [Specific F1F0 ATP hydrolysis vs. Maximal lifespan] (=0.0012795) &				
[Heart rate vs. Specific basal metabolic rate] (=0.000006) = 0.0000002				

Heart rate

Heart rate values were sourced from [29]. For species with a range of values disclosed therein, the middle value of the range was taken. This heart rate data comes from conscious animals, *except* for hamster: its values are from anesthetized animals. This disparity was ignored. But if instead it isn't, this can increase at least some of the correlations to heart rate, and their statistical significance. The anesthetized heart rate range for hamster in [29] is 375-425. And the value drawn was 400. But if the upper bound value is taken instead, 425, then at least some of the investigated Pearson correlation coefficient (R) values relating to heart rate are increased, and their associated (one-tailed) p-values decreased, i.e. increased statistical significance:

		Specific F1F0 ATP hydrolysis	Specific basal metabolic rate	Maximal lifespan	log10(Body mass)
Heart rate	R	0.8139	0.9476	-0.8648	-0.9439
	p	0.000637	0.0000015	0.000295	0.000002

Birds

Conceptually, a different way to decrease ROS generation is, instead of (or in addition to) reducing metabolic rate and O_2 consumption rate, modifying the respiratory chain such that it fumbles a lower percentage of the electrons it passages (i.e. increased efficiency) [129]. Some species, possibly at least some bird species, may have availed themselves of such increased efficiency. For example, there is data suggesting that the particularly long-lived (for its size) pigeon species, *Columba livia*, has such increased efficiency [130]. An observed strategy, for increased efficiency, is to reduce the amount of Complex I [131-134].

Moreover, long-lived (for their size) bird species' membranes (e.g. the mitochondrial inner membrane) tend to have less propensity to amplify ROS damage (wherein lipid peroxidation PUFA products are themselves ROS, which can attack further PUFA molecules, a chain reaction, which can go on to damage other cellular components, e.g. membrane proteins, mtDNA) because their polyunsaturated fatty acids (PUFAs) tend to have less double bonds [135-140].

To generate the principal correlative Results of this paper I used data from [29], which was published 34 years ago. Including its data from pigeon. But [29] doesn't specify which particular pigeon species it used. I made the estimation that [29] used the common wood pigeon (*Columba palumbus*), which has a maximal lifespan of 17.7 years [5]. Although I concede that [29] may instead have used the rock pigeon (*Columba livia*), which has a very different maximal lifespan. Of 35 years [5]. So, nearly twice as long. Given this uncertainty, I reason that a maximal lifespan of 17.7 years (that for *Columba palumbus*) is the best value to use for pigeon, by the balance of probabilities, as I explain later. And so this is the maximal lifespan that I allocated to pigeon. Which is of the order of the maximal lifespan (in brackets after each name) of most other pigeon and dove {Columbidae family} species in [5]: *Leucosarcia melanoleuca* (16.3), *Patagioenas leucocephala* (14.4), *Columba oenas* (12.6), *Cepphus Columba* (15.2), *Caloenas nicobarica* (20.5), *Patagioenas fasciata* (18.5), *Streptopelia decaocto* (17.9), *Streptopelia risoria* (12), *Streptopelia turtur* (13.2), *Columbina passerina* (7.2), *Streptopelia chinensis* (9.8), *Geopelia striata* (14), *Leptotila verreauxi* (8.6), *Columbina inca* (13.3). ***But*** there are three longer-lived, outlier species: *Columba livia* (35), *Zenaida macroura* (31.3), *Zenaida asiatica* (25) [5]. The particularly long-lived *Columba livia* (*particular breed thereof unspecified*) has been shown to have low Complex I content, in the aforementioned [131]. And a low number of double bonds in its PUFAs, in the aforementioned [136-137]. If [29] used *Columba livia*, which is more of an outlier species, living longer (maximal lifespan of 35 years) for its size, instead of *Columba palumbus*, then the Pearson correlation coefficients (R, and their p-values, one-tailed because each alternative hypothesis is directional) are as follows: wherein the second line of R shown is if pigeon is omitted from the data set, and the third line of R shown is if the other bird species (chicken) is omitted also, such that all the remaining species are mammals (N.B. [5] didn't, and presently {*July 2021*} doesn't, have metabolic data for any pigeon, so the specific basal metabolic rate value of pigeon [particular species unknown] is singly from [36]):

		Specific F1F0 ATP hydrolysis	Specific basal metabolic rate	Heart rate	log10(Body mass)
Maximal lifespan	R	-0.5041	-0.6008	-0.66	0.6221
	p	0.0569265	0.025307	0.013556	0.0204885
Maximal lifespan	R	-0.7535	-0.8413	-0.8744	0.8915
	p	0.005924	0.0011405	0.000467	0.0002655
Maximal lifespan	R	-0.8189	-0.8387	-0.8993	0.9042
	p	0.0034685	0.002361	0.000483	0.0004075

A complication of *Columba livia* is that there are many (hundreds of) different breeds thereof. Different "fancy pigeons". Which can be very morphologically diverse. And which, at least in some cases, have had very different maximal lifespans reported, which *may* reflect true differences in maximal lifespan. Perhaps reflecting, deliberate and/or inadvertent, artificial selection for longer lifespan in at least some breeds. For example, discussing different breeds of *Columba livia*, a Cropper pigeon reportedly lived to 35 years old, but (from the *same* source paper) the "limit of the age of the Pouter Pigeon is only 10 to 12 years, the "great proportion dying in less than half that time"" [141] (*incidentally, [141] is the {once removed} upstream source of the 35 year maximal lifespan reported for Columba livia in [5], for which [141] cites a further upstream source, dating from 1911*). Whilst as regards the original/ancestor *Columba livia*, without any breeding/selecting by man: in captivity, in Egypt, at the Giza zoo, "two Rock-Pigeons [*Columba livia*] from the Dongola Province of the Sudan lived certainly for 8 years and possibly for 12 years 10 months" [141]. In captivity, at the same location, a hybrid cross pigeon, of *Columba livia* x *Columba lumbus*, lived for 5 years, 7 months, 17 days [141]. So, it *might* be that *some* breeds of *Columba livia* have a maximal lifespan that is less than, or comparable to, that of *Columba palumbus*. Given that we don't truly know which species of pigeon [29] used, nor which breed thereof (*if* it used *Columba livia*), nor definitively how different breeds of *Columba livia* map to maximal lifespan, moreover wherein at least some bird species tend to live much/anomalously longer than similarly sized mammal species, where mammals are my primary focus, there is a case for omitting pigeon from the data/investigation. But in the Results section of this present paper, wherever a pigeon maximal lifespan is utilized/presented, a relatively conservative maximal lifespan value (17.7 years), that of a very common pigeon species (*Columba lumbus*) [5], of the order of the maximal lifespan of most other pigeon species [5], and *possibly* of *some* breeds of *Columba livia*, is used. Instead of omission.

If omission is selected instead, as shown below, the Pearson correlation coefficients (R) between maximal lifespan and the presented variables are *greater*, and some of the (one-tailed) p-values are accordingly lower (despite the smaller value of *n*):

		Specific F1F0 ATP hydrolysis	Specific basal metabolic rate	Heart rate	log10(Body mass)
WITH pigeon					
Maximal lifespan	R	-0.7192	-0.8144	-0.8572	0.8573
	p	0.0063065	0.001136	0.000373	0.000761
WithOUT pigeon					
Maximal lifespan	R	-0.7535	-0.8413	-0.8744	0.8915
	p	0.005924	0.0011405	0.000467	0.0002655

Wherein "WITH pigeon" data is that presented in the Results section herein. And "WithOUT pigeon" is the same as presented in the preceding table, in this present section.

Replication of the specific F_1F_0 ATP hydrolysis data (utilized herein) by other studies

In the table below, Paper [α] is [29] (whose data is used in the Results section of this present paper), Paper [β] is [142], Paper [γ] is [143], Paper [δ] is [144], Paper [ε] is [145], and Paper [ψ] is [146]. All these papers are from the same laboratory. But with varied authorship. Probably (at least partly) because their publication dates span 9 years. Notably, the co-author of Paper [γ] is Maynard E. Pullman, who co-discovered the IF1 protein in 1963 [147]. There are some differences in protocol between at least some of the papers. For (non-exhaustive) example, to prepare Sub-Mitochondrial Particles (SMPs), Paper [α] uses sonication only. But Papers [γ] and [ψ] use sonication *and* at least one subsequent centrifugation step. Centrifugation is for mitochondrial debris clearing, e.g. of large mitochondrial remnants and membrane fragments. But it must be implemented judiciously, lest it remove some of the IF1 protein. Confusingly, at least some of these papers use an idiosyncratic terminology. Where they refer to mitochondrial preparations that have undergone both sonication and centrifugation as Sub-Mitochondrial Particles (SMPs). Whilst referring to those that have only undergone sonication as "sonicated mitochondria". This terminology is somewhat misleading because *both* these preparations contain SMPs (it is the sonication step that breaks up the mitochondria into SMPs). A constant for the data in the table below is that the mitochondria, broken up to form SMPs, were sourced from ischemic heart tissue. If body mass is reported as a range in a source paper, I report its middle value in the table below. An uncontrolled aspect is body mass differences, in some cases large, between the different

(paper's) studies.

	Paper [α]		**Paper [β]**		**Paper [γ]**		**Paper [δ]**		**Paper [ε]**		**Paper [ψ]**	
	[A]	[B]	[A]	[B]	[A]	[B]	[A]	[B]	[A]	[B]	[A]	[B]
Cow	500	1.32										
Pig	100	0.81	17.01	1.33 (±0.15)								
Human	90	1.31										
Sheep	60	1.49										
Dog	25	1			NS	0.87 (±0.11)	30	1.12 (±0.12)	10	1.75 (±0.08)		
Rabbit	2	1.12	1	1.32 (±0.18)							1	1.18 (±0.08)
Chicken	2	2.89										
Pigeon	0.6	2.66	0.4	2.99 (±0.12)							0.6	3.35 (±0.16)
Guinea Pig	0.4	2.71	0.4	3.04 (±0.06)								
Rat	0.2	3.02	0.3	3.27 (±0.11)			0.25	2.91 (±0.24)	0.5	2.66 (±0.17)		
Hamster	0.1	3.9										
Mouse	0.03	2.73	0.025	3.31 (±0.07)								
	[A] **= Body mass (*kg*), [**B] **= F1F0 ATP hydrolysis (*μmol/min/mg*)**; NS= Not Specified											

Firstly, to compare just Paper [α] and Paper [β]. Their source papers, [29] and [142] respectively, were published 7 years apart, in different peer-reviewed journals, by the same laboratory, wherein the latter paper has two additional authors. Paper [β] specifies its tested species more precisely: *Sus scrofa* ("farm pig"), *Oryctolagus cuniculus* (rabbit), *Columba livia* (rock pigeon, Indian Fantail breed), *Cavia porcellus* (guinea pig), *Rattus norvegicus* (brown rat), *Mus musculus* (mouse). Note the large difference in pig body mass between the two studies. Where Paper [β] presumably reports upon piglets/adolescents rather than adults (I took the middle value of its weight range: "thirty-five to 40-lb. farm pigs" = 17.01 kg). Which *might* be why it reports a greater specific F_1F_0 ATP hydrolysis for pig. Because, to speculate, piglets/adolescents are smaller than adult pigs, so have a higher surface-area to volume ratio, thence require greater heat generation per unit mass, and so a faster specific basal metabolic rate, driven by greater specific F_1F_0 ATP hydrolysis.

From the table above, only using data from the lines that present data from both studies: The Pearson correlation coefficient (R) between the specific F_1F_0 ATP hydrolysis data of Paper [α] and Paper [β] is 0.98751 (one-tailed, because the alternative hypothesis is directional, p-value = 0.0001165). This is without applying the error bars. If these are instead applied, R is instead 0.97423. Ignoring the error bars, comparing the specific F_1F_0 ATP hydrolysis data of Paper [α] and Paper [β]: they are <u>*not*</u> significantly different from each other: independent (two-tailed) t-test statistic = -0.6706, p-value = 0.517661; Mann-Whitney U test (two-tailed): U-value = 9, z-score = -1.36109, p-value = 0.17384; Kruskal-Wallis test: H statistic = 2.0769, p-value = 0.14954; Levene's test of homogeneity of variance: f-ratio = 0.00078, p-value = 0.978277. If the error bar is added or subtracted (operation independently selected in each

case) from each datum of Paper [β], whichever manipulation makes each value further from the corresponding value from Paper [α], again the data sets are *not* significantly different from each other: independent (two-tailed) t-test statistic = -0.89801, p-value = 0.390289; Mann-Whitney U test (two-tailed): U-value = 8, z-score = -1.52122, p-value = 0.12852; Kruskal-Wallis test: H statistic = 2.5641, p-value = 0.10931; Levene's test of homogeneity of variance: f-ratio = 0.02019, p-value = 0.889822.

Now to compare, as regards specific F_1F_0 ATP hydrolysis, for their shared species/genera, Paper [α] with the mean of Papers [β], [γ], [δ], [ε], [ψ]. Ignoring error bars. The Pearson correlation coefficient (R) = 0.9708 (one-tailed, because the alternative hypothesis is directional, p-value = 0.0001375). These two data sets are *not* significantly different from each other: independent (two-tailed) t-test statistic = -0.60998, p-value = 0.553253; Mann-Whitney U test (two-tailed): U-value = 13, z-score = -1.40553, p-value = 0.15854; Kruskal-Wallis test: H statistic = 2.1592, p-value = 0.14172; Levene's test of homogeneity of variance: f-ratio = 0.03268, p-value = 0.859571. Incidentally, the pigeon species used by Paper [ψ] is *Columba livia* (White Carneaux breed).

IF1 protein content

Under normal conditions *in vivo*, the inhibitory capability of a species' IF1 protein population is at least a function of (*a*) how much IF1 protein it has per ATP synthase molecule, (*b*) how potently (how much inhibition, per unit amount) its IF1 protein can inhibit *its* F_1F_0 ATP hydrolysis, and (*c*) it's IF1 protein's tendency/self-affinity for tetramerization and higher oligomerization (self-sequesteration) at the alkaline pH of the mitochondrial matrix. Assaying, at pH 7.8, for 5 minutes, F_1F_0 ATP hydrolysis in Sub-Mitochondrial Particles (SMPs), which are derived (by sonication) from mitochondria that have been isolated from an ischemic tissue of the species, reflects upon (*a*), (*b*) and (*c*). Their combination. Enabling species comparisons. Such data has been utilized up until this point (e.g. utilized in Figure 2). By contrast, this present section uses a more limited assay, which doesn't as fully reflect upon (*a*) and (*b*), and doesn't reflect upon (*c*) at all. Only capturing the IF1 protein quantity (and not its ratio to ATP synthase) aspect of (*a*). And (aside from for rat) not capturing the "*its* F_1F_0 ATP hydrolysis" aspect to (*b*). This present assay reports the combination of (*i*) IF1 protein amount, with (*ii*) IF1 protein potency against rat F_1F_0 ATP hydrolysis. Although in the literature, the latter potency element is overlooked/discounted, and this assay is considered to

simply report upon “IF1 protein amount” or “IF1 protein content”. Hereafter I align with this terminology, with the caveat of what has been said. For different species, the table below utilizes “IF1 protein content”, which is the amount of mitochondrial extract {measured as mg of mitochondrial protein} from a species that can decrease F_1F_0 ATP hydrolysis of rat Sub-Mitochondrial Particles (SMPs) by 1 μmol/min. Assay performed at pH 6.2. This assay works because rat has very little endogenous IF1 protein, and so a high rate of F_1F_0 ATP hydrolysis. Moreover, because IF1 protein sequences, and ATP synthase protein sequences, are incredibly conserved across species. Such that IF1 proteins are typically interoperable between species, e.g. yeast IF1 protein can inhibit bovine F_1F_0 ATP hydrolysis [148]. In the table below, IF1 protein content data, for 12 different species, is used from Paper [α] [29] (*from column titled “ATPase Inhibitor Content, IU/mg” in its Table 1*). And from 6 different species from Paper [β] [141] (*from column titled “IF1 content (I.U./mg)” in its Table III*; those species of same genera as found in Paper [α], comprising the 5 species it {most probably} shares with Paper [α], and the specified pigeon species in Paper [β], *Columba livia* {Indian Fantail breed}, which I allocated a maximal lifespan of 35 years [5]). Pearson correlation coefficients are reported, and one-tailed (because each alternative hypothesis is directional) p-values.

			Specific basal metabolic rate	Heart rate	Maximal lifespan	log10(Body mass)
Paper [α]	IF1 protein content	R	-0.6669	-0.6051	0.6261	0.486
		p	0.0089225	0.018549	0.019661	0.054583
Paper [β]	IF1 protein content	R	-0.8211	-0.9285	0.6677	0.7488
		p	0.0225725	0.003743	0.073644	0.0433635

Comparing corresponding species/genus data (*i.e. comparing corresponding pig, rabbit, guinea pig, rat, mouse, and pigeon data*), the Pearson correlation coefficient (R) between the IF1 protein content data from Papers [α] and [β] is 0.8971. For which the one-tailed (because the alternative hypothesis is directional) p-value is 0.007669. Comparing corresponding species/genus data, the IF1 protein content data from Papers [α] and [β] is <u>*not*</u> significantly different from each other: independent (two-tailed) t-test statistic = -0.42674, p-value = 0 .677802; Mann-Whitney U test (two-tailed): U-value = 14, z-score = 0.56045, p-value = 0.57548; Kruskal-Wallis test: H statistic = 0.4103, p-value = 0.52184; Levene's test of homogeneity of variance: f-ratio = 0.29322, p-value = 0.600018. The IF1 protein content data of Paper [α] doesn’t have error bars. But that of Paper [β] does. If the error bar is added or subtracted (operation independently selected in each case) from each datum of Paper [β], whichever manipulation makes each value further from the corresponding value from Paper

[α], again these IF1 protein content data sets are *not* significantly different from each other: independent (two-tailed) t-test statistic = 0.35084, p-value = 0.73299; Mann-Whitney U test (two-tailed): U-value = 14, z-score = 0.56045, p-value = 0.57548; Kruskal-Wallis test: H statistic = 0.4103, p-value = 0.52184; Levene's test of homogeneity of variance: f-ratio = 0.32067, p-value = 0.58369.

The IF1 protein content data, as used to produce the table (most immediately) above, aligns with the other data herein, supporting the conclusions drawn therefrom.

Incidentally, relating to what was discussed in the earlier section titled "Birds", if the pigeon of Paper [β] is considered to have a maximal lifespan of 17.7 (instead of 35) years, its R (between IF1 protein content and maximal lifespan) is much greater than presented in the table above, being 0.8023 (one-tailed p-value = 0.027382). If the pigeon of Paper [α] is considered to have a maximal lifespan of 35 (instead of 17.7) years, its R (between IF1 protein content and maximal lifespan) is greater than presented in the table above, being 0.6444 (one-tailed p-value = 0.0161685).

Combining specific F_1F_0 ATP hydrolysis and IF1 protein content data

The Pearson correlation coefficient between the afore-used specific F_1F_0 ATP hydrolysis and IF1 protein content data, of [29], is -0.5292. With a one-tailed (because the alternative hypothesis is directional) p-value of 0.038426. So, the greater the IF1 protein content, the less the specific F_1F_0 ATP hydrolysis. In earlier sections, both these entities have been independently correlated, by Pearson correlation coefficient, to specific basal metabolic rate, heart rate, and maximal lifespan. As shown below, Fisher's combined probability test was used to combine their p-values for each of these correlations. The independence requirement of Fisher's method is met here, because specific F_1F_0 ATP hydrolysis and IF1 protein content are different measures, assayed by different experimental protocols. These combined p-values are presented in the table below, on the row labelled "*Combined*". Along with, on lower rows, some afore-presented correlations. Lower down in the table below, all these p-values are combined by two different methods: the asymptotically exact harmonic mean p-value for combining independent/dependent tests [7] (its post-published corrected method, as corrected on 7 October 2019), and using Fisher's combined probability test.

p-value (one-tailed)						
	Specific basal metabolic rate	Heart rate	Maximal lifespan			
Combined	0.00053569	0.0001955	0.00123938			
	Specific basal metabolic rate	0.0000015	0.001136			
		Heart rate	0.0003725			
Asymptotically exact harmonic mean p-value for combining independent/dependent tests						
Of all the p-values above (in this present table) = 0.000008850359 = **0.000009**						
Fisher's combined probability test						
Using p-values for [*Combined* vs. Maximal lifespan] (=0.00123938) &						
[Heart rate vs. Specific basal metabolic rate] (=0.0000015) = 0.00000004						

Bradford Hill criteria

Historically, the Bradford Hill criteria (also known as Hill's criteria for causation) [149] were used to persuade that lung cancer *correlates* with smoking in epidemiological data, because smoking *causes* lung cancer. The present work reports a correlation between more IF1 protein activity (less F_1F_0 ATP hydrolysis) and longer maximal lifespan. This correlation, although not epidemiological, satisfies (at least the spirit of) at least most of the Bradford Hill criteria.

Confirmatory

The multi-pronged hypothesis, that IF1 protein activity (by curtailing F_1F_0 ATP hydrolysis, setting specific basal metabolic rate [which sets heart rate]) is a molecular determinant of maximal lifespan, was set before the consistent/supporting data above was in hand. So, in statistical terminology, this study is "confirmatory" (hypothesis before data, and the data is consistent with {supports} the hypothesis). Rather than "exploratory" (data before hypothesis: hypothesis sourced from data).

Supplementary content for the Results section titled "Numerical prediction observed"

The table below shows correlations (R is the Pearson correlation coefficient, and p-values are one-tailed, because each alternative hypothesis is directional) to the *absolute* value of the resting mitochondrial membrane potential, $|\Psi_{IM}|$. Ψ_{IM} data (mV) is from [151], from isolated hepatocytes. For correlations to (s/v) and l, $n = 6$, because the number of overlapping species was 6. For the other correlations shown, $n = 5$. There weren't enough overlapping species to calculate correlations to g and w. At least across species, for these species, the greater the proton leak, l, the smaller the value of $|\Psi_{IM}|$, i.e. the less hyperpolarised the mitochondrial membrane potential. Proton leak is attenuating to the proton motive force (pmf), and its Ψ_{IM}

component. As is futile cycling of F_1F_0 ATP synthesis (pmf dissipation) and F_1F_0 ATP hydrolysis (pmf creation), because no energy conversion can be 100% efficient (2nd Law of Thermodynamics). At least across species, for these species, the less hyperpolarised the mitochondrial membrane potential (i.e. the smaller the value of $|\Psi_{IM}|$), the shorter the maximal lifespan.

		(*s* /*v*)	*l*	*h*	Specific basal metabolic rate	Heart rate	Maximum lifespan
|ΨIM|	R	-0.6482	-0.7588	-0.7818	-0.8956	-0.899	0.8712
	p	0.081938	0.0401	0.05913	0.0199265	0.018971	0.027202

Proton leak is not only an (attenuating) input into Ψ_{IM}, but also a function of it. Wherein greater Ψ_{IM} is an Ohmic, or supra-Ohmic, drive to greater proton leak. The proton leak variable used herein, *l*, is the proton leak when Ψ_{IM} is fixed at a value of -170 mV (and when ATP synthase is blocked by oligomycin). But, as referred to earlier, the different species don't have the same (resting) value of Ψ_{IM}. And so then there is a question mark over the fidelity of *l* to the actual proton leaks of these species. So use of *l* herein is with this caveat.

A new variable, *l* divided by resting Ψ_{IM}, would be interesting to explore. But there weren't enough shared species to calculate Pearson correlation coefficients for it.

Caveat

For expediency of explanation, at some points in the paper I write as though all homeothermic species maintain a body temperature of (around) 37°C. Although this is true for many (possibly most) homeothermic mammals (e.g. mice and humans [5]), it certainly isn't true for all. For example, the naked mole rat (*Heterocephalus glaber*) maintains a body temperature of (around) 32°C instead [5].

Synthesis of 7a and 7b (*anti-cancer activity in Figure 11*)

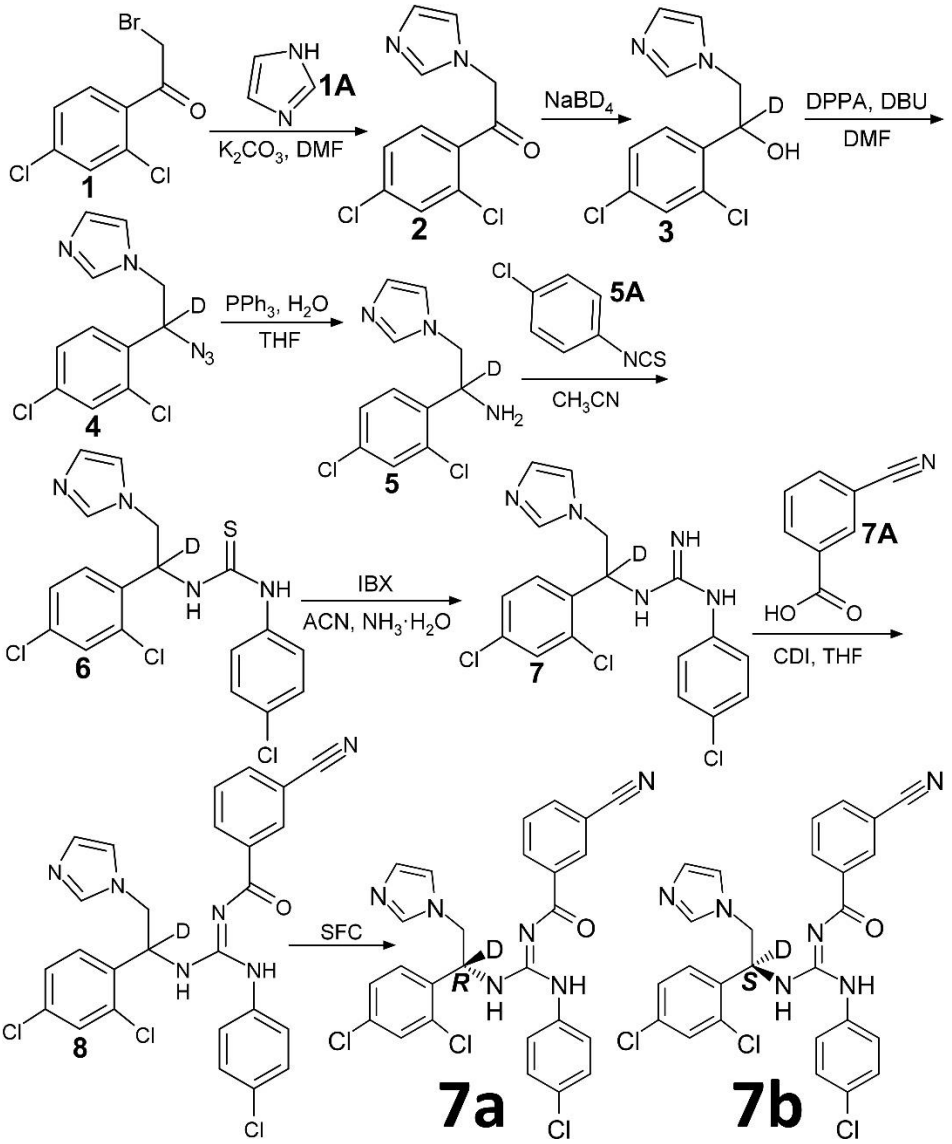

7a (enantiomeric excess (ee) ≥97%): Liquid Chromatography-Mass Spectrometry (LC-MS): LC Retention Time (RT) = 2.685 minutes, MS (electrospray ionization, positive mode): *m/z* 538.1 $[M+H]^+$, 560.1 $[M+Na]^+$, 269.6 $[M+2H]^{2+}$. High Resolution Mass Spectrometry (HRMS): Liquid Chromatography-Time of Flight (LC-TOF) MS (electrospray ionization, positive mode): LC Retention Time (RT) = 0.163 minutes, *m/z* 538.0727757864 $[M+H]^+$, *m/z* 560.0513502753 $[M+Na]^+$, *m/z* 576.0327248583 $[M+K]^+$, molar percent deuterium incorporation at chiral carbon = 99.14%.

^{1}H NMR (400 MHz, DMSO-*d6*) δ 11.46 (s, 1H), 8.32 (s, 1H), 8.24 (d, J = 7.9 Hz, 1H), 7.95 (d, J = 7.7 Hz, 2H), 7.70 – 7.59 (m, 3H), 7.59 – 7.49 (m, 4H), 7.21 (s, 1H), 7.12 (d, J = 7.9 Hz, 2H), 6.99 (s, 1H), 4.36 (d, J = 13.9 Hz, 1H), 4.22 (s, 1H). {*NMR probe temperature = 300.7 K*}.

7b (enantiomeric excess (ee) ≥97%): LC-MS: LC Retention Time (RT) = 2.685 minutes, MS (electrospray ionization, positive mode): *m/z* 538.1 $[M+H]^+$, 560.1 $[M+Na]^+$, 269.6 $[M+2H]^{2+}$. HRMS: LC-TOF MS (electrospray ionization, positive mode): LC RT = 0.166 minutes, *m/z* 538.0745928061 $[M+H]^+$, *m/z* 560.0600137508 $[M+Na]^+$, *m/z* 576.0250917093 $[M+K]^+$, molar percent deuterium incorporation at chiral carbon = 99.13%.
^{1}H NMR (400 MHz, DMSO-*d6*) δ 11.48 (s, 1H), 8.33 (s, 1H), 8.25 (dt, J = 7.8, 1.5 Hz, 1H), 7.96 (dt, J = 7.7, 1.5 Hz, 1H), 7.92 (s, 1H), 7.71 – 7.60 (m, 3H), 7.60 – 7.49 (m, 4H), 7.23 (s, 1H), 7.14 (s, 2H), 7.00 (s, 1H), 4.38 (d, J = 14.1 Hz, 1H), 4.23 (s, 1H). {*NMR probe temperature = 301 K*}.

Presented NMR peaks are from using the "Auto Assignment" algorithm in MestReNova version 12 software (Mestrelab Research, Santiago de Compostela, Spain). Which picks peaks in an inputted NMR spectrum, influenced by an inputted structure, which was structure 8 in the reaction scheme above. However, after automatic assignment, I manually made a single change for 7a: I changed the number of hydrogens at 7.95 ppm from 1H to 2H. I executed this change by manually extending the integration line (this manipulation automatically changes the MestReNova program's integration calculation method from "peak" to "sum") in this 7.95 ppm region for 7a, making it the same length as the integration line in the same region for 7b. Which then rendered/integrated this region with 2H as compared to 1H. The same as for 7b in this region (by "Auto Assignment" algorithm: 7b has peaks at 7.96 [1H] and 7.92 [1H] = 2H in 7.95 ppm region). This change in integration increases the nuclide count to the correct number for the structure (18H). This manipulation is best explained in pictures and so please refer to Figures 39 and 40. Which both show 7b data in the upper panel, 7a data in the lower panel. Wherein Figure 39 shows how this region was automatically integrated. And Figure 40 shows how I manually extended the integration line for 7a, to match the length of that for 7b. Such that both integrated to 2H in this region.

<u>Performed synthesis of 7a and 7b in detail</u>

In this section, numbers in square brackets are CAS numbers.

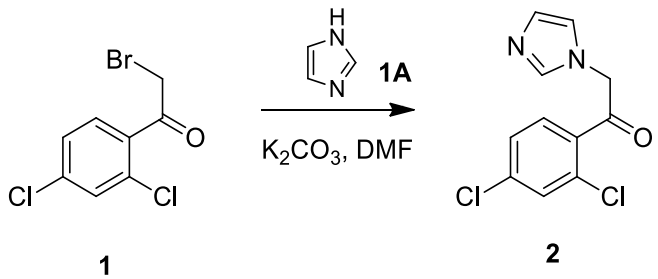

1. Charged Compound 1 [170894-53-8] (15.0 g, 55.9 mmol) and DMF [68-12-2] (150 mL) into the reactor at 25°C under N_2.
2. Charged K_2CO_3 [584-08-7] (23.2 g, 167 mmol) into the reactor at 25°C.
3. Charged imidazole [288-32-4] (11.4 g, 167 mmol) into the reactor at 25°C.
4. The mixture was stirred at 25°C for 3 hours.
5. TLC (petroleum ether:ethyl acetate = 5:1, R_f = 0.0) showed raw material was consumed.
6. The mixture was quenched with water (100 mL).
7. The aqueous phase was extracted with ethyl acetate (100 mL x 2). The combined organic phase was washed with brine (50 mL), dried with anhydrous Na_2SO_4, filtered and concentrated in vacuum.
8. The residue was purified by silica gel chromatography (column height: 250 mm, diameter: 100 mm, 100-200 mesh silica gel, petroleum ether/ethyl acetate=20/1, 3/1) to give Compound 2 (13.0 g, 38.8 mmol, 69.3% yield, 76.1% purity) as yellow solid.

Compound 2: ^{1}H NMR ($CDCl_3$, 400 MHz) δ (ppm) 7.55 (d, J = 8.0 Hz, 1H), 7.50 (s, 1H), 7.35-7.37 (dd, J = 8.0 Hz, 8.0 Hz, 1H), 7.09 (d, J = 8.0 Hz, 1H), 6.93 (s, 1H), 5.32 (s, 2H).

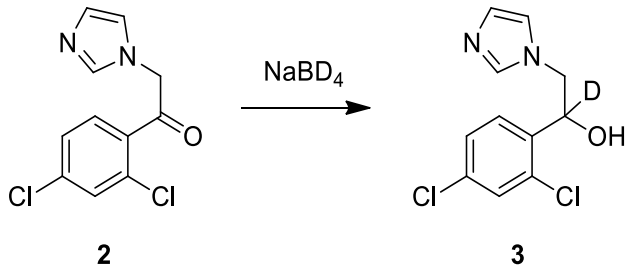

1. Charged Compound 2 (8.00 g, 31.3 mmol) and MeOH (40 mL) into the reactor at 25°C under N_2.
2. Charged $NaBD_4$ [15681-89-7] (1.31 g, 34.5 mmol) to the solution.
3. The mixture was stirred at 50°C for 3 hours.
4. LC-MS (product: RT= 0.914 min) showed raw material was consumed.
5. The reaction was quenched with water (100 mL).

6. The aqueous phase was extracted with ethyl acetate (50 mL x 2). The combined organic phase was washed with brine (50 mL), dried with anhydrous Na_2SO_4, filtered and concentrated in vacuum.

7. The residue was purified by silica gel chromatography (column height: 250 mm, diameter: 100 mm, 100-200 mesh silica gel, petroleum ether/ethyl acetate=10/1, 0/1) to give Compound 3 (5.50 g, 21.3 mmol, 67.9% yield) as white solid.

Compound 3: ^{1}H NMR ($CDCl_3$, 400 MHz) δ (ppm) 7.57 (d, J = 8.0 Hz, 1H), 7.39 (m, 1H), 7.28-7.30 (dd, J = 8.0 Hz, 8.0 Hz, 1H), 6.88 (d, J = 8.0 Hz, 2H), 4.20 (d, J = 12 Hz, 1H), 3.84-3.88 (d, J = 16 Hz, 1H).

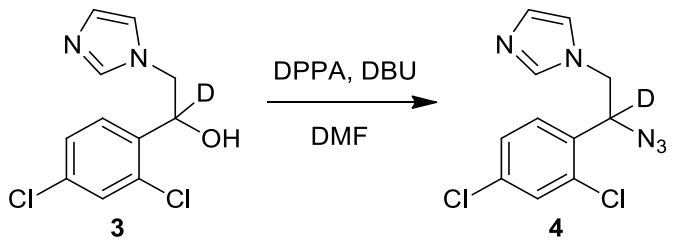

1. Set up a reactor R-1. (Note: R-1 is a 100 mL three-necked bottle)

2. Charged Compound 3 (4.50 g, 17.4 mmol) and DPPA [26386-88-9] (4.80 g, 17.4 mmol, 3.78 mL), DMF (22.5 mL) into the reactor R-1 at 25-30°C.

3. Charged DBU [6674-22-2] (2.65 g, 17.4 mmol, 2.63 mL) into the mixture under nitrogen atmosphere at 0-5°C, then the mixture was stirred for about 15 minutes.

4. After that, the reaction mixture was stirred for 24 hours at 20-30°C.

5. TLC (DCM/MeOH = 10/1, SM R_f = 0.55, product R_f = 0.72) showed raw material was consumed, LC-MS (product: RT = 0.764 min) and HPLC (product: RT = 1.893 min) indicated reaction mixture has desired product.

6. The reaction mixture was extracted with EtOAc (40 mL x 3).

7. The combined organic phase was washed with brine (40 mL), dried with Na_2SO_4, filtered and concentrated in vacuum to get the residue.

8. The residue was purified by column chromatography (SiO_2, dichloromethane: methanol = 1/0 to 100/1) to give Compound 4 (3.80 g, crude) as yellow oil.

Compound 4: ^{1}H NMR ($CDCl_3$, 400 MHz) δ (ppm) 7.50 (s, 1H), 7.44 (s, 1H), 7.35 (d, J = 2.0 Hz, 1H), 7.33 (d, J = 2.0 Hz, 1H), 7.29-7.30 (m, 1H), 6.94-7.10 (m, 1H), 4.25 (d, J = 14.4 Hz, 1H), 4.04 (d, J = 14.4 Hz, 1H).

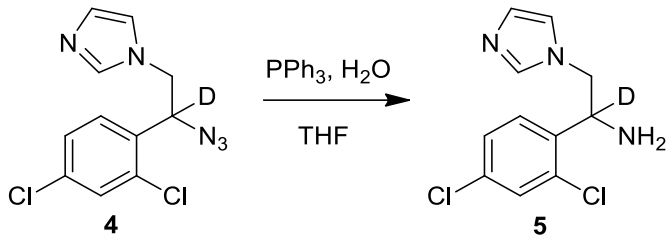

1. Set up a reactor R-1. (Note: R-1 is a 100 mL three-necked bottle)
2. Charged Compound 4 (3.80 g, 13.4 mmol), PPh_3 [603-35-0] (10.5 g, 40.2 mmol), THF [109-99-9] (12.6 mL) and H_2O (1.26 mL) into the reactor R-1 at 25-30°C.
3. Stirred at 65-70°C for 16 hours.
4. Checked the reaction mixture by TLC (dichloromethane: methanol=10:1, SM: R_f = 0.54, product: R_f = 0.45) and LC-MS (product: RT = 1.253min) showed that reactant was consumed completed.
5. The reaction mixture was concentrated under reduced pressure to remove THF.
6. The reaction mixture was added with H_2O (38 mL), adjusted pH to 3 with con. HCl and washed with EtOAc (38 mL).
7. The water phase was adjusted pH to 13 with 1N aq. NaOH, then exacted with EtOAc (38 mL x 2).
8. The combined organic phase was washed with brine (38 mL), dried with Na_2SO_4, filtered and concentrated in vacuum to give Compound 5 (2.60 g, crude) as a yellow liquid.

Compound 5: ^{1}H NMR ($CDCl_3$, 400 MHz) δ (ppm) 7.44 (d, J = 14 Hz, 1H), 7.41 (s, 1H), 7.29 (d, J = 2.0 Hz, 1H), 7.27 (d, J = 1.2 Hz, 1H), 7.07 (s, 1H), 6.92 (s, 1H), 4.21 (d, J = 14 Hz, 1H), 3.92 (d, J = 14 Hz, 1H).

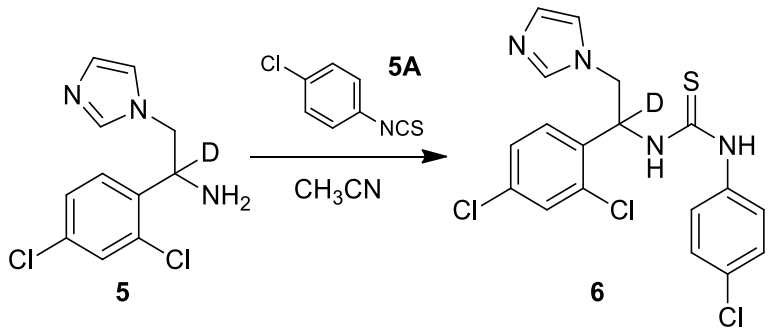

1. Charged Compound 5 (2.50 g, 9.72 mmol), Compound 5A [2131-55-7] (1.65 g, 9.72 mmol) and MeCN (37.5 mL) into the reactor at 25°C.
2. The mixture was stirred at 25°C for 12 hours.

3. TLC (dichloromethane: methanol=10:1, SM: R_f = 0.5, product: R_f = 0.2) showed raw material was consumed completed.

4. The mixture was concentrated in vacuum.

5. The residue was purified by silica gel chromatography (column height: 250 mm, diameter: 100 mm, 100-200 mesh silica gel, petroleum ether/ethyl acetate=3/1, 0/1) to give Compound 6 (3.60 g, 8.44 mmol, 86.7% yield) as white solid.

Compound 6: ^{1}H NMR ($CDCl_3$, 400 MHz) δ (ppm) 9.08 (s, 1H), 7.48 (d, J = 2.0 Hz, 1H), 7.33 (d, J = 8.0 Hz, 1H), 7.25-7.28 (m, 1H), 7.16 (d, J = 2.0 Hz, 1H), 7.00 (s, 1H), 6.88 (d, J = 8.0 Hz, 1H), 6.72 (s, 1H), 4.46 (dd, J = 14.4 Hz, 14 Hz, 1H), 1.84 (s, 1H).

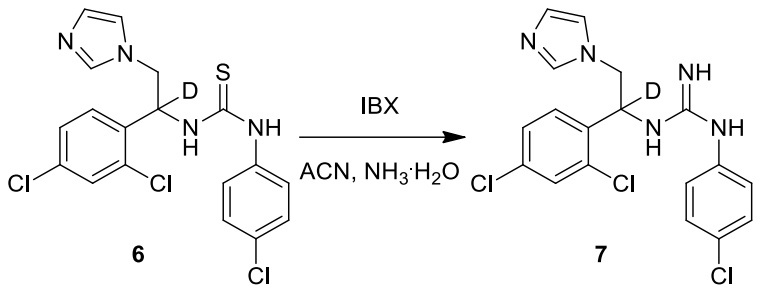

1. Charged Compound 6 (3.00 g, 7.03 mmol) and MeCN (30 mL) into the reactor at 25°C.

2. Charged IBX [61717-82-6] (2.17 g, 7.73 mmol) into the reactor at 25°C.

3. Charged $NH_3.H_2O$ [1336-21-6] (13.6 g, 116 mmol, 15 mL, 30% purity) into the reactor at 25°C.

4. The mixture was stirred at 25°C for 12 hours.

5. LC-MS (product: RT = 0.717 min) showed raw material was consumed completed.

6. The mixture was filtered and the filter cake was concentrated in vacuum to give Compound 7 (2.50 g, 6.10 mmol, 86.8% yield) as white solid.

Compound 7: ^{1}H NMR ($CDCl_3$, 400 MHz) δ (ppm) 7.87 (d, J = 8.0 Hz, 1H), 7.67 (s, 1H), 7.55-7.60 (m, 2H), 7.37-7.41 (m, 2H), 7.23 (s, 1H), 7.07-7.09 (m, 1H), 6.92 (s, 1H), 4.33 (dd, J = 14.4 Hz, 14 Hz, 1H).

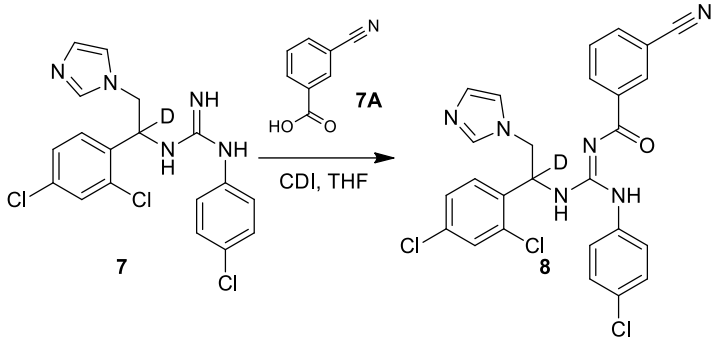

1. Charged Compound 7 (538 mg, 3.66 mmol), CDI [530-62-1] (593 mg, 3.66 mmol) and THF [109-99-9] (30 mL) into the reactor at 25°C.
2. The solution was stirred at 25°C for 3 hours.
3. Charged compound 7A [1877-72-1] (1.50 g, 3.66 mmol) into the reactor at 25°C.
4. The mixture was stirred at 25°C for 12 hours.
5. LC-MS (SM: RT = 0.730 min, product: RT = 1.030 min) showed the raw material was consumed/completed.
6. The mixture was concentrated in vacuum.
7. Separating stereoisomers of Compound 8: the residue was purified with Prep-HPLC (column: DAICEL CHIRALPAKAD-H (250 mm*30 mm, 5 µm); mobile phase: [0.1% NH_3H_2O IPA]; B%: 44%-44%, 6.45 min) to give 7b (0.025 g, 45.8 µmol, 1.25% yield, 98.8% purity) as white solid and 7a (0.025 g, 45.5 µmol, 1.24% yield, 98.1% purity) as white solid.

<u>Spectral data for 7b</u>

Its expected/calculated *m/z*, from its structure (Figure 11A), using the "exact molecular weight" calculator in MarvinSketch software (Chemaxon, Budapest, Hungary), which uses the mass of the *most prevalent* isotope of each element in the molecule:
538.08 $[M+H]^+$, 560.06 $[M+Na]^+$, 269.54 $[M+2H]^{2+}$, 576.04 $[M+K]^+$).

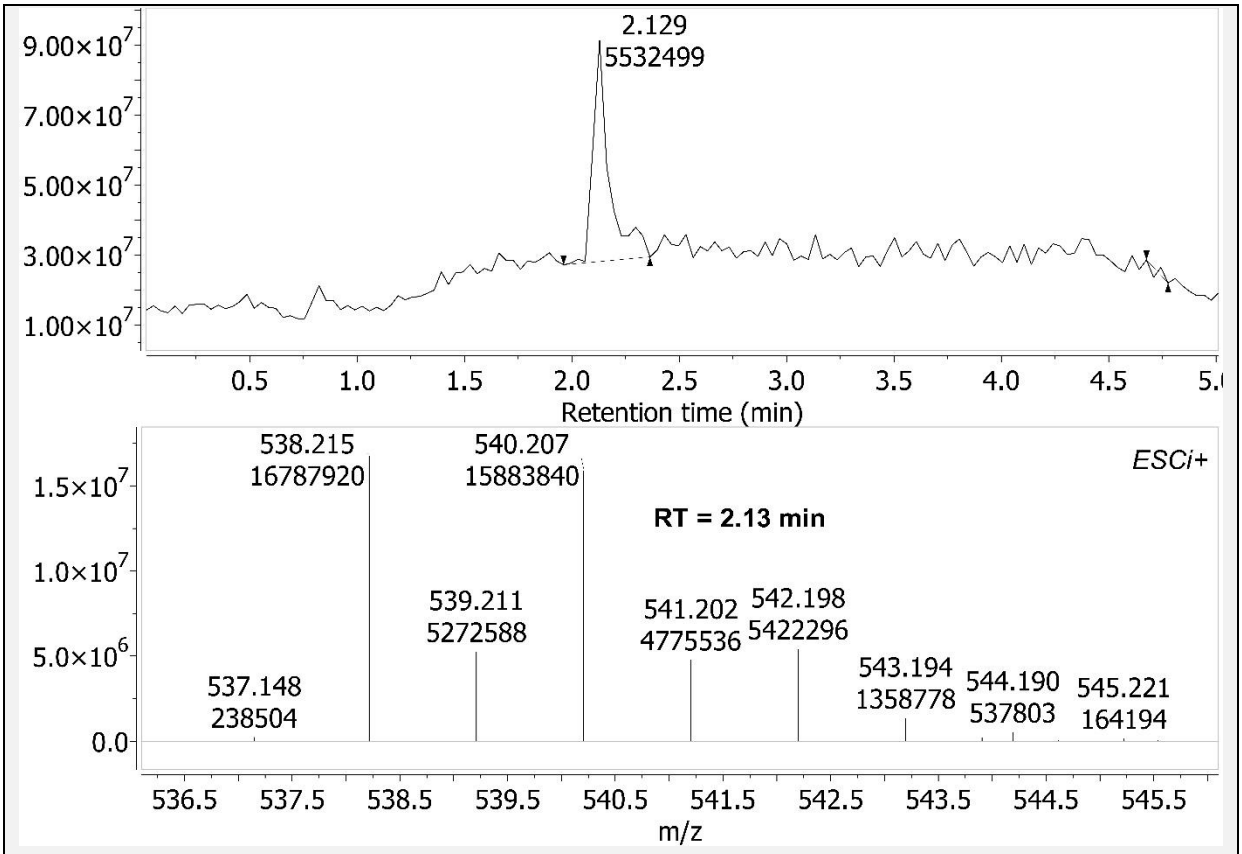

Figure 26 – Chiral SFC-MS for 7b sample. *Upper panel*: Chiral-SFC annotated with Retention Time (RT, minutes) and area under peak. *S* stereoisomer is found in [RT=2.13] peak. *Lower panel*: component of mass spectrum of [RT=2.13] peak. And therein is *m/z* 538.215 $[M+H]^+$ (*0.135 removed from Expected. Better concordance in subsequent spectra*).

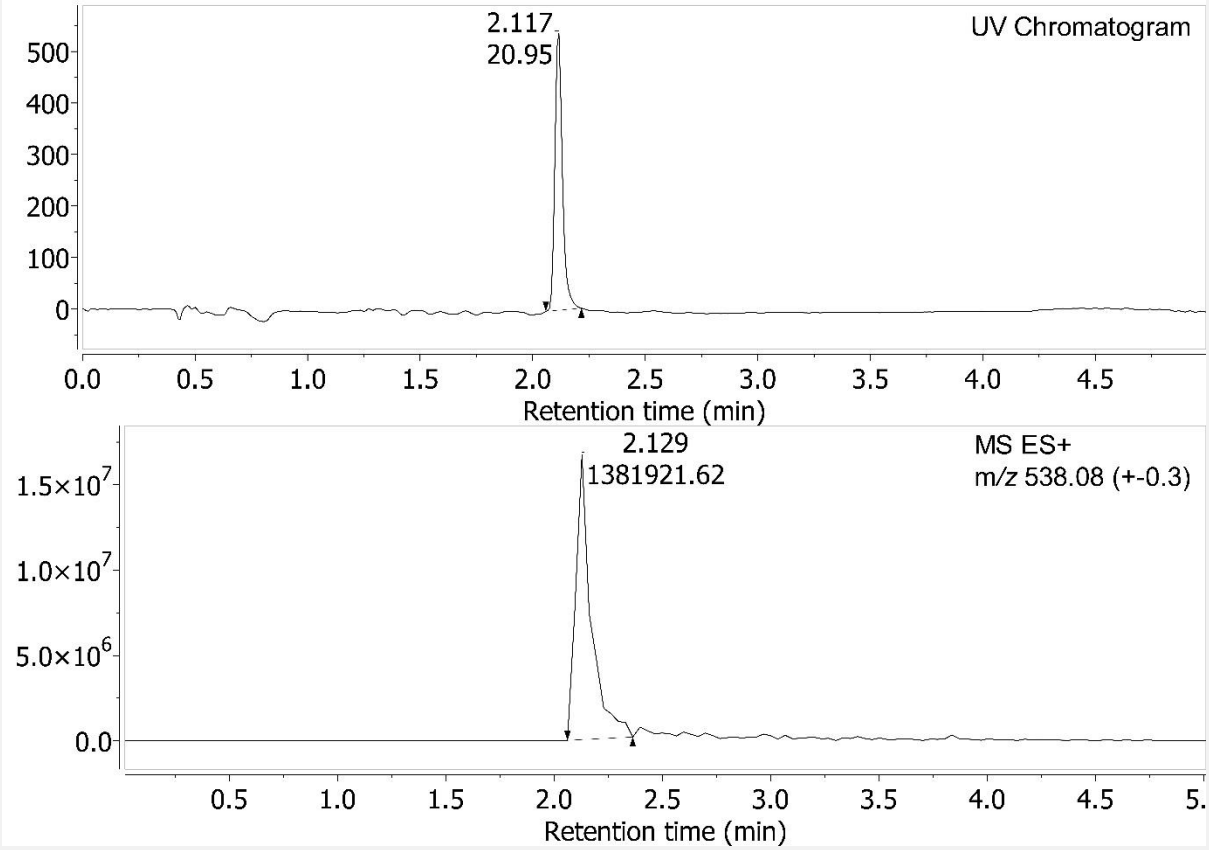

Figure 27 – Chiral-SFC of 7b sample. *S* stereoisomer excess = 100% (no other peak in the UV chromatogram). Enantiomeric excess (ee) = (100-50)*2 = 100%.

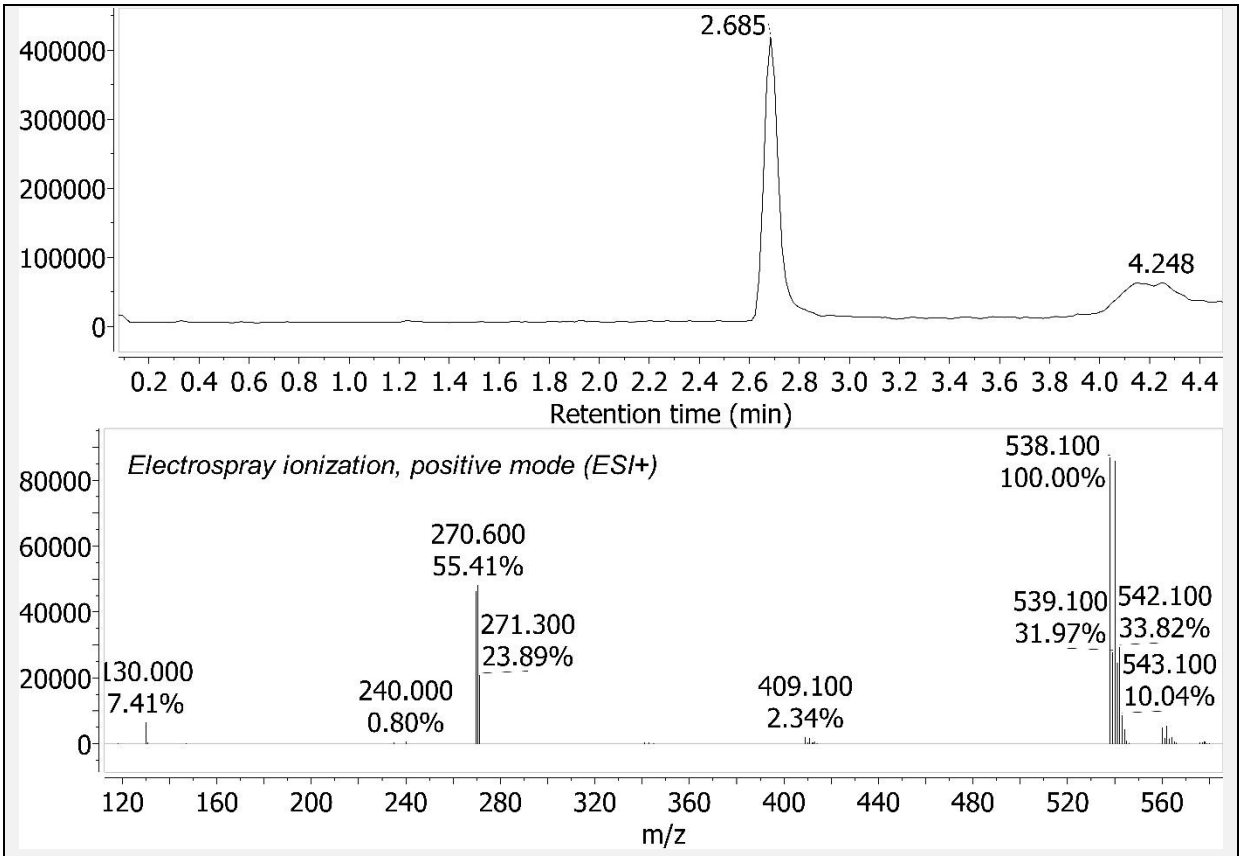

Figure 28 – LC-MS spectrum for 7b sample. *Upper panel*: Liquid Chromatography (LC) Retention Time (RT) = 2.685 minutes. *Bottom panel*: Mass Spectrum (MS) of [RT=2.685 peak]. Shows positively charged species (API-ES positive). Percentages are relative abundance.

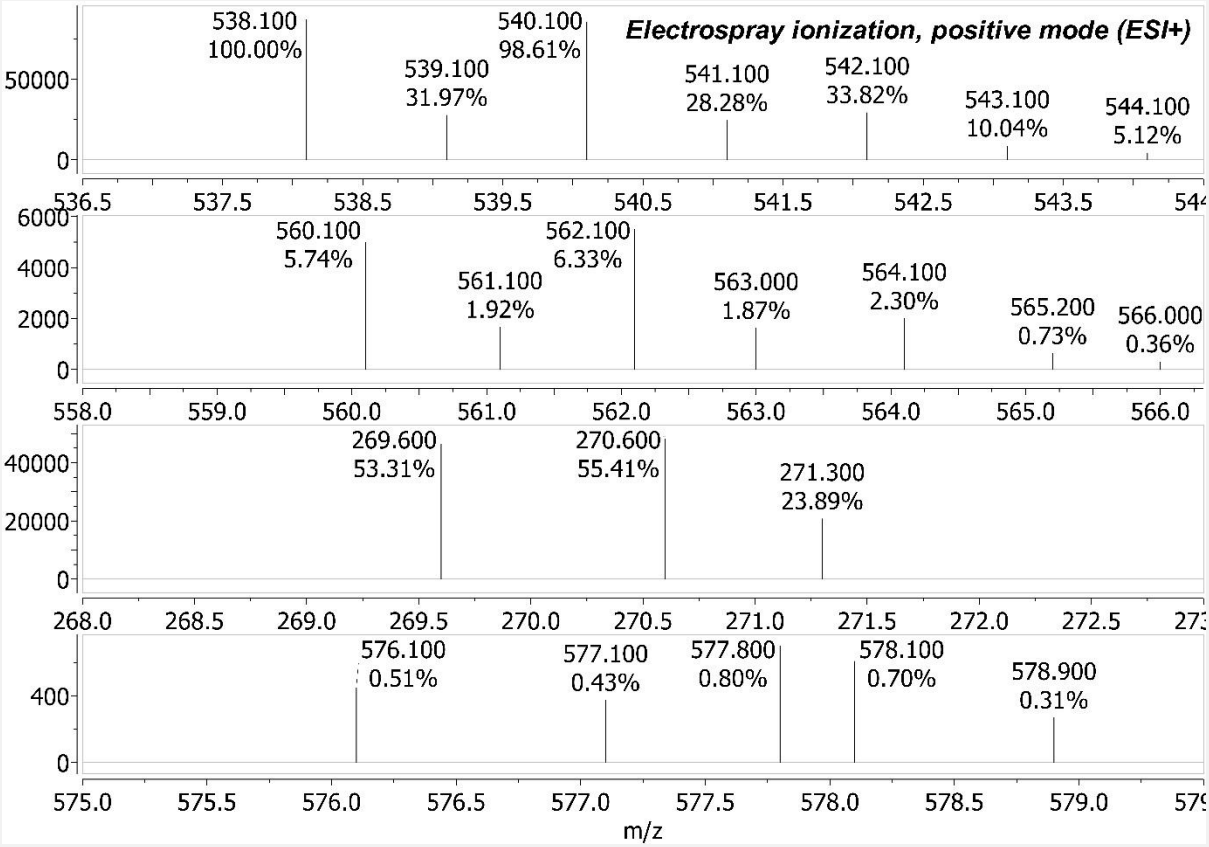

Figure 29 – Some Mass Spectrum (MS) components of Figure 28. *Upper panel*: *m/z* 538.1 $[M+H]^+$. *2nd panel*: *m/z* 560.1 $[M+Na]^+$. *3rd panel*: *m/z* 269.6 $[M+2H]^{2+}$. *Bottom panel*: *m/z* 576.1 $[M+K]^+$. All these Observed *m/z* are within 0.06 of Expected.

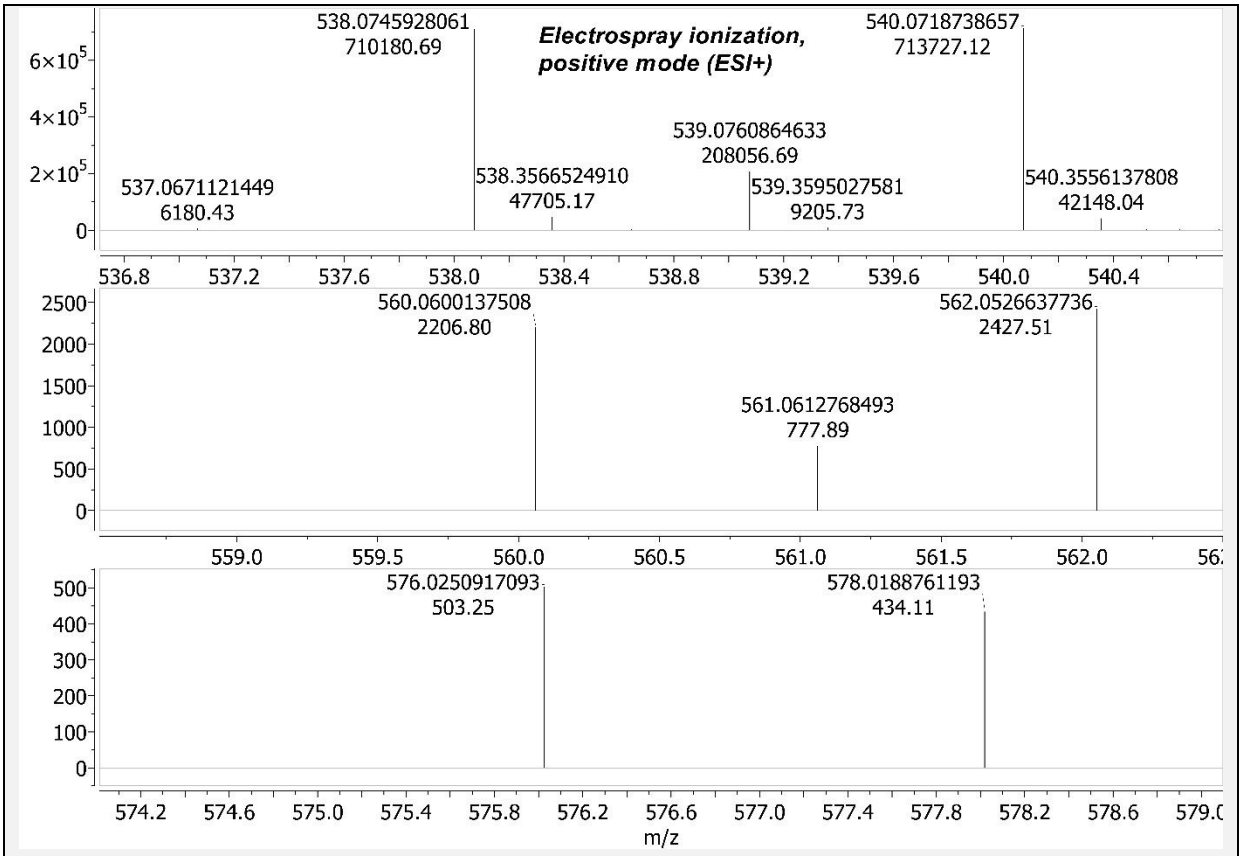

Figure 30 – High Resolution Mass Spectrometry (HRMS): Liquid Chromatography-Time of Flight (LC-TOF) Mass Spectrometry (MS) for 7b sample. LC Retention Time (RT) = 0.166 minutes (LC data not shown). *Upper panel*: OBSERVED *m/z* 538.0745928061 $[M+H]^+$. CALCULATED from structure *m/z* 538.0821456 $[M+H]^+$. So, Observed mass is only 0.0075527939 Daltons (0.7% the mass of a proton) removed from calculation. The species with *m/z* 537.0671121449 $[M+H]^+$ has hydrogen instead of deuterium on the chiral carbon. And indeed is the mass of a neutron (1.008664 Daltons) lighter: (538.0745928061-537.0671121449) = 1.0074806612 Daltons mass difference (0.12% removed from being the exact mass of a neutron difference). Absolute abundance is shown on the y-axis. And the molar percent deuterium incorporation for 7b sample at the chiral carbon is 100% - ((6180.43/710180.69)*100=0.87%) = 99.13%. *2nd panel*: OBSERVED *m/z* 560.0600137508 $[M+Na]^+$. CALCULATED from structure *m/z* 560.0640898 $[M+Na]^+$. So, Observed mass is only 0.0040760492 Daltons (0.4% the mass of a proton) removed from calculation. The species with hydrogen instead of deuterium on chiral carbon is too low abundance to be observed here. *Bottom panel*: OBSERVED *m/z* 576.0250917093 $[M+K]^+$. CALCULATED from structure *m/z* 576.0380270 $[M+K]^+$. So, Observed mass is only 0.0129352907 Daltons (1.3% the mass of a proton) removed from calculation. The species with hydrogen instead of deuterium on chiral carbon is too low abundance to be observed here.

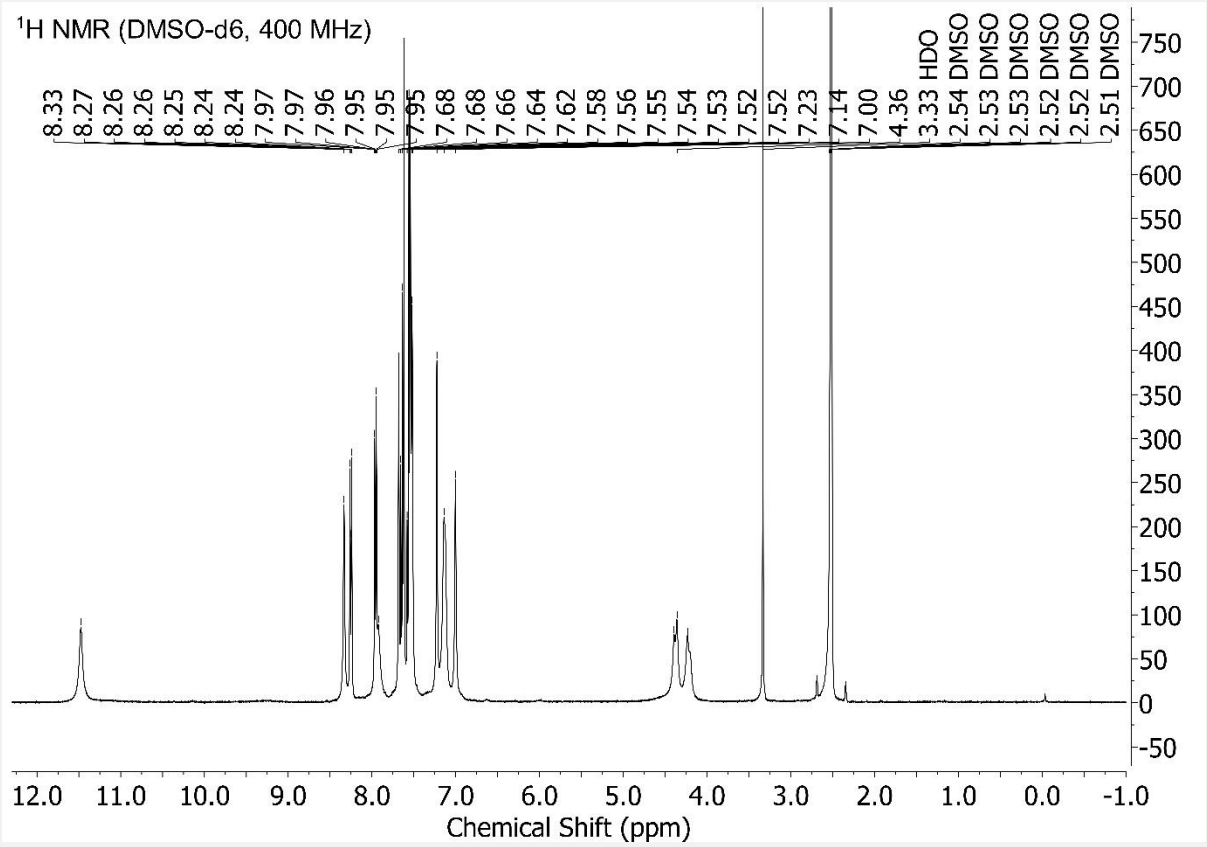

Figure 31 – ^{1}H NMR {*NMR probe temperature = 301 K*} for 7b sample. Scaled to highest compound peak. Peaks identified by "Auto peak picking" algorithm of MestReNova v12 software. With default program settings used. And no chemical structure used/inputted to guide/constrain this peak picking.

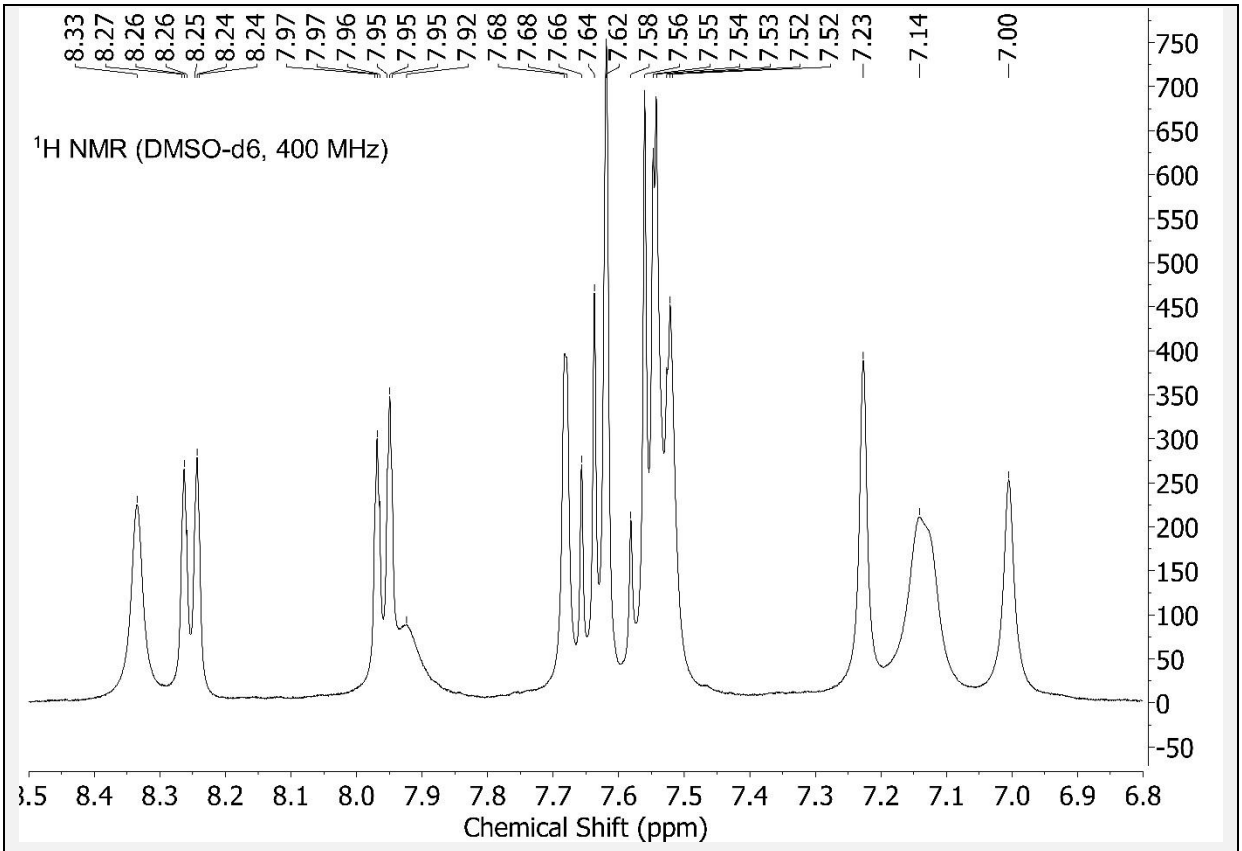

Figure 32 – Aromatic region of Figure 31 expanded.

Spectral data for 7a

Note that for 7a, its LC-MS, HRMS and NMR data are not all correspondent. To explain, LC-MS, HRMS and ^{1}H NMR were performed for 7a. And its ^{1}H NMR showed a high amount of impurities (spectrum not shown). Further mass based purification steps were taken as a result. And the ^{1}H NMR was repeated (spectrum shown herein). And ^{13}C NMR performed. All showing a much lower, acceptable level of impurity. And it is this purer form that was entered into anti-cancer testing at the National Cancer Institute (Figure 11B). However, LC-MS and HRMS were not repeated. But the LC-MS and HRMS are clear enough to identify the [M+ion] species needed. All be it with some additional species/impurities also observed, which aren't in the LC-MS and HRMS spectra for 7b (e.g. compare Figures 30 and 36).

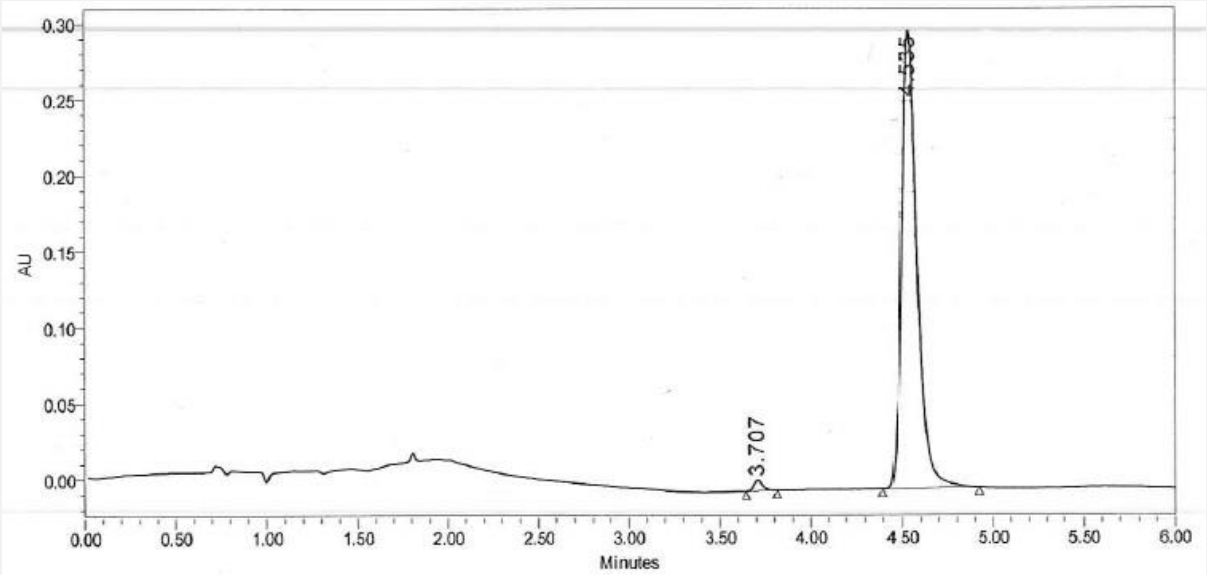

	RT	Area	% Area	Height
1	3.707	23021	1.29	6747
2	4.535	1765686	98.71	301165

Figure 33 – The chiral SFC-MS machine broke down. And so a different machine, with only chiral-SFC capability, had to be used. So, only chiral-SFC was performed for the 7a sample. Retention Time (RT) = 4.535 min.

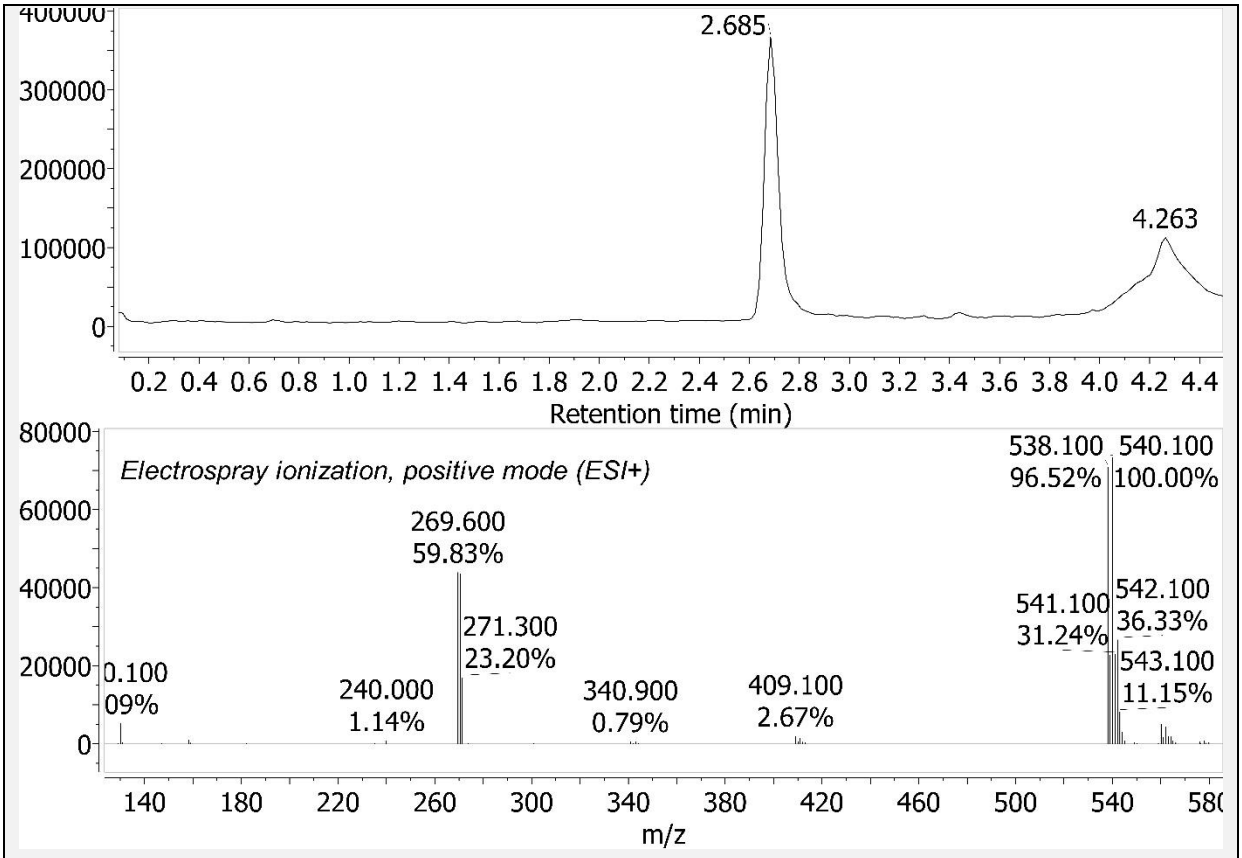

Figure 34 – LC-MS spectrum for 7a sample. Retention Time (RT) = 2.685 minutes.

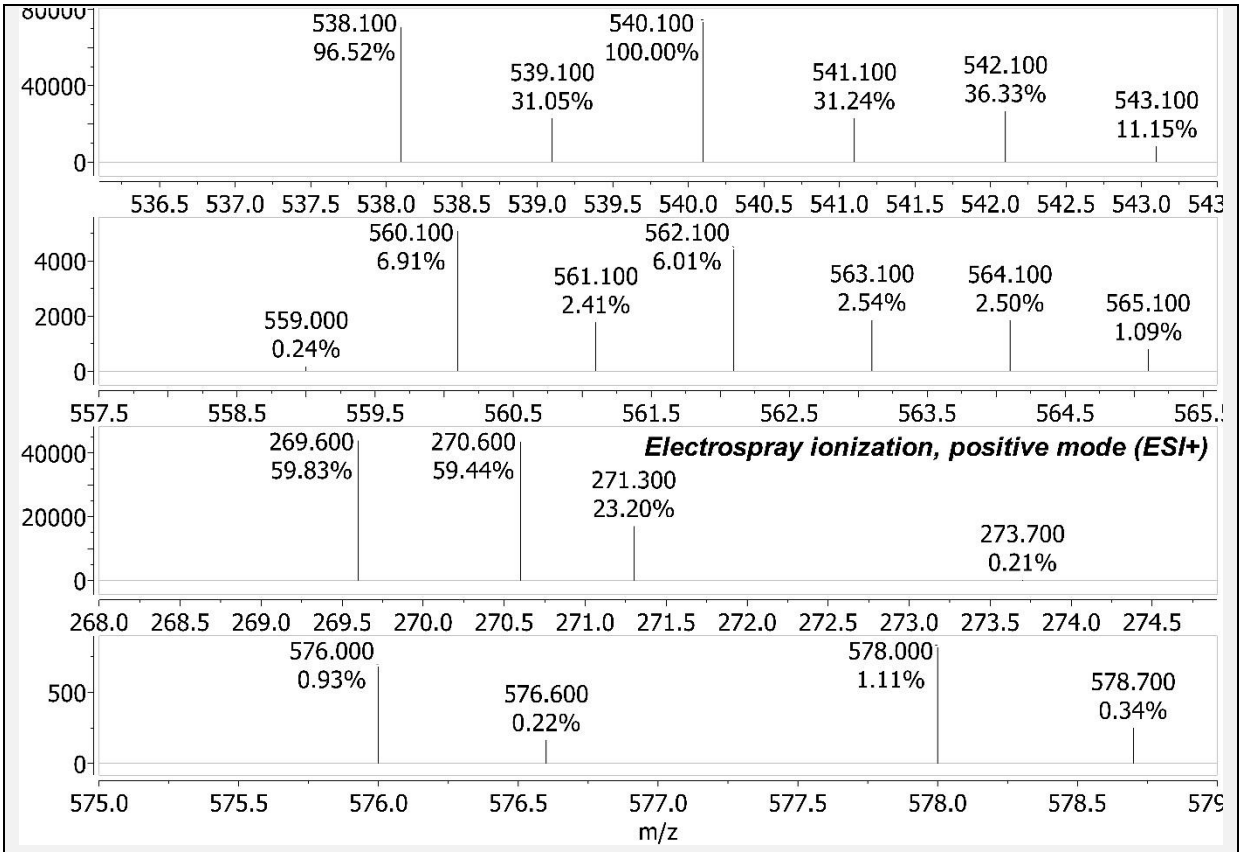

Figure 35 – Some Mass Spectrum (MS) components of Figure 34. *Upper panel*: *m/z* 538.1 $[M+H]^+$. *2nd panel*: *m/z* 560.1 $[M+Na]^+$. *3rd panel*: *m/z* 269.6 $[M+2H]^{2+}$. *Bottom panel*: *m/z* 576.0 $[M+K]^+$. All these Observed *m/z* are within 0.06 of Expected.

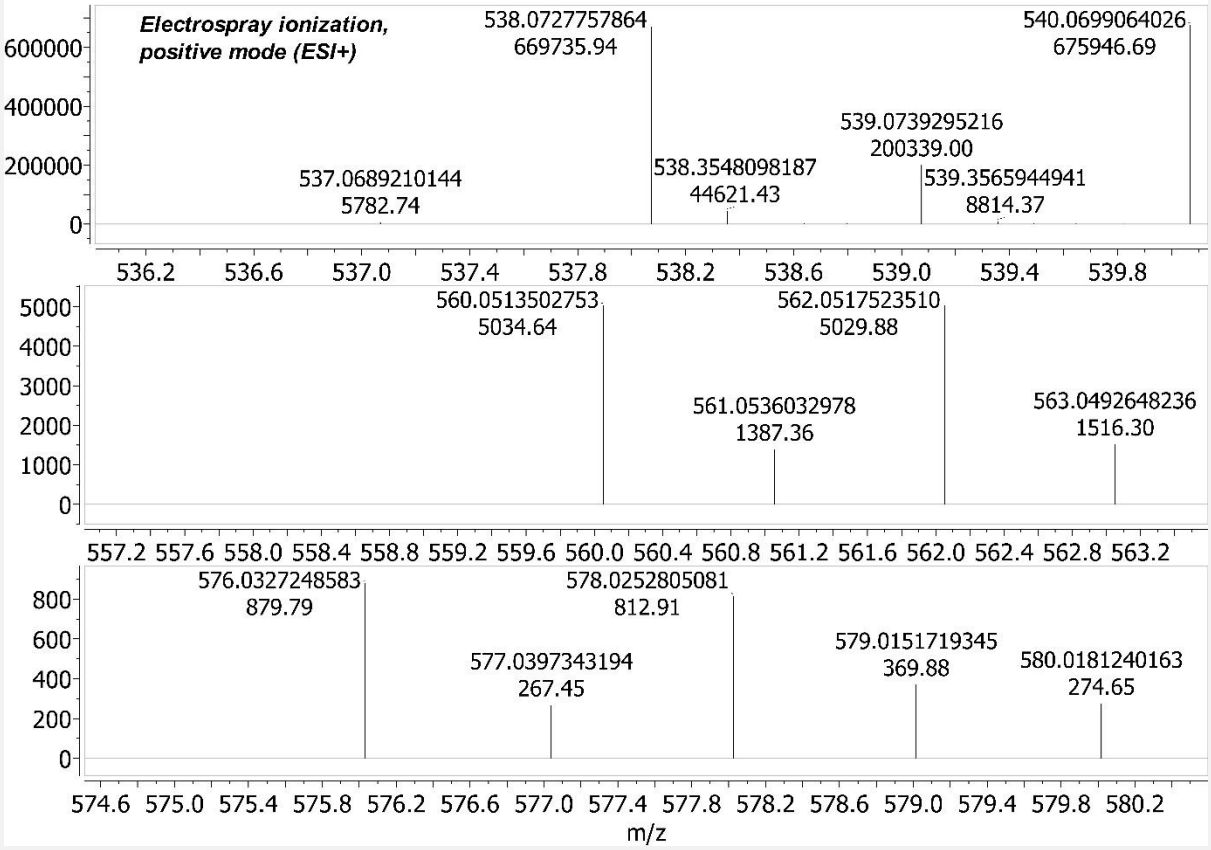

Figure 36 – HRMS: LC-TOF MS for 7a sample. LC Retention Time (RT) = 0.163 minutes (LC data not shown). *Upper panel*: *m/z* 538.0727757864 $[M+H]^+$. The species with *m/z* 537.0689210144 $[M+H]^+$ has hydrogen instead of deuterium on the chiral carbon. Absolute abundance is shown on the y-axis. And the molar percent deuterium incorporation for 7a at the chiral carbon is 100% - ((5782.74/669735.94)*100=0.86%) = 99.14%. *2nd panel*: *m/z* 560.0513502753 $[M+Na]^+$. *Bottom panel*: *m/z* 576.0327248583 $[M+K]^+$.

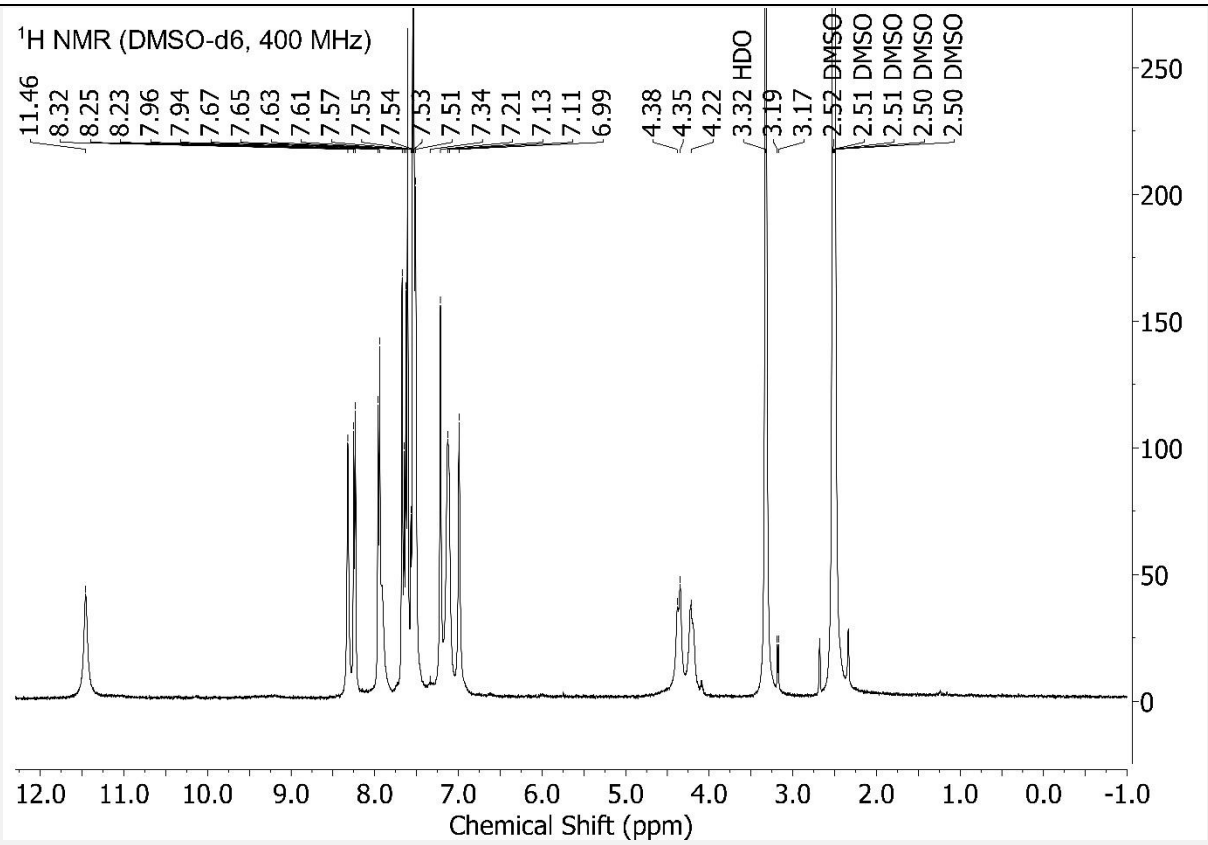

Figure 37 – ^{1}H NMR {*NMR probe temperature = 300.7 K*} for 7a sample. Scaled to highest compound peak. "Auto peak picking" algorithm in MestReNova v12 used to pick peaks shown. With default program settings used. And no chemical structure used/inputted to guide/constrain this peak picking.

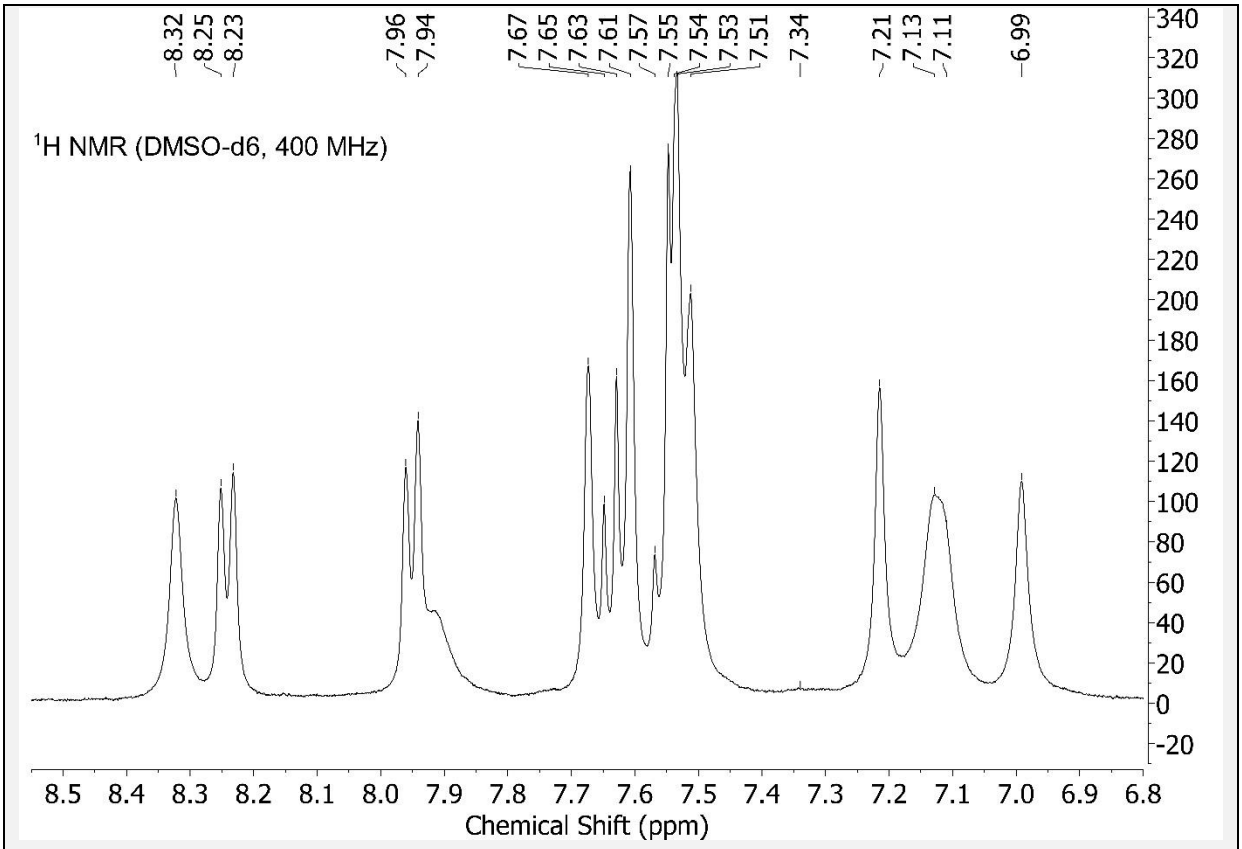

Figure 38 – Aromatic region of Figure 37 expanded.

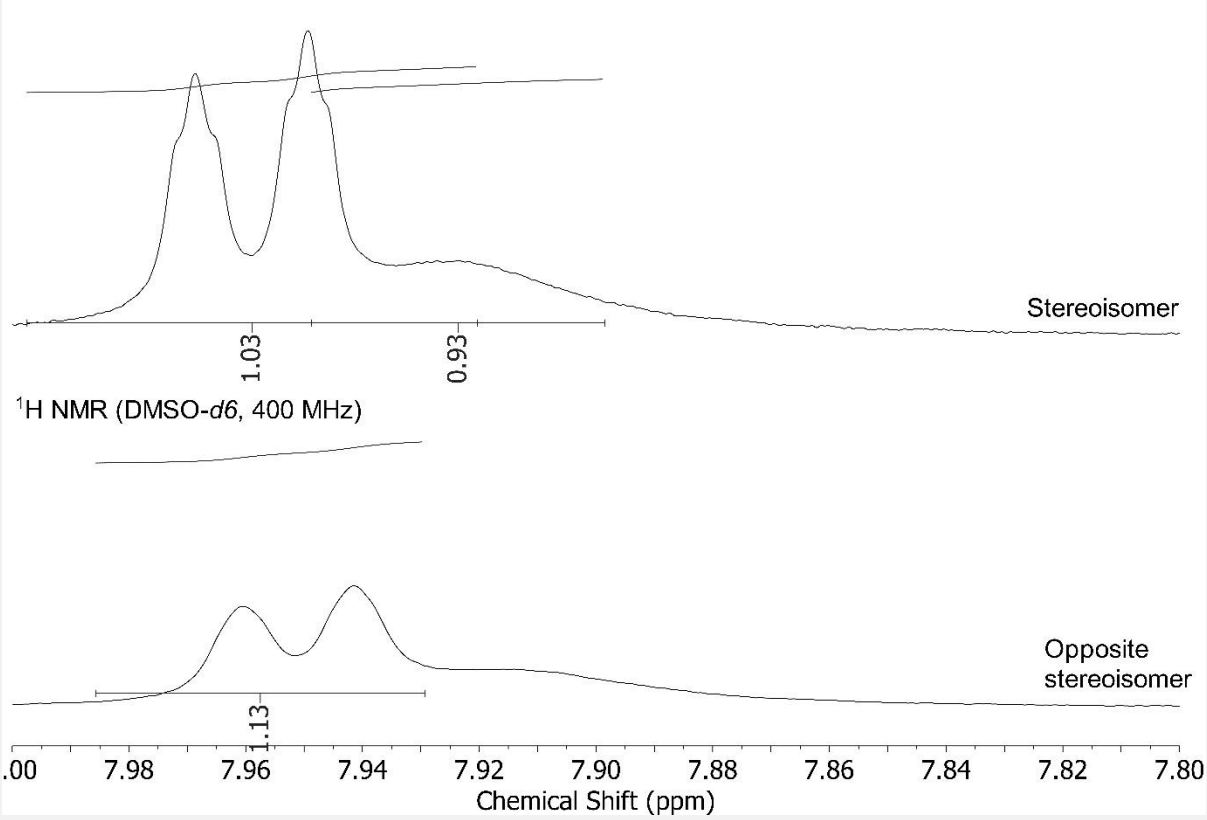

Figure 39 – 7b data in upper panel, 7a data in lower panel. Figure shows integration values in this ppm region as automatically assigned by the MestReNova v12 software used. 7b has 2H assigned (1.03+0.93=1.96, rounds to 2), whilst 7a has 1H assigned (1.13, rounds to 1), in this ppm region.

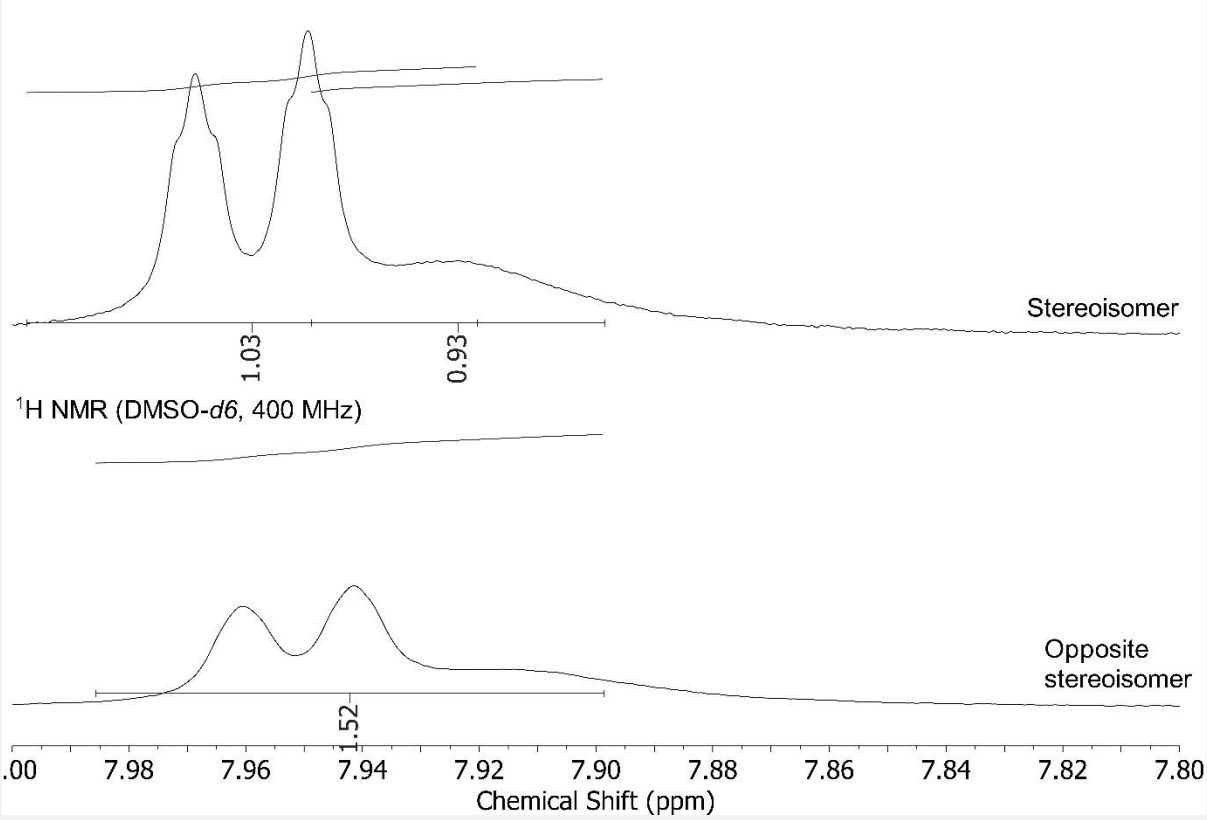

Figure 40 – Shown here, I manually extended the integration line (N.B. this automatically changes the MestReNova v12 integration calculation method from "peak" to "sum") for 7a to be the same length as that for 7b. Which changes its integration value from 1.13 (prior) to 1.52, which rounds to 2H. This improves the 7a assignment because now it has the correct number of hydrogen nuclides (18H), whereas before it had (incorrectly) 17H. It is true that 1.52 only narrowly crosses the threshold for 2H. But interestingly, the integration value is also very low in this ppm region for the hydrogen on chiral carbon stereoisomers (integration value at 7.93 ppm = 1.51 for 6b, 1.57 for 6a. As assigned by "Auto Assignment" algorithm of MestReNova v12).

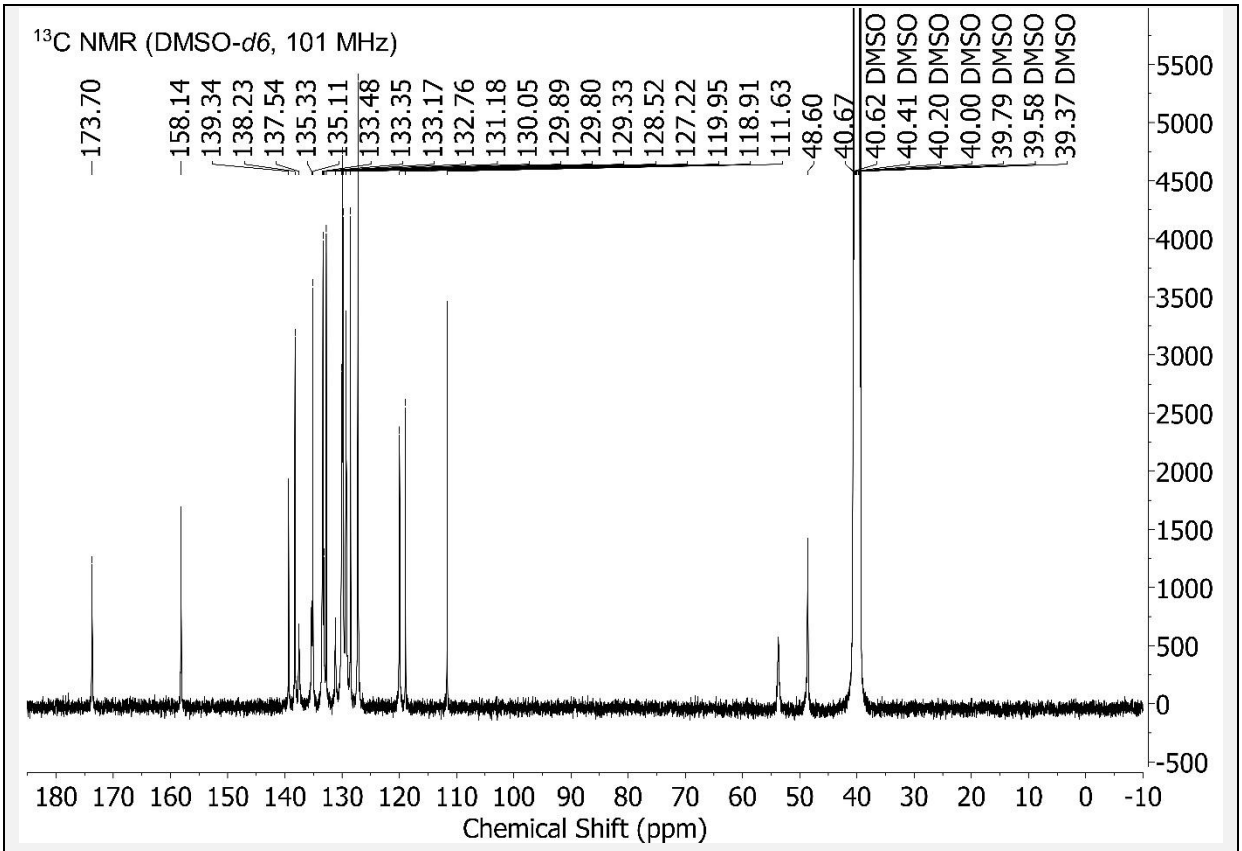

Figure 41 – ^{13}C NMR {*NMR probe temperature = 311.9 K*} for 7a. Scaled to highest compound peak. "Auto peak picking" algorithm in MestReNova v12 used to pick peaks shown. With default program settings used. And no chemical structure used/inputted to guide/constrain this peak picking.

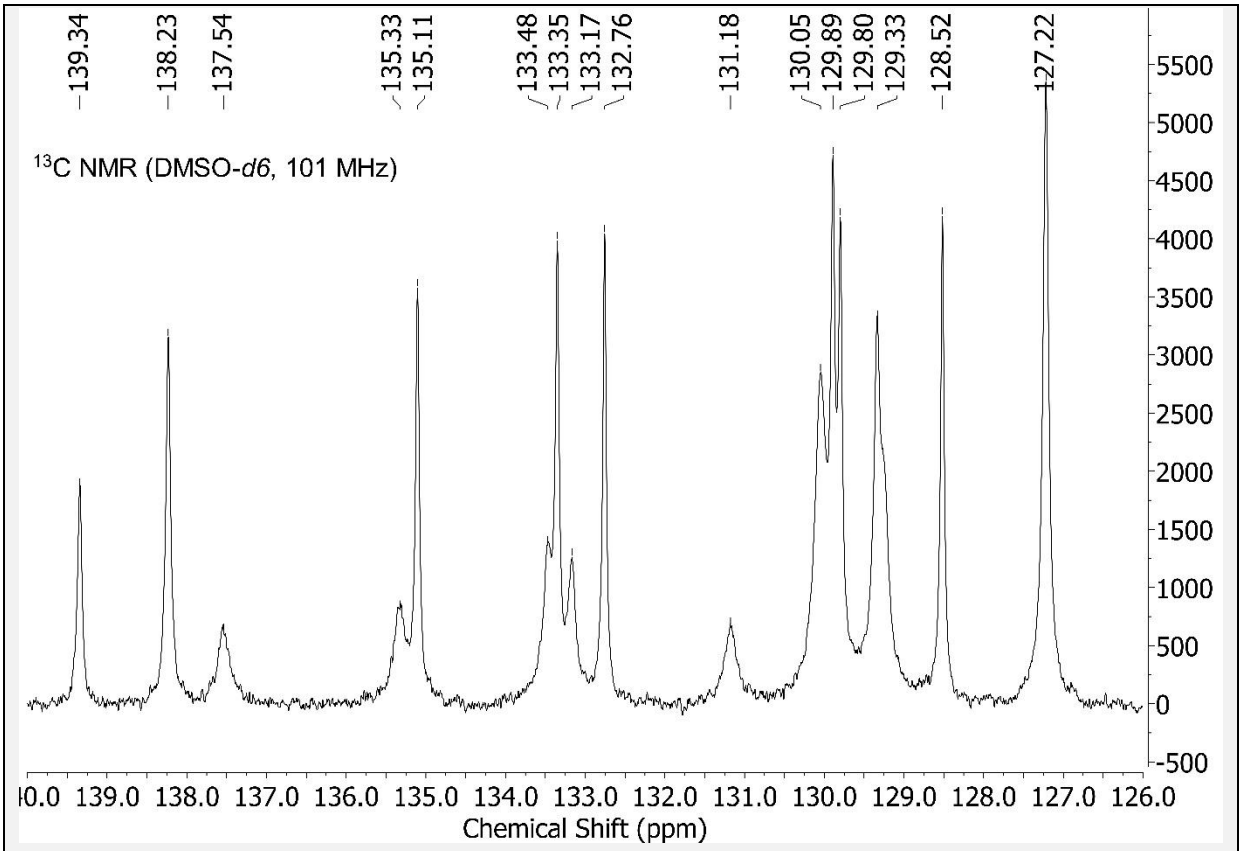

Figure 42 – Region of Figure 41 expanded.

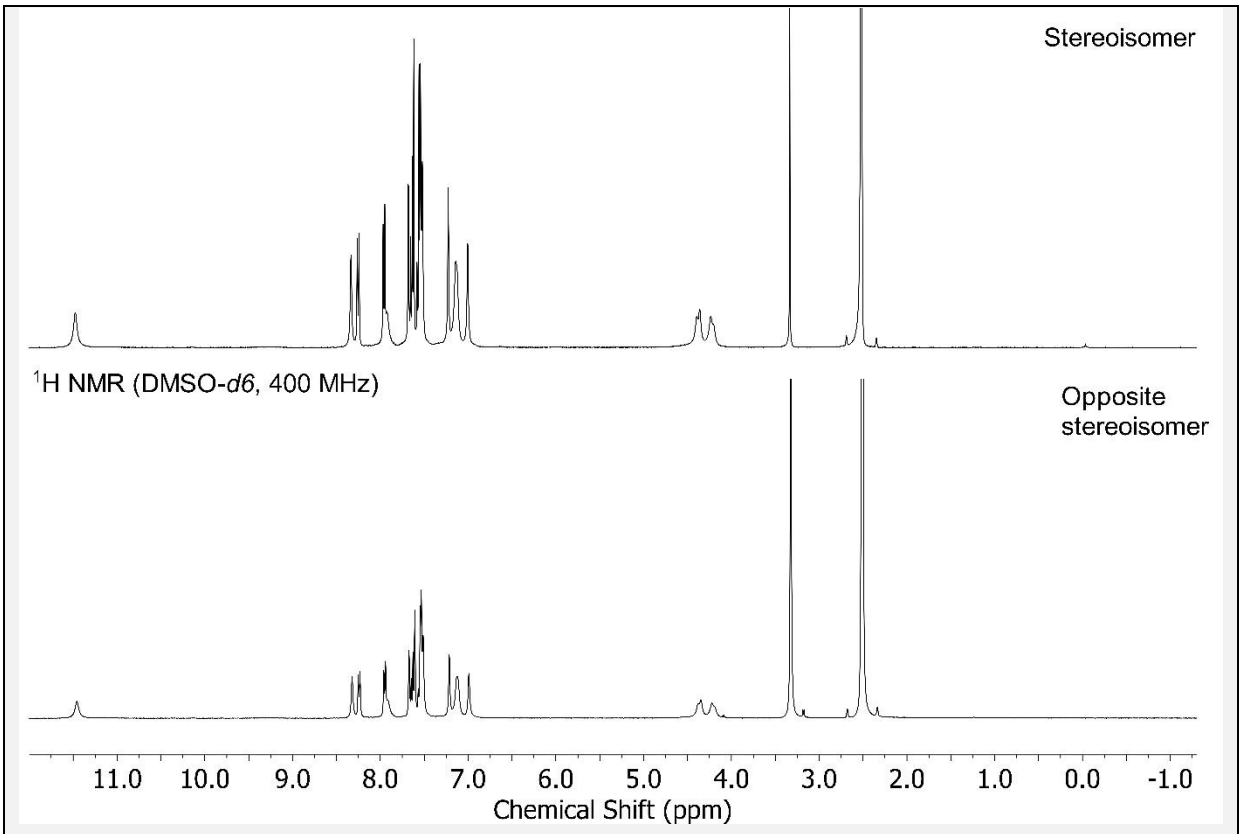

Figure 43 – 7b data in upper panel, 7a data in lower panel.

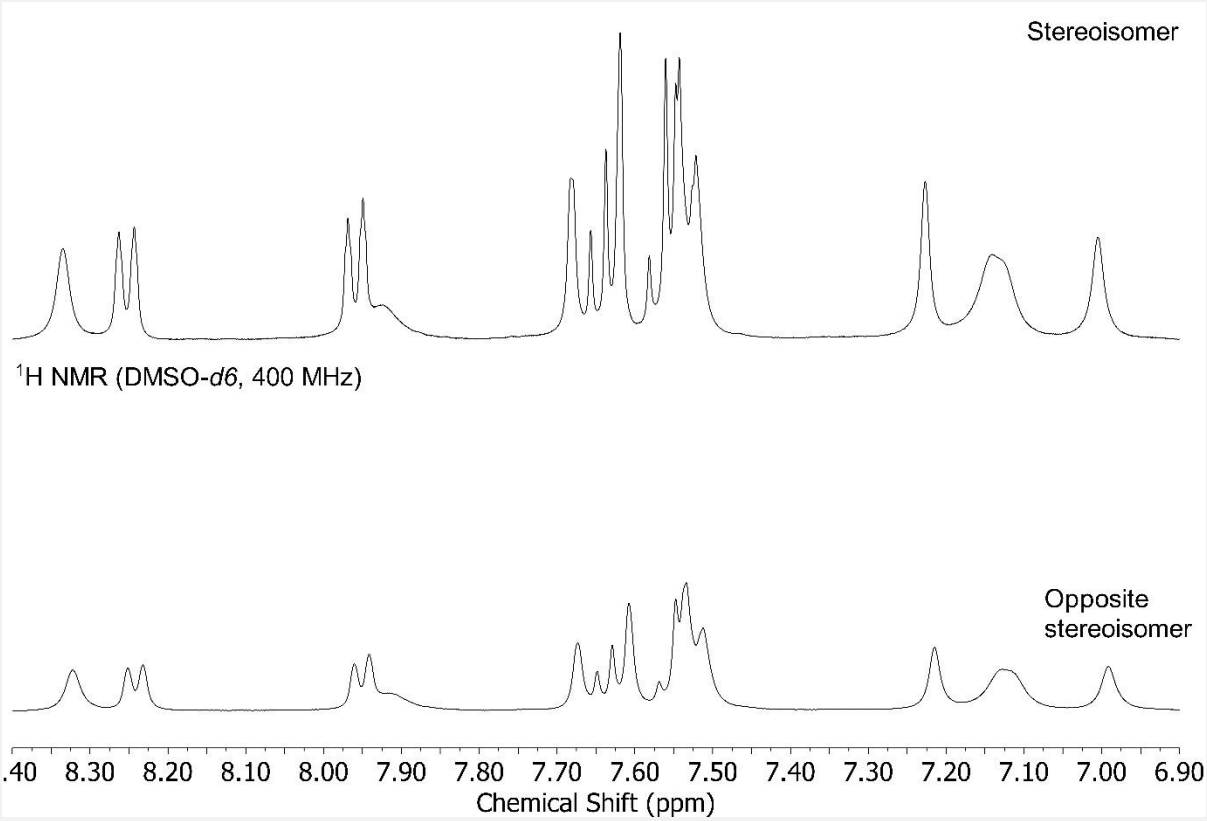

Figure 44 – Aromatic region. 7b data in upper panel, 7a data in lower panel.

Hydrogen vs. deuterium on chiral carbon

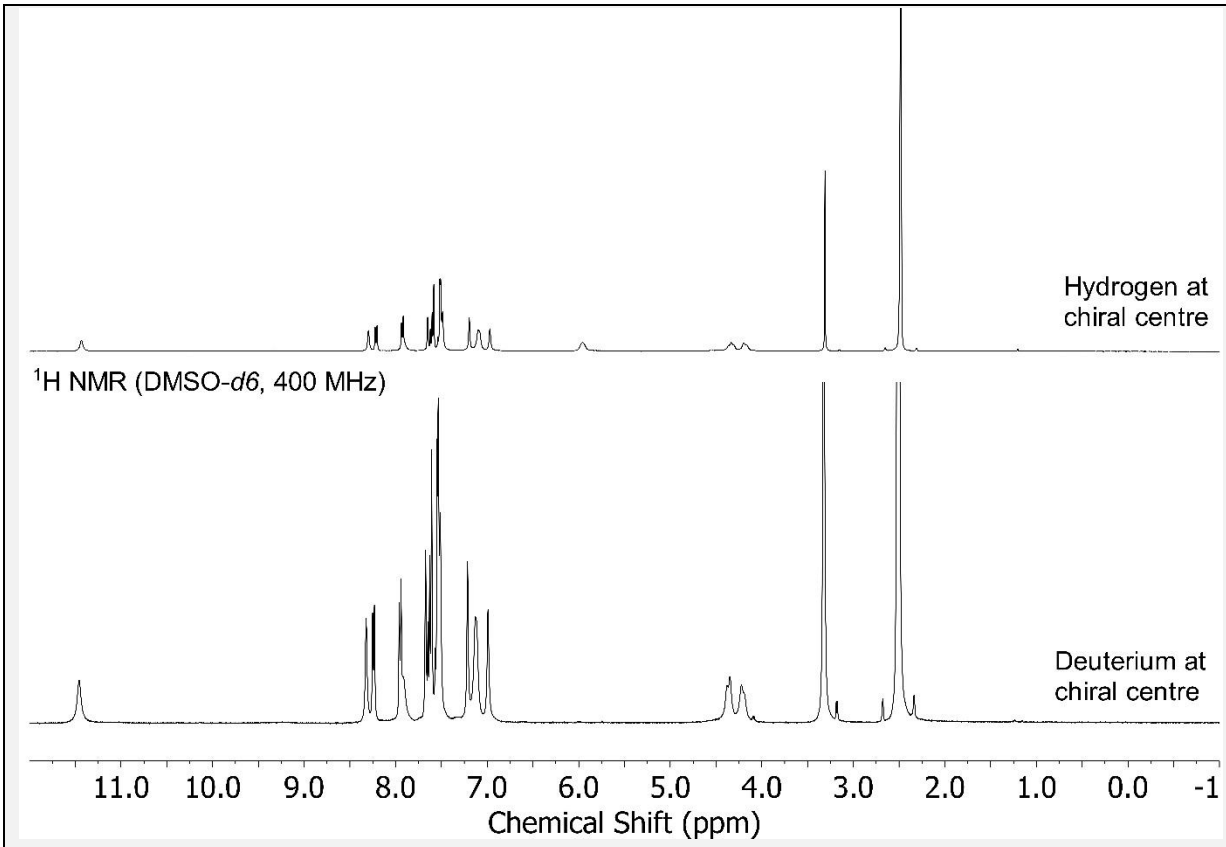

Figure 45 – *Upper panel*: ^{1}H NMR spectrum for 6b. *Lower panel*: ^{1}H NMR spectrum for 7a. The upper has a peak at 5.96 ppm from the hydrogen attached to its chiral carbon. The lower has this hydrogen replaced with a deuterium, and thence this 5.96 ppm peak is absent in its ^{1}H NMR spectrum.

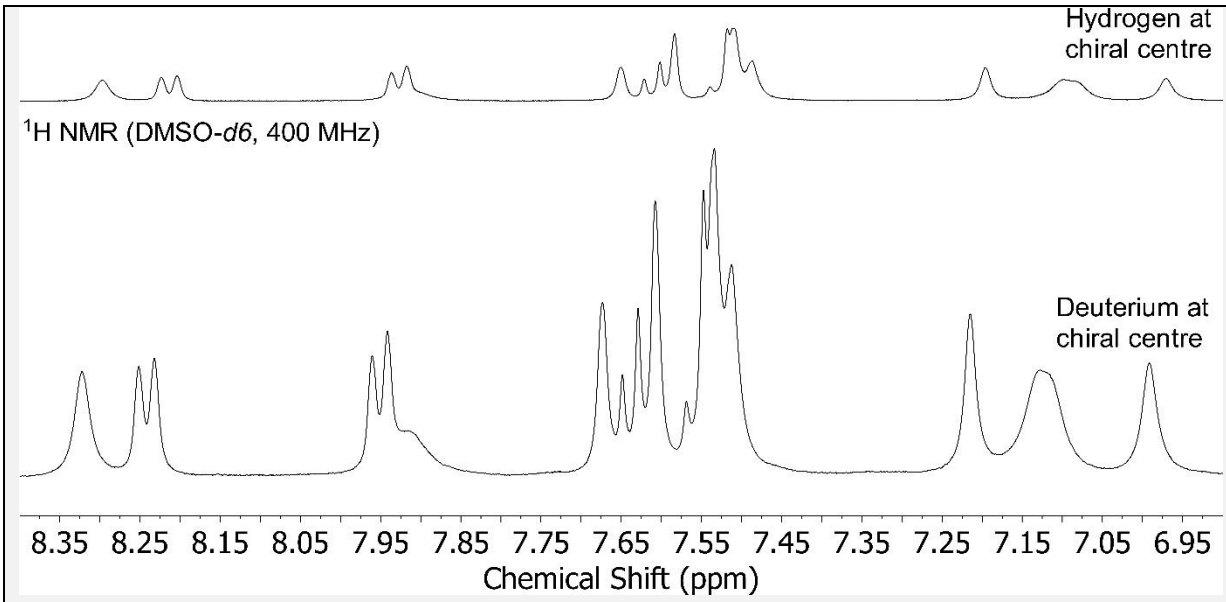

Figure 46 – Aromatic region. *Upper panel*: ^{1}H NMR spectrum for 6b. *Lower panel*: ^{1}H NMR spectrum for 7a.

Supplementary content for the Results section titled "Anti-cancer"

Consolidated absolute excess, and enantiomeric excess, data:

[From MassLynx 4.1 software on							
the Chiral SFC-MS machine used]				**[*SAME data in different software: Mestrelab*]**			
	Chiral SFC			**Chiral SFC**			
	(UV chromatogram)			**(UV chromatogram)**		***Chiral SFC-MS***	
	Absolute(%)	ee(%)		Absolute(%)	ee(%)	Absolute(%)	ee(%)
6a	98.79	97.58		98.83	97.66	99.64	99.28
6b	99.02	98.04		98.23	96.46	97.9	95.8
7a	98.71	97.42		*Done on a different machine (other broke) **			
7b	100	100		100	100	*Can't calculate #*	
		Enantiomeric excess (ee) = (Absolute excess-50)*2					
Wavelength (λ) for UV chromatogram = 220 nm							
* This other machine *only* has Chiral SFC capability. It is *not* a Chiral SFC-MS machine.							
Its shown data is *not* from MassLynx 4.1, but from Empower 3 software instead.							
This data won't open in Mestrelab (incompatibility).							
Chiral SFC-MS machine used = Thar analytical SFC with UV & mass detectors.							
Chiral SFC machine used = Waters Acquity UPC2 with PDA detector.							
# Without equivalent Chiral-SFC data for 7a, it isn't possible to calculate from the Chiral							
SFC-MS data of 7b. Because the Retention Time (RT) of 7a on this machine is unknown.							

As shown earlier, the mean of 7a and 7b median anti-cancer activity (63.30) is slightly greater (0.54) than the mean of 6a and 6b median anti-cancer activity (62.76). Similarly, the mean of 7a and 7b mean anti-cancer activity (62.58) is slightly greater (0.85) than the mean of 6a and 6b mean anti-cancer activity (61.73). These differences are small enough (<1) to be within a margin of experimental error. This is their most likely explanation. But, alternatively, perhaps, they might actually reflect features of the data. Because (*i*) 7b has slightly greater enantiomeric excess than 6b, (*ii*) 7a has slightly less enantiomeric excess than 6a. Meaning, for absolute excess values, (7b-7a) is 1.06 greater than (6b-6a). Wherein values 0.54, 0.85, and 1.06 all round to 1.

AFTERWORD

The forest shrew has a maximal lifespan of just 2 years, whilst the bowhead whale has a maximal lifespan of at least 211 years [5]. Why? How can an old dog be younger chronologically, but older biologically, than its human owner? Why do dogs age faster than humans? Why do different species age at different rates, and have different maximal lifespans? There ***must*** be a reason(s).

COMPETING INTERESTS

The author has filed for related patents. These disclose, and protect, well beyond the scope of this present disclosure. Most are yet to publish (as of August 2021, and won't publish for some time, e.g. PCT filed on 24th January 2021, with no priority claim, which will publish 18 months thereafter). One of the author's related Australian (AU) patent applications, 2018209175, has already passed examination and been accepted.

FUNDING

None. This work was conducted without funding.

ACKNOWLEDGEMENTS

Under the author's direction, two Contract Research Organisation (CROs) were utilized to generate the data of Figure 1, and Figures 10-46. WuXi AppTec synthesized the compounds. Crown Bioscience performed the experimentation in mice.

REFERENCES

[1] Nicholls DG, Ferguson SJ (2002) Bioenergetics 3 (Vol. 3). Gulf Professional Publishing.

[2] Cabezon E, Butler PJG, Runswick MJ, Walker JE (2000) Modulation of the oligomerization state of the bovine F1-ATPase inhibitor protein, IF1, by pH. Journal of Biological Chemistry. 275(33):25460-25464.

[3] Michael David Forrest. "Therapeutic Modulators of the Reverse Mode of ATP Synthase". U.S. Patent Application No. 16/629,390. Published as US20200306253A1.
In PDF format, on the Google Patents website:
https://patentimages.storage.googleapis.com/2b/ad/07/f9e06bda62ec75/US20200306253A1.pdf
This US patent application is a 371 national entry of PCT/EP2018/069175 (filed 13 July 2018), which published as WO2019/012149A1 (on 17 January 2019).

[4] Cabanac A, Briese E (1992) Handling elevates the colonic temperature of mice. Physiology & behavior. 51(1):95-8.

[5] Tacutu R, Thornton D, Johnson E, Budovsky A, Barardo D, Craig T, Diana E, Lehmann G, Toren D, Wang J, Fraifeld VE, de Magalhaes JP (2018) Human Ageing Genomic Resources: new and updated databases. Nucleic Acids Research 46(D1):D1083-D1090.

[6] Marschner JA, Schäfer H, Holderied A, Anders HJ (2016) Optimizing mouse surgery with online rectal temperature monitoring and preoperative heat supply. Effects on post-ischemic acute kidney injury. PLoS One. 11(2):e0149489.

[7] Wilson DJ (2019) The harmonic mean p-value for combining dependent tests. Proceedings of the National Academy of Sciences. 116(4):1195-1200.
[8] Formentini L, Pereira MP, Sánchez-Cenizo L, Santacatterina F, Lucas JJ, Navarro C, Martínez-Serrano A, Cuezva JM (2014) In vivo inhibition of the mitochondrial H+-ATP synthase in neurons promotes metabolic preconditioning. The EMBO journal. 33(7):762-78.
[9] Santacatterina F, Sánchez-Cenizo L, Formentini L, Mobasher MA, Casas E, Rueda CB, Martínez-Reyes I, de Arenas CN, García-Bermúdez J, Zapata JM, Sánchez-Aragó M (2016) Down-regulation of oxidative phosphorylation in the liver by expression of the ATPase inhibitory factor 1 induces a tumor-promoter metabolic state. Oncotarget. 7(1):490.
[10] Formentini L, Santacatterina F, de Arenas CN, Stamatakis K, López-Martínez D, Logan A, Fresno M, Smits R, Murphy MP, Cuezva JM (2017) Mitochondrial ROS production protects the intestine from inflammation through functional M2 macrophage polarization. Cell reports. 19(6):1202-13.
[11] Harman D (1972) The biologic clock: the mitochondria? Journal of the American Geriatrics Society. 20(4):145-147.
[12] De Grey AD (1999) The mitochondrial free radical theory of aging. Austin, TX: RG Landes.
[13] Barja G (2013) Updating the mitochondrial free radical theory of aging: an integrated view, key aspects, and confounding concepts. Antioxidants & redox signalling. 19(12):1420-1445.
[14] Alpert NM, Guehl N, Ptaszek L, Pelletier-Galarneau M, Ruskin J, Mansour MC, ... & El Fakhri G (2018) Quantitative in vivo mapping of myocardial mitochondrial membrane potential. PloS one. 13(1):e0190968.
[15] Porcelli AM, Ghelli A, Zanna C, Pinton P, Rizzuto R, Rugolo M (2005) pH difference across the outer mitochondrial membrane measured with a green fluorescent protein mutant. Biochemical and biophysical research communications. 326(4):799-804.
[16] Davies KM, Strauss M, Daum B, Kief JH, Osiewacz HD, Rycovska A, ... Kühlbrandt W (2011) Macromolecular organization of ATP synthase and complex I in whole mitochondria. Proceedings of the National Academy of Sciences. 108(34):14121-14126.
[17] Llopis J, McCaffery JM, Miyawaki A, Farquhar M, Tsien RY (1998) Measurement of cytosolic, mitochondrial, and Golgi pH in single living cells with green fluorescent proteins. Proc. Natl. Acad. Sci. USA 95:6803–6808.

[18] Heidrick ML, Hendricks LC, Cook DE (1984) Effect of dietary 2-mercaptoethanol on the life span, immune system, tumor incidence and lipid peroxidation damage in spleen lymphocytes of aging BC3F1 mice. Mechanisms of ageing and development. 27(3):341-358.
[19] Milgram NW, Racine RJ, Nellis P, Mendonca A, Ivy GO (1990) Maintenance on L-deprenyl prolongs life in aged male rats. Life Sciences. 47(5):415-420.
[20] Schriner SE, Linford NJ, Martin GM, Treuting P, Ogburn CE, Emond M, Rabinovitch PS (2005) Extension of murine life span by overexpression of catalase targeted to mitochondria. Science. 308(5730):1909-1911.
[21] Podmore ID, Griffiths HR, Herbert KE, Mistry N, Mistry P, Lunec J (1998) Vitamin C exhibits pro-oxidant properties. Nature. 392(6676):559-559.
[22] Sohal RS, Orr WC (2012) The redox stress hypothesis of aging. Free Radical Biology and Medicine. 52(3):539-555.
[23] Rebrin I, Sohal RS (2008) Pro-oxidant shift in glutathione redox state during aging. Advanced drug delivery reviews. 60(13-14):1545-1552.
[24] Wood JM, Decker H, Hartmann H, Chavan B, Rokos H, Spencer JD, Schallreuter KU (2009) Senile hair graying: H2O2-mediated oxidative stress affects human hair color by blunting methionine sulfoxide repair. The FASEB Journal. 23(7):2065-2075.
[25] Gledhill JR, Montgomery MG, Leslie AG, Walker JE (2007) How the regulatory protein, IF1, inhibits F1-ATPase from bovine mitochondria. Proceedings of the National Academy of Sciences. 104(40):15671-15676.
[26] Bason JV, Runswick MJ, Fearnley IM, Walker JE (2011) Binding of the inhibitor protein IF1 to bovine F1-ATPase. Journal of molecular biology. 406(3):443-453.
[27] Bason JV, Montgomery MG, Leslie AG, Walker JE (2014) Pathway of binding of the intrinsically disordered mitochondrial inhibitor protein to F1-ATPase. Proceedings of the National Academy of Sciences, 111(31):11305-11310.
[28] Shi Y, Buffenstein R, Pulliam DA, Van Remmen H (2010) Comparative studies of oxidative stress and mitochondrial function in aging. Integrative and comparative biology. 50(5):869-879.
[29] Rouslin WI (1987) The mitochondrial adenosine 5'-triphosphatase in slow and fast heart rate hearts. American Journal of Physiology-Heart and Circulatory Physiology. 252(3):H622-7.
[30] Sasaki T, Unno K, Tahara S, Shimada A, Chiba Y , Hoshino M, Kaneko T (2008) Age-related increase of superoxide generation in the brains of mammals and birds. Aging cell. 7(4):459-469.

[31] Foksinski M, Rozalski R, Guz J, Ruszkowska B, Sztukowska P, Piwowarski M, Olinski R (2004) Urinary excretion of DNA repair products correlates with metabolic rates as well as with maximum life spans of different mammalian species. Free Radical Biology and Medicine. 37(9):1449-1454.
[32] Hamilton ML, Van Remmen H, Drake JA, Yang H, Guo ZM, Kewitt K, Richardson A (2001) Does oxidative damage to DNA increase with age? Proceedings of the National Academy of Sciences. 98(18):10469-10474.
[33] Kaneo T, Tahara S, Matsuo M (1996) Non-linear accumulation of 8-hydroxy-2′-deoxyguanosine, a marker of oxidized DNA damage, during aging. Mutation Research/DNAging. 316(5-6):277-285.
[34] Barja G, Herrero A (2000) Oxidative damage to mitochondrial DNA is inversely related to maximum life span in the heart and brain of mammals. The FASEB Journal. 14(2): 312-318.
[35] Pamplona R, Portero-Otın M, Ruiz C, Gredilla R, Herrero A, Barja G (2000) Double bond content of phospholipids and lipid peroxidation negatively correlate with maximum longevity in the heart of mammals. Mechanisms of ageing and development. 112(3):169-183.
[36] Kleiber M (1932) Body size and metabolism. Hilgardia. 6(11):315-353.
[37] Kleiber M (1947) Body size and metabolic rate. Physiological reviews. 27(4):511-541.
[38] Savage VM, Gillooly JF, Woodruff WH, West GB, Allen AP, Enquist BJ, Brown JH (2004) The predominance of quarter-power scaling in biology. Functional Ecology. 18(2):257-282.
[39] Prinzinger R (2005) Programmed ageing: the theory of maximal metabolic scope: How does the biological clock tick? EMBO reports. 6(S1):S14-S19.
[40] Porter RK, Hulbert AJ, Brand MD (1996) Allometry of mitochondrial proton leak: influence of membrane surface area and fatty acid composition. American Journal of Physiology-Regulatory, Integrative and Comparative Physiology. 271(6):R1550-R1560.
[41] Kleiber M (1941) Body size and metabolism of liver slices in vitro. Proceedings of the Society for Experimental Biology and Medicine. 48(2):419-423.
[42] Biesanz JC, Falk CF, Savalei V (2010) Assessing mediational models: Testing and interval estimation for indirect effects. Multivariate Behavioral Research. 45(4):661-701.
[43] Rosseel Y (2012) Lavaan: An R package for structural equation modeling and more. Version 0.5–12 (BETA). Journal of statistical software. 48(2):1-36.

[44] Conti B, Sanchez-Alavez M, Winsky-Sommerer R, Morale MC, Lucero J, Brownell S, Bartfai T (2006) Transgenic mice with a reduced core body temperature have an increased life span. Science. 314(5800):825-828.

[45] Conti B (2008) Considerations on temperature, longevity and aging. Cellular and Molecular Life Sciences. 65(11):1626-1630.

[46] Peto MV, De la Guardia C, Winslow K, Ho A, Fortney K, Morgen E (2017) MortalityPredictors.org: a manually-curated database of published biomarkers of human all cause mortality. Aging (Albany NY). 9(8):1916.

[47] Shoemaker RH (2006) The NCI60 human tumour cell line anticancer drug screen. Nature Reviews Cancer. 6(10):813-823.

[48] Bigeleisen J (1949) The relative reaction velocities of isotopic molecules. The journal of chemical physics. 17(8):675-678.

[49] O'Ferrall RM (2010) A pictorial representation of zero-point energy and tunnelling contributions to primary hydrogen isotope effects. Journal of Physical Organic Chemistry. 23(7):572-579.

[50] Slaughter LM, Wolczanski PT, Klinckman TR, Cundari TR (2000) Inter- and Intramolecular Experimental and Calculated Equilibrium Isotope Effects for $(silox)_2(^tBu_3SiND)TiR$ + RH(silox= $^tBu_3SiO$): Inferred Kinetic Isotope Effects for RH/D Addition to Transient $(silox)_2Ti{=}NSi^tBu_3$. Journal of the American Chemical Society. 122(33):7953-7975.

[51] Holbeck SL, Collins JM, Doroshow JH (2010) Analysis of Food and Drug Administration–approved anticancer agents in the NCI60 panel of human tumor cell lines. Molecular cancer therapeutics. 9(5):1451-1460.

[52] Warburg O (1956) On the origin of cancer cells. Science. 123(3191):309-314.

[53] Hatano E, Ikai I, Higashi T, Teramukai S, Torizuka T, Saga T, ... & Shimahara Y (2006) Preoperative positron emission tomography with fluorine-18-fluorodeoxyglucose is predictive of prognosis in patients with hepatocellular carcinoma after resection. World journal of surgery. 30(9):1736-1741.

[54] Seo S, Hatano E, Higashi T, Hara T, Tada M, Tamaki N, ... & Uemoto S (2007) Fluorine-18 fluorodeoxyglucose positron emission tomography predicts tumor differentiation, P-glycoprotein expression, and outcome after resection in hepatocellular carcinoma. Clinical cancer research. 13(2):427-433.

[55] Cerfolio RJ, Bryant AS, Ohja B, Bartolucci AA (2005) The maximum standardized uptake values on positron emission tomography of a non-small cell lung cancer predict stage,

recurrence, and survival. The Journal of Thoracic and Cardiovascular Surgery. 130(1):151-159.
[56] Downey RJ, Akhurst T, Gonen M, Vincent A, Bains MS, Larson S, Rusch V (2004) Preoperative F-18 fluorodeoxyglucose-positron emission tomography maximal standardized uptake value predicts survival after lung cancer resection. Journal of Clinical Oncology. 22(16):3255-3260.
[57] il Lee M, Jung YJ, Kim DI, Lee S, Jung CS, Kang SK, ... & Kim HY (2021) Prognostic value of SUVmax in breast cancer and comparative analyses of molecular subtypes: A systematic review and meta-analysis. Medicine. 100(31).
[58] Stryer L, Berg JM, Tymoczko JL (2002) Biochemistry, 4th Ed. New York, NY: WH Freeman.
[59] Forrest MD (2015) Why cancer cells have a more hyperpolarised mitochondrial membrane potential and emergent prospects for therapy. bioRxiv, 025197.
[60] Hanahan D, Weinberg RA (2000) The hallmarks of cancer. Cell. 100(1):57-70.
[61] von Haehling S, Anker MS, Anker SD (2016) Prevalence and clinical impact of cachexia in chronic illness in Europe, USA, and Japan: facts and numbers update 2016.
[62] Walenta S, Wetterling M, Lehrke M, Schwickert G, Sundfør K, Rofstad EK, Mueller-Klieser W (2000) High lactate levels predict likelihood of metastases, tumor recurrence, and restricted patient survival in human cervical cancers. Cancer research. 60(4):916-21.
[63] Zamzami N, Kroemer G (2001) The mitochondrion in apoptosis: how Pandora's box opens. Nature reviews Molecular cell biology. 2(1):67-71.
[64] Brizel DM, Sibley GS, Prosnitz LR, Scher RL, Dewhirst MW (1997) Tumor hypoxia adversely affects the prognosis of carcinoma of the head and neck. International Journal of Radiation Oncology* Biology* Physics. 38(2):285-289.
[65] Höckel M, Knoop C, Schlenger K, Vorndran B, Baußnann E, Mitze M, ... Vaupel P (1993) Intratumoral pO2 predicts survival in advanced cancer of the uterine cervix. Radiotherapy and Oncology. 26(1):45-50.
[66] Brizel DM, Scully SP, Harrelson JM, Layfield LJ, Bean JM, Prosnitz LR, Dewhirst MW (1996) Tumor oxygenation predicts for the likelihood of distant metastases in human soft tissue sarcoma. Cancer research. 56(5):941-943.
[67] Höckel M, Schlenger K, Aral B, Mitze M, Schäffer U, Vaupel P (1996) Association between tumor hypoxia and malignant progression in advanced cancer of the uterine cervix. Cancer research. 56(19):4509-4515.

[68] Höckel M, Schlenger K, Höckel S, Aral B, Schäffer U, Vaupel P (1998) Tumor hypoxia in pelvic recurrences of cervical cancer. International journal of cancer. 79(4):365-369.
[69] Sundfør K, Lyng H, Rofstad EK (1998) Tumour hypoxia and vascular density as predictors of metastasis in squamous cell carcinoma of the uterine cervix. British journal of cancer. 78(6):822-827.
[70] Barker HE, Paget JT, Khan AA, Harrington KJ (2015) The tumour microenvironment after radiotherapy: mechanisms of resistance and recurrence. Nature reviews Cancer. 15(7):409.
[71] Gatenby RA, Kessler HB, Rosenblum JS, Coia LR, Moldofsky PJ, Hartz WH, Broder GJ (1988) Oxygen distribution in squamous cell carcinoma metastases and its relationship to outcome of radiation therapy. International Journal of Radiation Oncology* Biology* Physics. 14(5):831-838.
[72] Sullivan R, Pare GC, Frederiksen LJ, Semenza GL, Graham CH (2008) Hypoxia induced resistance to anticancer drugs is associated with decreased senescence and requires hypoxia-inducible factor-1 activity. Molecular cancer therapeutics. 7(7):1961-73.
[73] Doktorova H, Hrabeta J, Khalil MA, Eckschlager T (2015) Hypoxia-induced chemoresistance in cancer cells: The role of not only HIF-1. Biomedical Papers of the Medical Faculty of Palacky University in Olomouc. 159(2).
[74] Michael David Forrest. “Therapeutic Inhibitors of the Reverse Mode of ATP Synthase”. U.S. Patent Application No. US16/478,497. Published as US20200247758A1.
In PDF format, on the Google Patents website:
https://patentimages.storage.googleapis.com/32/92/56/ffe5afbff03bf0/US20200247758A1.pdf
This US patent application is a 371 national entry of PCT/EP2018/051127 (filed 17 January 2018), which published as WO2018/134265A1 (on 26 July 2018).
[75] de Magalhães JP, Toussaint O (2004) Telomeres and telomerase: a modern fountain of youth? Rejuvenation research. 7(2):126-133.
[76] Artandi SE, Alson S, Tietze MK, Sharpless NE, Ye S, Greenberg RA, ... & DePinho RA (2002) Constitutive telomerase expression promotes mammary carcinomas in aging mice. Proceedings of the National Academy of Sciences. 99(12):8191-8196.
[77] Bernardes de Jesus B, Vera E, Schneeberger K, Tejera AM, Ayuso E, Bosch F, Blasco MA (2012) Telomerase gene therapy in adult and old mice delays aging and increases longevity without increasing cancer. EMBO molecular medicine. 4(8):691-704.

[78] Miller RA, Harrison DE, Astle CM, Fernandez E, Flurkey K, Han M, ... & Strong R (2014) Rapamycin-mediated lifespan increase in mice is dose and sex dependent and metabolically distinct from dietary restriction. Aging cell. 13(3):468-477.
[79] https://dtp.cancer.gov/dtpstandard/dwindex/index.jsp (accessed on 16 November 2021).
[80] Yuan R, Kay A, Berg WJ, Lebwohl D (2009) Targeting tumorigenesis: development and use of mTOR inhibitors in cancer therapy. Journal of hematology & oncology. 2(1):1-12.
[81] Laconi E, Marongiu F, DeGregori J (2020) Cancer as a disease of old age: changing mutational and microenvironmental landscapes. British journal of cancer. 122(7):943-952.
[82] Armstrong GT, Kawashima T, Leisenring W, Stratton K, Stovall M, Hudson MM, Sklar CA, Robison LL, Oeffinger KC (2014) Aging and risk of severe, disabling, life threatening, and fatal events in the childhood cancer survivor study. Journal of clinical oncology. 32(12):1218.
[83] Ng J, Shuryak I (2015) Minimizing second cancer risk following radiotherapy: current perspectives. Cancer management and research. 7:1.
[84] Huxley AF (1959) Ion movements during nerve activity. Annals of the New York Academy of Sciences. 81(2):221-46.
[85] Chapman RA (1967) Dependence on temperature of the conduction velocity of the action potential of the squid giant axon. Nature. 213(5081):1143.
[86] Maldonado CA, Wooley BD, Pancrazio JJ. The excitatory effect of temperature on the Hodgkin-Huxley model.
[87] Fitzhugh R (1966) Theoretical effect of temperature on threshold in the Hodgkin-Huxley nerve model. The Journal of general physiology. 49(5):989-1005.
[88] Kuang S, Wang J, Zeng T, Cao A (2008) Thermal impact on spiking properties in Hodgkin-Huxley neuron with synaptic stimulus. Pramana. 70(1):183-90.
[89] Goldin MA, Mindlin GB (2017) Temperature manipulation of neuronal dynamics in a forebrain motor control nucleus. PLoS computational biology. 13(8):e1005699.
[90] Papa S, Zanotti F, Cocco T, Perrucci C, Candita C, Minuto M (1996) Identification of functional domains and critical residues in the adenosinetriphosphatase inhibitor protein of mitochondrial F0F1 ATP synthase. European journal of biochemistry. 240(2):461-7.
[91] Zanotti F, Raho G, Vuolo R, Gaballo A, Papa F, Papa S (2000) Functional domains of the ATPase inhibitor protein from bovine heart mitochondria. FEBS letters. 482(1-2):163-6.
[92] Zanotti F, Raho G, Gaballo A, Papa S (2004) Inhibitory and anchoring domains in the ATPase inhibitor protein IF1 of bovine heart mitochondrial ATP synthase. Journal of bioenergetics and biomembranes. 36(5):447-57.

[93] de Chiara C, Nicastro G, Spisni A, Zanotti F, Cocco T, Papa S (2002) Activity and NMR structure of synthetic peptides of the bovine ATPase inhibitor protein, IF1. Peptides. 23(12):2127-41.
[94] Rothbard JB, Garlington S, Lin Q, Kirschberg T, Kreider E, McGrane PL, ... & Khavari PA (2000) Conjugation of arginine oligomers to cyclosporin A facilitates topical delivery and inhibition of inflammation. Nature medicine. 6(11):1253-1257.
[95] Altschul SF, Gish W, Miller W, Myers EW, Lipman DJ (1990) Basic local alignment search tool. Journal of molecular biology. 215(3):403-410.
[96] Lin MT, Beal MF (2006) Mitochondrial dysfunction and oxidative stress in neurodegenerative diseases. Nature. 443(7113):787-795.
[97] Gella A, Bolea I (2011) Oxidative stress in Alzheimer's disease: pathogenesis, biomarkers and therapy. Alzheimer's Disease Pathogenesis-Core Concepts, Shifting Paradigms and Therapeutic Targets, (contents VII, chapter 15), 319-344.
[98] Beal MF (1996) Mitochondria, free radicals, and neurodegeneration. Current opinion in neurobiology. 6(5):661-666.
[99] Dias V, Junn E, Mouradian MM (2013) The role of oxidative stress in Parkinson's disease. Journal of Parkinson's disease. 3(4):461-491.
[100] Hagemeier J, Geurts JJ, Zivadinov R (2012) Brain iron accumulation in aging and neurodegenerative disorders. Expert review of neurotherapeutics. 12(12):1467-1480.
[101] Zecca L, Youdim MB, Riederer P, Connor JR, Crichton RR (2004) Iron, brain ageing and neurodegenerative disorders. Nature Reviews Neuroscience. 5(11):863-873.
[102] Moreira PI, Smith MA, Zhu X, Nunomura A, Castellani RJ, Perry G (2005) Oxidative stress and neurodegeneration. Annals of the New York Academy of Sciences. 1043(1):545-552.
[103] Forster MJ, Dubey A, Dawson KM, Stutts WA, Lal H, Sohal RS (1996) Age-related losses of cognitive function and motor skills in mice are associated with oxidative protein damage in the brain. Proceedings of the National Academy of Sciences. 93(10):4765-4769.
[104] Halliwell B (2001) Role of free radicals in the neurodegenerative diseases. Drugs & aging. 18(9):685-716.
[105] Abou-Sleiman PM, Muqit MM, Wood NW (2006) Expanding insights of mitochondrial dysfunction in Parkinson's disease. Nature Reviews Neuroscience. 7(3):207-219.
[106] Halliwell B (1992) Reactive oxygen species and the central nervous system. Journal of neurochemistry. 59(5):1609-1623.

[107] Radi Isola RA, Castro Peyronel LA, Rodríguez Rey MI, Cassina Gómez AM, Thomson Garibotti ML, Flint Beal M, ... & Bodis-Wollner I (1997) Free radical damage to mitochondria. Mitochondria and Free Radicals in Neurodegenerative Diseases.
[108] Pope S, Land JM, Heales SJ (2008) Oxidative stress and mitochondrial dysfunction in neurodegeneration; cardiolipin a critical target? Biochimica et Biophysica Acta (BBA)-Bioenergetics. 1777(7-8):794-799.
[109] Bender A, Krishnan KJ, Morris CM, Taylor GA, Reeve AK, Perry RH, ... & Turnbull DM (2006) High levels of mitochondrial DNA deletions in substantia nigra neurons in aging and Parkinson disease. Nature genetics. 38(5):515-517.
[110] Massaad CA, Pautler RG, Klann E (2009) Mitochondrial superoxide: a key player in Alzheimer's disease. Aging (Albany NY). 1(9):758.
[111] Massaad CA, Washington TM, Pautler RG, Klann E (2009) Overexpression of SOD-2 reduces hippocampal superoxide and prevents memory deficits in a mouse model of Alzheimer's disease. Proceedings of the National Academy of Sciences. 106(32):13576-13581.
[112] Perry G, Nunomura A, Hirai K, Zhu X, Prez M, Avila J, ... & Smith MA (2002) Is oxidative damage the fundamental pathogenic mechanism of Alzheimer’s and other neurodegenerative diseases? Free Radical Biology and Medicine. 33(11):1475-1479.
[113] Harman D (2002) Alzheimer's disease: role of aging in pathogenesis. Annals of the New York Academy of Sciences. 959(1):384-395.
[114] Naoi M, Maruyama W (1999) Cell death of dopamine neurons in aging and Parkinson’s disease. Mechanisms of ageing and development. 111(2):175-88.
[115] Bender A, Krishnan KJ, Morris CM, Taylor GA, Reeve AK, Perry RH, Turnbull DM (2006) High levels of mitochondrial DNA deletions in substantia nigra neurons in aging and Parkinson disease. Nature genetics. 38(5):515-517.
[116] Kraytsberg Y, Kudryavtseva E, McKee AC, Geula C, Kowall NW, Khrapko K (2006) Mitochondrial DNA deletions are abundant and cause functional impairment in aged human substantia nigra neurons. Nature genetics. 38(5):518-520.
[117] Wong WL, Su X, Li X, Cheung CM, Klein R, Cheng CY, Wong TY (2014) Global prevalence of age-related macular degeneration and disease burden projection for 2020 and 2040: a systematic review and meta-analysis. The Lancet Global Health. 2(2):e106-16.
[118] Michael David Forrest. “Therapeutic Modifiers of the Reverse Mode of ATP Synthase”. Australian Patent Application Number AU2019208238A1. Filed on 26 July 2019. Published on 11 February 2021.

[119] Michael David Forrest. “Therapeutic Modifiers of the Reverse Mode of ATP Synthase”. Canadian Patent Application Number CA3050553. Filed on 25 July 2019. Published on 25 January 2021.
[120] Rieger B, Arroum T, Villalta J, Busch KB (2021) Mitochondrial F_1F_O ATP synthase determines the local proton motive force in cristae tips. bioRxiv.
[121] McCullough L, Arora S (2004) Diagnosis and treatment of hypothermia. American family physician. 70(12):2325-32.
[122] Gordon CJ (2012) Thermal physiology of laboratory mice: defining thermoneutrality. Journal of thermal biology. 37(8):654-685.
[123] Gaskill BN, Rohr SA, Pajor EA, Lucas JR, Garner JP (2009) Some like it hot: mouse temperature preferences in laboratory housing. Applied Animal Behaviour Science. 116(2):279-85.
[124] Gordon CJ, Puckett ET, Repasky ES, Johnstone AF (2017) A Device that Allows Rodents to Behaviorally Thermoregulate when Housed in Vivariums. Journal of the American Association for Laboratory Animal Science. 56(2):173-6.
[125] Boily P (2009) Role of voluntary motor activity on menthol-induced hyperthermia in mice. Journal of Thermal Biology. 34(8):420-5.
[126] Pennycuik PR (1967) A comparison of the effects of a variety of factors on the metabolic rate of the mouse. Australian Journal of Experimental Biology and Medical Science. 45(4):331-346.
[127] Gordon CJ (1990) Thermal biology of the laboratory rat. Physiology & behavior. 47(5):963-991.
[128] Magalhães JPD, Costa J, Church GM (2007) An analysis of the relationship between metabolism, developmental schedules, and longevity using phylogenetic independent contrasts. The Journals of Gerontology Series A: Biological Sciences and Medical Sciences. 62(2):149-160.
[129] Barja G (2007) Mitochondrial oxygen consumption and reactive oxygen species production are independently modulated: implications for aging studies. Rejuvenation research. 10(2):215-224.
[130] Barja G, Cadenas S, Rojas C, Perez-Campo R, Lopez-Torres M (1994) Low mitochondrial free radical production per unit O2 consumption can explain the simultaneous presence of high longevity and high aerobic metabolic rate in birds. Free radical research. 21(5):317-327.

[131] Lambert AJ, Buckingham JA, Boysen HM, Brand MD (2010) Low complex I content explains the low hydrogen peroxide production rate of heart mitochondria from the long-lived pigeon, Columba livia. Aging cell. 9(1):78-91.
[132] Pamplona R, Portero-Otín M, Sanz A, Ayala V, Vasileva E, Barja G (2005) Protein and lipid oxidative damage and complex I content are lower in the brain of budgerigar and canaries than in mice. Relation to aging rate. Age. 27(4):267-280.
[133] Miwa S, Jow H, Baty K, Johnson A, Czapiewski R, Saretzki G, Von Zglinicki T (2014) Low abundance of the matrix arm of complex I in mitochondria predicts longevity in mice. Nature communications. 5(1):1-12.
[134] Pamplona R, Jové M, Mota-Martorell N, Barja G (2021) Is the NDUFV2 subunit of the hydrophilic complex I domain a key determinant of animal longevity? The FEBS Journal.
[135] Hulbert AJ, Pamplona R, Buffenstein R, Buttemer WA (2007) Life and death: metabolic rate, membrane composition, and life span of animals. Physiological reviews. 87(4):1175-1213.
[136] Pamplona R, Prat J, Cadenas S, Rojas C, Perez-Campo R, Torres ML, Barja G (1996) Low fatty acid unsaturation protects against lipid peroxidation in liver mitochondria from long-lived species: the pigeon and human case. Mechanisms of ageing and development. 86(1):53-66.
[137] Pamplona R, Portero-Otın M, Requena JR, Thorpe SR, Herrero A, Barja G (1999) A low degree of fatty acid unsaturation leads to lower lipid peroxidation and lipoxidation-derived protein modification in heart mitochondria of the longevous pigeon than in the short-lived rat. Mechanisms of ageing and development. 106(3):283-296.
[138] Pamplona R, Portero-Otin M, Riba D, Ledo F, Gredilla R, Herrero A, Barja G (1999) Heart fatty acid unsaturation and lipid peroxidation, and aging rate, are lower in the canary and the parakeet than in the mouse. Aging Clinical and Experimental Research. 11(1):44-49.
[139] Buttemer WA, Battam H, Hulbert AJ (2008) Fowl play and the price of petrel: long-living Procellariiformes have peroxidation-resistant membrane composition compared with short-living Galliformes. Biology Letters. 4(4):351-354.
[140] Hulbert AJ, Faulks S, Buttemer WA, Else PL (2002) Acyl composition of muscle membranes varies with body size in birds. Journal of Experimental Biology. 205(22):3561-3569.

[141] Major SS Flower (1925) Contributions to our Knowledge of the Duration of Life in Vertebrate Animals. - IV. Birds. Proceedings of the Zoological Society of London. 95(4):1365-1422. Blackwell Publishing Ltd.
[142] Rouslin W, Frank GD, Broge CW (1995) Content and binding characteristics of the mitochondrial ATPase inhibitor, IF1 in the tissues of several slow and fast heart-rate homeothermic species and in two poikilotherms. Journal of bioenergetics and biomembranes. 27(1):117-125.
[143] Rouslin W, Pullman ME (1987) Protonic inhibition of the mitochondrial adenosine 5′-triphosphatase in ischemic cardiac muscle. Reversible binding of the ATPase inhibitor protein to the mitochondrial ATPase during ischemia. Journal of molecular and cellular cardiology. 19(7):661-668.
[144] Rouslin W (1988) Factors affecting the loss of mitochondrial function during zero-flow ischemia (autolysis) in slow and fast heart-rate hearts. Journal of molecular and cellular cardiology. 20(11):999-1007.
[145] Rouslin W, Broge CW, Grupp IL (1990) ATP depletion and mitochondrial functional loss during ischemia in slow and fast heart-rate hearts. American Journal of Physiology-Heart and Circulatory Physiology. 259(6):H1759-H1766.
[146] Rouslin W, Broge CW (1989) Regulation of mitochondrial matrix pH and adenosine 5′-triphosphatase activity during ischemia in slow heart-rate hearts: Role of Pi/H+ symport. Journal of Biological Chemistry. 264(26):15224-15229.
[147] Pullman ME, Monroy GC (1963) A naturally occurring inhibitor of mitochondrial adenosine triphosphatase. Journal of biological chemistry. 238(11):3762-3769.
[148] Satre M, De Jerphanion MB, Huet J, Vignais PV (1975) ATPase inhibitor from yeast mitochondria. Purification and properties. Biochimica et Biophysica Acta (BBA)-Bioenergetics. 387(2):241-55.
[149] Hill AB (1965) The environment and disease: association or causation?
[150] https://www.nhs.uk/live-well/healthy-weight/understanding-calories/ (accessed on 16 August 2021).
[151] Porter RK, Brand MD (1995) Causes of differences in respiration rate of hepatocytes from mammals of different body mass. American Journal of Physiology-Regulatory, Integrative and Comparative Physiology. 269(5):R1213-R1224.